UNIVERSITY OF GENOA

POLYTECHNIC SCHOOL

DIME: SECTION OF MATHEMATICAL METHODS AND MODELS

PhD Thesis

for the award of the degree of

DOCTOR OF PHILOSOPHY

XXXII CYCLE

Astrophysical and Cosmological applications of Extended Theories of Gravity

Supervisors:

Prof. Roberto Cianci

Prof. Stefano Vignolo

Prof. Salvatore Capozziello

Candidate:

Pasquale Feola

S4178505

Academic year 2018 – 2019

Acknowledgements

First and foremost I would like to express my sincere gratitude to my thesis supervisors Prof. Roberto Cianci, Prof. Stefano Vignolo and Prof. Salvatore Capozziello for their relentless support, guidance and motivation throughout the course of PhD. In addition to teaching and guiding, on various projects in this thesis, they inculcated the attitude to understand, formulate and accomplish any given task for which I'll always be thankful to them.

I would also like to thank Prof. Ester Piedipalumbo for giving me the opportunity to work on her project and for her continued support and guidance.

I thank Prof. Sante Carloni for his collaboration in this project.

I am also grateful to all my excellent PhD course instructors, especially to Prof. Mariafelicia De Laurentis for the support and advices that she have given me during and after the course work.

I am very grateful to my work partner, as well as a friend, Dr. Xisco Jiménez Forteza, for having successfully collaborated on my research project and for the advices that he gave me constantly during and after our collaboration.

And finally, last but by no means least, I would like to express my heartfelt gratitude to my family and my girlfriend Teresa for their continuous encouragement and belief in me!

To Antonio and aunt Alda

Abstract

The aim of this thesis is to study the possible astrophysical and cosmological applications of *Extended Theories of Gravity*. In particular, we will study Neutron Stars, both on astrophysical and cosmological scale where, at cosmological level, they can assume a macroscopic configuration, i.e. a cosmological probe, which can be represented like a Fermionic condensate. The goal is to provide answers consistent with observational evidences that are not justified by General Relativity. In fact, in the Einstein theory and on astrophysical scale, the maximum allowed mass for the Neutron Stars, called *Chandrasekhar's limit*, is not confirmed by the observations since there exist observational evidences of Neutron Stars that exceed this limit, i.e. exceed the upper limit that the mass of a stable body composed of degenerate matter can have. So, the canonical theories need to be reviewed and integrated with new models that can provide a description that is compatible with the observations. Furthermore, on cosmological scale, standard theories fail to perfectly describe the formation of the large-scale structure of the universe (*dark matter* concept) and the accelerated expansion of the universe (*dark energy* concept). A cosmological theory, with Fermionic condensate non-minimally coupled with the gravitational field, tries to describe a cosmological model using a classical approach where the condensate, being a Neutron Star a good approximation, could provide us an evolutionary model that

can be consistent with the *Lambda Cold Dark Matter* ΛCDM model.

Having problems on different scales, we will study first Neutron Stars as a single, non-rotating object in *Extended Theories of Gravity*. In particular, we will use the $f(R)$ theory, i.e. described by all classes of lagrangians that are written as a generic function of the Ricci scalar. We shall derive the stellar structure equations, namely the *Tolman-Oppenheimer-Volkoff* equations, both in the metric and in the metric-affine case (with torsion and spin). We will see how the torsion and the spin terms could be gravitational field sources for these stars and how these two theories, comparing them, could provide us information on the mass excess obtained from the observations. Therefore, the goal is to identify possible stable configurations of Neutron Stars not justified and foreseen by General Relativity. This is possible by solving numerically the *Tolman-Oppenheimer-Volkoff* equations and plot the *Mass-Radius relation*, which is the most important representation of this stars and it is uniquely related to the choice of the equation of state of the dense matter.

We will consider the *Starobinsky model* and then we will study realistic Neutron Stars using appropriate equations of state that are compatible with the *LIGO* experiment constraints, which allow us to discard a consistent number of equations of state that could be incompatible with a internal structure of a compact star. Since there are no observational evidences that allow to obtain information on the internal structure of a Neutron Star, in the literature there are a hundred possible candidates of equations of state. Therefore, the choice of these equations is very important. By making this opportune choice, we will plot these diagrams, will quantify the parameters

of these objects and, then, will compare the results of the two theories and we will see what the effects will produce. We will see how the effects due to torsion tend to oppose the increases of the star mass, while this effect does not happen in the metric case. We will see how it is possible to obtain stable configurations not justified by General Relativity and, in addition, we will see how a metric theory is better suited to describe more compact objects respect than a torsion theory more suited to describing less compact objects.

Then, subsequently, on cosmological case, we will compare theoretical predictions with observations for a class of cosmological models in which the dark energy component is modeled as a Fermionic condensate, non-minimally coupled with the gravitational field and characterized by some specific self-interaction potentials. Our analysis will be based on the *Markov Chain Monte Carlo Method* and will be employed different data sets. It turns out that, with an appropriate choice of parameters, our models are fully compatible with several observed data. We will combine these parameter values with phase space analysis to deduce the features of the entire cosmic history of the considered models. Moreover, in the phase space analysis, the strong constraint that comes from the Dirac equations allows us a detailed design of the cosmology of the models considered, guaranteeing an evolution towards a state indistinguishable from the general relativistic cosmological models. In fact, these specific potentials are able to reproduce in a natural way an accelerated expansion phase, where the exponential potential is able to induce two de Sitter phases separated by an expansion with a power law that could be for the unification of a phase inflationary and a dark energy era.

Publications

The thesis is based on several papers developed during the three years of PhD that correspond to a published or to be submitted papers as follows:

Chapter 5

S. Capozziello, R. Cianci, P. Feola, S. Vignolo, **Compact Objects with Torsion and Spin in $f(R)$ Gravity**, arXiv:...

Chapter 6

P. Feola, Xisco Jimenez Forteza, S. Capozziello, R. Cianci, S. Vignolo, **Mass-radius relation for neutron stars in $f(R) = R+\alpha R^2$ gravity: a comparison between purely metric and torsion formulations**, *Phys. Rev. D*, **101**, 044037, (2020).

Chapter 7

S. Carloni, R. Cianci, P. Feola, E. Piedipalumbo, S. Vignolo., **Non minimally coupled condensate cosmologies: matching observational data with phase space**, *JCAP*, **09**, 014, (2019).

Contents

List of Figures

List of Tables

Chapter 1

Introduction

Many fundamental physical problems, in General Relativity context, concern the limitations of the Einstein theory, both on astrophysical and cosmological scales, in extreme/strong gravitational regimes has. In fact, on astrophysical scales, compact objects, such as Neutron Stars, are astrophysical objects that can only be described with the General Relativity theory. These relativistic stars are natural laboratories for studying the behavior of high-density nuclear matter using an appropriate equation of state, which relates the pressure and density of degenerate matter. This allows us to obtain the Mass-Radius relation and other macroscopic properties such as the tidal deformability and the stellar moment of inertia [1].

Since the internal structure of a Neutron Star can not be reproduced in the laboratory because of the extreme conditions in which it operates, only theoretical models can be formulated where there are a very large number of candidate equation of state. The astrophysical measurements of the macroscopic properties of the Neutron Star are very useful because they allow us to understand what can be the realistic equation of state. In fact, they can provide information on whether the equation of state is soft, i.e. more compact and less deformable,

or stiff, i.e. less compact and more deformable, and what is the pressure and density of nuclear saturation [2; 3; 4; 5]. Therefore, measuring the mass value of an Neutron Star could help us to describe matter at extreme gravity regimes.

Einstein's theory describes accurately the physical properties that govern the stability of Neutron Stars where Chandrasekhar, considering degenerate matter, fixed a theoretical upper limit of $1.44M_{\odot}$ so that the stability of a non-rotating degenerate star is conserved [6]. Instead, as confirmed by various astrophysical observations, there exist binary systems with Neutron Star with a mass larger than this well known limit [7; 8; 9; 10; 11].

These observational evidences, have already been studied in several previous works (in the metric formalism) [12; 13; 14; 15; 16; 17], where Extended Theories of Gravity are used and in particular the $f(R)$ gravity, i.e. classes of Lagrangians that are written as a generic function of Ricci scalar. The primary goal is to obtain the Mass-Radius relation for a Neutron Star that allows us, in principle, given an equation of state, to derive the maximum mass value, radius and all other macroscopic observables of Neutron Stars.

The use of $f(R)$ theories and the presence of these objects in the Universe, could give useful gravitational probes to survey still unresolved questions such as the problem of the accelerated expansion of the universe, called *dark energy*, where the expansion is confirmed by several observations highlighted in many works [18; 19; 20; 21; 22; 23], and the problem of the formation of large-scale structures, called *dark matter*. Unlike the cosmological model called as *Concordance Lambda Cold Dark Matter* (ΛCDM) Model [24; 25; 26], with the $f(R)$ theories, instead, are obtained similar results without considering any dark component but expanding the gravitational sector (see [27; 28; 29; 30; 31; 32; 33; 34; 35] for more information).

Furthermore, these theories, are having a growing interest because they allow a

good description of the gravitating structures by providing the main contribution to the non-baryonic dark matter of the Universe by means of the extra scalar mode ([36; 37] for explicit examples), together with the possibility to unify the cosmic acceleration [38] and the early-time inflation through, for instance, the Starobinsky inflationary R2-model [39], thus leading to a complete picture of the evolution of the Universe [29; 40; 41; 42; 43; 44; 45; 46] and large-scale structures therein [47; 48; 49].

Unlike the works present in the literature, in this thesis we will plot the $\mathcal{M} - \mathcal{R}$ diagram, using realistic equation of state compatible with the LIGO constraints [50] for a particular Lagrangian, using two different theories, the purely metric theory (that is the one used in literature) and the $f(R)$ gravity with torsion theory, allow to introduce the spin in General Relativity [51]. In this theory, the torsion field is due to the non-linearity of $f(R)$ model. These theories allow us to use spin, which is as important as the mass of particles, introducing torsion where mass (energy) is a source of curvature and spin is a source of torsion. In this way the torsion contributions could provide us additional information to various astrophysical scales, including compact stars, thus obtaining more compatible results in extreme gravity regimes where General Relativity has its own limits.

Studying massive Neutron Star means having an excellent investigation tool, in extreme regimes where General Relativity exhibits some limitations too, both on astrophysical and cosmological scales and could be what is called the *Prova Regina* to test the validity of modified theories of gravity, verify their compatibility with observations and to distinguish General Relativity from its extensions. All this could provide more information so that a consistent description can be given to unsolved problems above, i.e. the *dark matter* problem in the astrophysical context and the *dark energy* problem and early inflation at cosmological level.

Studying these objects means writing the modified Tolman-Oppenheimer-Volkoff equations for $f(R)$ gravity. These equations describe or constrain the structure of a spherically symmetric body composed of isotropic material which is in static gravitational equilibrium. In General Relativity, are derived starting from the Einstein field equations considering a general spherically symmetric metric time-independent. These equations, connected by an equation of state which relates the pressure to the density, completely determine the structure of a spherically symmetric body of isotropic material in equilibrium [52].

Considering the Extended Theories, the various derivation steps are the same but the starting from field equations are different both from General Relativity and between the two formalisms used, i.e. the metric and the metric-affine formalisms. In this thesis, we will be write the Tolman-Oppenheimer-Volkoff equations in $f(R)$ gravity using both formalisms. In the torsional theory, torsion will be introduced considering fluids without spin and, subsequently, we will consider Weyssenhoff spin fluids in addition to torsion.

One of the goal of this thesis is to obtain realistic $\mathcal{M} - \mathcal{R}$ relation by solving numerically the Tolman-Oppenheimer-Volkoff completely modified system equations [52], where we consider the quadratic corrections to the Ricci scalar. All this allows us to compare exactly the data of the two theories and to see how these differ from those of General Relativity and bring out the strong gravity regimes that condition the aforementioned relation.

The study of compact objects could be an excellent tool for confirming or refuting these theories because it would allow us to investigate situations in extreme gravity regimes, being able to distinguish general relativity from its extensions. In the literature, new theoretical star structures have been obtained that are important confirmations for extended gravity[53; 54] by making hypotheses as in [55].

Therefore, on astrophysical scale, studying the massive Neutrons Stars with the Extended Theories of Gravity, may provide answers concerning the existence of a class of objects not foreseen and justified by General Relativity that could be cosmological probes that could provide a description more consistent with cosmological models where the dark energy component is present. In fact, in this thesis, using a non-minimally coupled theory, we will see how the use of a Fermionic condensate non-minimally coupled with the gravitational field, allow us to describe the dark energy component quite faithfully. Condensate cosmology [56] is a way of describing the expanding accelerating universe. Indeed, on cosmological scales, the primary goal of modern cosmology is to solve the problem of accelerated expansion of the universe, confirmed by several observations highlighted in many works [18; 19; 20; 21; 22; 23], These observations show that the standard cosmological model is inadequate for describing the universe under extreme conditions because the hypotheses of a universe containing only matter and radiation is not sufficient.

An explanation for a possible solution to this problem is to assume the existence of a cosmic fluid consisting of non-standard matter with an equation of state $p = -\rho$ that is not stored on large-scale structures where *dark energy* is associated with the Einstein cosmological constant which includes 68.3% of the universe, while 31.7% of the universe consists of 4.9% for baryonic matter and cold dark matter for 26.8% which would explain the large scale structure.

This model is in agreement with the data provided from the observations and is called (ΛCDM) Model [24; 25; 26], but despite all this, presents some inconsistencies from the theoretical point of view. In fact, a discrepancy of 120 orders of magnitude emerged between the observed value of the cosmological constant at the cosmological level and the one predicted by any quantum gravity [57]. This inconsistency, is known as *the cosmological constant problem.* In the

last years, a large quantity of observational data revealed that the present universe is experiencing an accelerated expansion (see for instance [58; 59; 60; 61]), which is usually assumed to be driven by a new form of matter–energy: dark energy.

As previously stated on astrophysical scale, also on cosmological scale is possible to use another approach to study these problems, i.e. modify the Einstein theory where the General Relativity is limited to the description of the universe on solar system scales and, as a consequence, going beyond these scales, the observational effects of this inadequacy manifests itself in the dark matter and dark energy form. These considerations allow us to propose alternative theories of gravity where results are obtained without considering any dark component where, in previous works [27; 28; 29; 30; 31; 32; 33; 34; 35], an accelerated expansion of the universe consisting of observations has been obtained, expanding only the gravitational sector.

Going into more detail, these theories allowed to reproduce the Hubble diagram derived from *Type Ia Supernovae* surveys [62; 63], the anisotropies observed for *Cosmic Microwave Background* (CMB) [64; 65] and, recently, that the existence of a Noether symmetry in Extended Theories of Gravity gives rise to a further gravitational radius determining the dynamics at galactic scales, where it is possible to explain the baryonic Tully-–Fisher relation and the rotation curve of gas-rich galaxies without the dark matter hypothesis [66].

In the current state, the nature of dark energy is still completely unknown. Some of the theoretical frameworks proposed to understand this issue include a non zero cosmological constant, the potential energy of some scalar field, effects connected with non homogeneous distributions of matter and averaging procedures, and effects due to alternative theories of gravity. Among the latter, the so called scalar-tensor gravitational theories, arising in other contexts like for example the low energy limit of Kaluza-Klein gravity or the quantum field theory in

curved spacetimes [67; 68], have been widely investigated in both the scenarios of the early and late universe expansions. The peculiar feature of these theories is the non minimal coupling of gravity with a given scalar field. Recently, it is has been suggested that such a scalar field is not fundamental but it may be constituted by a fermion condensate.

In cosmology, fermion fields have been studied as possible sources of inflation and dark energy [69; 70; 71; 72]. In most cases, fermions fields are minimally coupled to gravity; only recently, few works have instead investigated the cosmological effects of non–minimally coupled condensates of semi–classical fermions [73; 74; 75; 76; 77]. Differently from other scalar-tensor models, the fermion condensate are characterized by an easier first order evolution equation. This induces a number of peculiar features which have been described for the first time via phase space analysis in [76] for a non–minimally coupled fermion condensate characterized by three different potentials. The dynamical system approaches and methods that have been used in [76] have been known for long time in General Relativity based cosmologies [78], and more recently in the context of modified gravity (see [79] for a recent review), allowing a relatively easy semi-quantitative interpretation of complex cosmological models.

In this thesis, we aim to perform a comparison of the models introduced in [76] with observations and more specifically with the *Union2 Type Ia Supernovae* data set, the *Gamma Ray Bursts Hubble* diagram, a sample of 28 measurements of the Hubble parameter compiled in [80], the gaussian priors on the distance from the *Baryon Acoustic Oscillations* and the *Hubble constant h* (such priors have been included in order to help break the degeneracies among model parameters). The statistical analysis on these datasets is based on *Monte Carlo Markov Chains* simulations which allow us to compute, simultaneously, the full probability density functions of all the parameters of interest. We will show that a value

of these parameters exists which is able to match these data to the non-minimally coupled condensate theory. Their values will be used in combination with phase space analysis to deduce global features of the cosmic history suggested by these theories. For this purpose, we will give here a set of dynamical system variables different from the ones employed in [76]. Such new setting is required because the phase space description in [76] was not compact and the data analysis suggests that the present universe is on an orbit that would go to the infinite boundary. The new formulation, instead, is compact and will allows us to explore without problems the entire cosmic history selected by the values the observational parameters.

Therefore, what we can say is that: in this thesis, we will see the possible astrophysical and cosmological applications of Extended Theories of Gravity. We will see how a theory $f(R)$ can be useful to describe Neutron Stars not justified by General Relativity and how they can be used as cosmological probes, i.e. Fermionic condensates non-minimally coupled to the gravitational field, which model the dark energy component present in the universe. The thesis is organized as follow. In chapter 2, we will see what are the Extended Theories of Gravity, why there is a need to extend Einstein's theory, what are the physical and mathematical motivations and how these theories relate to the Mach principle. In chapter 3, we will see the scenarios beyond Einstein's gravity. We will derive the field equations both in scalar-tensor and in higher-order theories. In chapter 4 we will give a brief, phenomenological, overview of what are compact objects, especially Neutron Stars, and Fermionic condensates. In chapter 5, we will derive the stellar structure equations for Neutron Stars in $f(R)$ gravity both in the metric and in the metric-affine case. In chapter 6, we will numerically solve the Tolman-Oppenheimer-Volkoff equations, we will plot the Mass-Radius diagrams for a Neutron Star, we will see the possible stable configurations of

these stars not justified by Einstein's theory and we will calculate the stellar parameters (maximum value of mass and radius) and compared in the two theories. In chapter 7, we compare theoretical predictions with observations for a class of cosmological models in which the dark energy component is modeled as a Fermionic condensate, non-minimally coupled with the gravitational field and characterized by some specific self-interaction potentials using the Markov Chain Monte Carlo Method and employs different data sets. Moreover, we will combine these parameter values with phase space analysis to deduce the features of the entire cosmic history of the considered models. In chapter 8, we will discuss the results, conclusions and future works.

Finally, unless other specified, in this thesis the metric signature is $(+,-,-,-)$, Latin and Greek indices run from 0 to 3; ∇ denotes the Levi-Civita covariant derivative associated with a metric tensor g_{ij}. Units are used in which the speed of light c, the reduced Planck constant $\hbar$, Newwton's constant G and $k_B = 8\pi G$ assume the value unity, i.e. $(\hbar = c = k_B = 8\pi G = 1)$. Round and square brackets around indices denote symmetrization and antisymmetrization, respectively, which include division by the number of permutations of the indices and g denotes the determinant of the metric tensor g_{ij}. The Riemann tensor is defined by

$$R^d_{cab} = \partial_a \Gamma_{bc}{}^d - \partial_b \Gamma_{ac}{}^d + \Gamma_{ap}{}^d \Gamma_{bc}{}^p - \Gamma_{bp}{}^h \Gamma_{ac}{}^p, \tag{1.1}$$

where the $\Gamma_{ab}{}^c$ are the Christoffel symbols associated with the metric g_{ij} defined by

$$\nabla_{\partial_a} \partial_b = \Gamma_{ab}{}^c \, \partial_c \, . \tag{1.2}$$

The Ricci tensor is obtained by contracting the first and the third index via the metric g_{ab}:

$$R_{ab} = R^c_{acb}, \tag{1.3}$$

while $R \equiv g^{ab}R_{ab}$ is the Ricci curvature, $\Box \equiv g^{ab}\nabla_a\nabla_b$ is d'Alembert's operator and the subscript 0 identifies quantities evaluated at the present instant of time in the history of the universe.

Chapter 2

Extended Theories of Gravity

Summary

In this chapter, we will see the main reasons to need extend Einstein theory, starting first with why we need to have an alternative theory of gravity. Then, we will move on to physical and mathematical motivations, also seeing General Relativity and its extensions. Moreover, we will see how important it is to implement the Mach principle in the two fundamental branches of extended theories, i.e. *Higher Order Corrections* theories to General Relativity and *Non-Minimal Coupled* theories. Finally, we will discuss how the Mach principle can be correlated with *The Equivalence Principle* and how it is connected with the variation of the Newton gravitational "constant" G [33].

2.1 Why extending gravity?

General Relativity, formulated by Einstein in 1916, is the most important physical theory that describes gravitational interaction. In the following years, several observations, have shown that this theory does not describe correctly all the

gravitational physical phenomena consistent with the observations.

The Einstein theory, basically elaborated with a classical approach, studies at macroscopic level the correlation that exists between space and time and between matter and gravity. Unlike Newtonian theory, where space and time were considered as absolute and static physical quantities, in Einsteinian theory, we have instead a dynamic description of the universe where both space and time are dynamic quantities that are derived taking into account the distribution and the matter and energy dynamics. Moreover, this theory has allowed us to describe the universe on a cosmological scale, thus obtaining the standard cosmological model that consistently describes some cosmological observables [81].

In recent years, astrophysical and cosmological observations have shown that General Relativity is inadequate to describe the gravitational interaction at various energy scales. In fact, for example at the cosmological level, a series of problems have emerged [82], called *The Standard Cosmology Problems*, which show how the standard Big Bang cosmological model fails to perfectly describe the universe at extreme gravitational regimes. In addition to all this, the gravitational interaction does not yet have a quantum field theory, therefore it cannot yet be described as a fundamental theory at the quantum level, which happens with the other fundamental interactions.

Because of all these motivations, a series of semiclassical theories have been formulated where the Einstein theory and its experimental and observational evidences can be reproduced. These theories, called *Extended Theories of Gravity*, aim to correct and expand General Relativity. This consists in adding higher order corrective terms in curvature invariants or minimally or non-minimally coupled scalar fields with gravity that emerge from an effective quantum gravity action [83].

The introduction of scalar fields in these theories also allows us to fully in-

tegrate the Mach principle [84]. According to Mach's principle the local inertial frame is determined by the average motion of distant astronomical objects [84]. This feature implies that the gravitational coupling at a spacetime point is not absolute but is determined by surrounding matter and, therefore, becomes a function of the spacetime location, a scalar field. As a consequence, both the concept of inertia and the principle of equivalence need to be revised. In this perspective, the Brans-Dicke theory [85] is the prototype of the extended theories of gravity. In fact, Newton's gravitation "constant", variable in this theory, corresponds to a scalar field non-minimally coupled with geometry and represents a more satisfactory implementation of the Mach's principle respect to General Relativity [85; 86; 87].

Furthermore, every scheme unifying the fundamental interactions produces effective actions in which non-minimal couplings to the geometry or higher order terms in the curvature invariants are necessarily present. Such contributions are due to first or higher loop corrections in the high curvature regime approaching the full quantum gravity regime [83]. This scheme was adopted in the quantization of matter fields on curved spacetimes and the result was that the interactions between quantum scalar fields and the background geometry, or the gravitational self-interactions, yield corrections to the Hilbert-Einstein Lagrangian [88]. Moreover, it has been realized that these corrective terms are unavoidable in the effective quantum gravity actions [89]. Thus, in these theories corrective terms are added, as soon as quantum corrections are introduced, to the Hilbert-Einstein Lagrangian [88], which can be the higher order invariants of the curvature tensor or non-minimal coupling terms between matter scalar fields and geometry.

In addition to motivations essentially of fundamental physics, Extended Theories show, at a cosmological level, an inflationary behavior that allows to overcome the gaps provided by the standard Big Bang model based on the Einstein the-

ory. These inflationary scenarios seem able to justify recent observations of the *Cosmic Microwave Background* CMB [40; 90; 91].

Finally, it has been shown that, by using of conformal transformations, the higher order corrective terms and the non-minimally coupled ones always correspond to one or more scalar fields minimally coupled to the curvature, which are added to the General Relativity [92; 93; 94; 95; 96; 97]. These properties allow us to describe multiple inflationary events where a primary phase could describe large-scale structures with very long wavelengths that then develop into today's galaxy cluster observations, while a later phase stage could choose smaller scale structures like the today's observed galaxies [98]. Consequently every inflationary era is linked to the dynamics of a scalar field.

2.2 Physical and Mathematical Motivations

The need to extend General Relativity is fundamentally due to physical (astrophysics and cosmology) and mathematical motivations. For a detailed quantum gravity motivations see [88; 99; 100; 101; 102; 103; 104].

The goal is to have descriptions that are consistent with the data taken in recent years. As mentioned in the previous section, these theories could play a fundamental role in the description of the early universe, i.e. to re-examine the standard cosmological scenarios that lead to inflation. Therefore, thanks to the data accumulated in the last period, could have a new cosmological model called ΛCDM model. The first evidence that the universe is actually in a phase of accelerated expansion it occurred by making measurements of the Hubble diagram of *Type Ia Supernovae* [18; 19; 105; 106] with $z \sim 1$. Other experiments [107; 108], determined the position of the first two Doppler peaks in the spectrum of CMB anisotropies, describing a universe with flat spatial sections.

Information originated by these data, indicates that the universe is dominated by a cosmic fluid with negative pressure (called *dark energy*) that is responsible for accelerated expansion. This phenomenon is further confirmed by recent measurements of the CMB spectrum from the *Wilkinson Microwave Anisotropy Probe* WMAP satellite experiment [21; 109; 110] and from the extension of the *Type Ia Supernovae* Hubble diagram to redshifts larger than one [20].

A simplest explanation for the cosmic acceleration is the well known cosmological constant Λ [111]. This one provides the best-fit to most of the available astrophysical data [21] but the ΛCDM model does not explain why the deduced value of Λ is 120 orders of magnitude lower in comparison with the typical value of the vacuum energy density predicted by particle physics, and why its present value is comparable to the matter density. This problem is called *Coincidence Problem*.

In literature, this problem has been faced developing some models known as *quintessence* [112; 113], i.e. replacing the cosmological constant Λ with a scalar field ϕ linked to a potential $V(\phi)$. This approach, while compatible with data, does not resolve the coincidence problem because the dark energy and matter densities have two completely different evolutions and their values are comparable on very short cosmological times that coincide precisely at the present era. This problem is *The Coincidence Problem of Quintessence*.

Unlike an approach that includes exotic matter, the problem has been studied completely differently. Taking into account the fact that dark energy has a component consisting of negative pressure matter, that comes to dominate the dynamics late in the matter era, then the expansion could be explained by considering a single fluid characterized by an equation of state that acts like dark matter at high densities, while at low densities it acts as a dark energy.

In these models, known as *Unified Dark Energy* or *Unified Dark Matter* mod-

els, at least at the phenomenological level the coincidence problem is solved naturally. A model used more often, for example, is the condensate cosmology [56]. A different class of *Unified Dark Energy* models with a single fluid has been proposed [114; 115]: its energy density scales with the redshift z in such a way that a radiation-dominated era, followed by a matter era and then by an accelerating phase can be naturally achieved. These models are extremely versatile since they can be interpreted both in the framework of *Unified Dark Energy* or as two-fluid scenarios containing dark matter and scalar field dark energy. A characteristic feature of this approach is that a generalized equation of state can always be obtained and the fit to the observational data can be attempted.

There is another, different, way to approach the problem of the cosmic acceleration. As highlighted in [116], it is the possibility that the observed acceleration is instead the first signal of a breakdown, in the infrared limit, of the laws of gravitation as we known them. Considering all this, the cosmological equations are modified and it is verified if the astrophysical data are still adaptable to the models that contain only standard matter. Examples are the Cardassian expansion [117] and Dvali-Gabadadze-Porrati gravity [118]. Moreover, it is possible to find alternative schemes in which a quintessential behavior is obtained by incorporating effective models coming from fundamental physics and giving rise to generalized or higher order gravity actions [27] (see [119] for a comprehensive review).

For instance, a cosmological constant may be recovered as a consequence of a non-vanishing torsion field, leading to a model consistent with both the *Type Ia Supernovae* Hubble diagram and observations of the Sunyaev–Zel'dovich effect in galaxy clusters [120]. *Type Ia Supernovae* data could also be efficiently fitted by including in the gravitational sector higher order curvature invariants [119; 121; 122; 123]. These alternative models provide naturally a cosmological

component with negative pressure originating in the geometry of the universe, thus overcoming the problematic nature of quintessence scalar fields.

All this issues concern cosmological and astrophysical events in strong field regimes. Coming to the weak-field limit, i.e. considering Solar System scales, the Extended Theories must reproduce General Relativity which, in any case, is firmly tested only in this limit and at these scales [124]. Even this limit is a matter of debate since several relativistic theories do not reproduce exactly the Einsteinian results in their Newtonian limit but, in some sense, generalize them. For example, in [125], the R^2-gravity give rise to Yukawa-like corrections to the Newtonian potential with potentially interesting physical consequences. In fact, such terms, can explain the flat rotation curves of galaxies [126].

Extended theories include a complex and distinct mathematical structure. In these theories, the gravitational field equations are modified in two ways:

1. The geometry can be non-minimally coupled to some scalar field (scalar-tensor theories);

2. Derivatives of the metric higher than second order appear (higher order theories).

The complexity of this mathematical formalism derives from the fact that more general theories must be reduced to the Einstein form. Through a Legendre transformation on the metric, higher order theories with Lagrangians satisfying minimal regularity conditions assume the form of Einstein theory with scalar fields sourcing the gravitational field [127; 128; 129; 130].

Another issue is the Palatini approach to gravity first analyzed by Einstein himself [131]. This formalism consider the (usually torsion-less) connection ${\Gamma_{ij}}^h$ defining by Ricci tensor R_{ij} as a quantity independent of the spacetime metric g_{ij}. The Palatini formulation of General Relativity is equivalent to the purely metric

theory [81; 132] because the field equations for the connection $\Gamma_{ij}{}^{h}$ regarded as a quantity independent of the metric, yield the Levi-Civita connection of the metric g_{ij}. Thus, the Palatini variational principle is completely equivalent to the metric one.

This equivalence, on the other hand, is not found in extended theories because the Palatini and the metric variational principles provide different gravitational field equations, so describing different physics phenomena [129; 133]. Palatini approach, in this framework, is useful for many cosmological applications [27; 119; 134; 135; 136; 137; 138]. When these formalisms are used, they must take into account the fact that, from the physical point of view, in the Palatini case, the metric structure of space-time is decoupled from the geodetic structure. Since the causal structure of space-time is described by the metric tensor g_{ij}, while the space-time trajectories of the particles are governed by the connection $\Gamma_{ij}{}^{h}$, (this connection, in general is different from Levi-Civita connection of g_{ij} for the metric case), this decoupling further defines the geometry of space-time and generalizes the purely metric formalism. Therefore, the metric-affine structure of spacetime is defined into a bimetric structure of spacetime. In addition to the physical metric g_{ij}, a second metric h_{ij} is present which is related, in the case of $f(R)$ gravity, to the connection. The connection $\Gamma_{ij}{}^{h}$ turns out to be the Levi-Civita connection of this second metric h_{ij} and provides the geodesic structure of spacetime.

Instead, in a scalar-tensor theories, if we consider non-minimal coupling interactions in the gravitational Lagrangian, the new metric h_{ij} is connected to this non-minimal coupling and h_{ij} can be related to a different geometric and physical aspect of the gravitational theory. With the Palatini formalism, the non-minimal coupling and the scalar field entering the evolution of the gravitational fields are separated from the metric structure of spacetime.

Finally, summarizing it can be said that: taking into account all the physical

and mathematical motivations, in general, any relativistic theory of gravitation yields corrections to the weak-field gravitational potentials (e.g., [139]) which, at the post-Newtonian level and in the Parametrized Post-Newtonian formalism, could constitute a test of these theories [124]. Furthermore, the gravitational lensing astronomy [140] is providing additional tests of gravity over small, large, and very large scales which will soon provide direct measurements of the variation of the Newton coupling [141], the potential of galaxies, clusters of galaxies, and several other features of self-gravitating systems. Likely, such data will be capable of confirming or ruling out as physically inconsistent General Relativity or Extended Theories of Gravity.

2.3 General Relativity and its extensions

A good relativistic theory of gravity, first of all, must justify a lot of astronomical observations such as mapping the orbits of planets and the potential well of self-gravitating structures such as galaxies and clusters. Then, a good theory, in weak-field slow-motion limit, must reproduce the Newtonian dynamics. Moreover, at the Post-Newtonian level, the theory must pass the classical Solar System tests [124]. At the galactic level, the theory should reproduce correctly the observed galactic dynamics taking into account the well-known baryonic constituents of the matter as stars, planets, dust, gas and radiation in order to reproduce the Newtonian potential extrapolated to galactic scales. Then, the theory must provide a consistent description the problem of the generation of large scale structures (galaxy clusters, superclusters, etc). Finally, the cosmological dynamics must be reproduced: i.e. reproduce cosmological observables such as Hubble parameter H_0 , the deceleration parameter q_0, the density parameters, etc.

Einstein's theory satisfies [142], in a certain way, the various requirements set forth above. This theory describes the structure of the universe as a cosmic network where space and time intertwine forming a single space-time structure where, in the limit of zero gravity, he recovers Minkowski's flat space-time. Using Riemann ideas, i.e. that the universe is a curved manifold and that its curvature must be measured by means of astronomical observations [143], Einstein hypothesized that the matter distribution determines, point by point, the local curvature of this spacetime manifold and, its formulation, assumes three hypothesis on gravity:

1. *The Principle of Relativity*: all observers are equally valid for describing physics. Then, inertial frames are not *a priori* preferred.

2. *The Equivalence Principle*: acceleration effects to be locally indistinguishable from gravitational effects (i.e. the equivalence between inertial and gravitational mass).

3. *The Principle of General Covariance*: the field equations be "generally covariant" tensor equations whose form is the same in all coordinate systems, and states that all coordinate systems are in principle equivalent in the description of physics [144].

Moreover, one imposes that causality is conserved (*Principle of Causality*, i.e., that each spacetime point should admit a notion of past, present, and future which is the same for all physical observers). It is generally felt that the notion of causality forbids the presence of closed timelike curves and time travel, although this belief is rather superficial (see [145] for a discussion and references). In any case, to enforce the absence of closed timelike curves it is necessary to impose restrictions on the matter distribution (*energy conditions*) [132; 146; 147].

Einstein, in his theory, had to recover the Newtonian gravitation in the low speed limit and in the weak field limit where space and time are absolute entities. Then, particles are required to move, in a preferred inertial frame, along curved trajectories, the curvature of which (i.e. the acceleration) was a function of the strength of the sources through the "forces". Therefore, Einstein postulated that gravitational forces should be described by the curvature of a metric tensor field g_{ij} related to the line element:

$$ds^2 = g_{ij}dx^i dx^j, \tag{2.1}$$

and that the curvature is locally determined by the distribution of the sources. He also postulated that spacetime curves onto itself and that its curvature is locally determined by the distribution of the sources described by the four-dimensional generalization of the matter stress-energy tensor Σ_{ij} (a rank-two symmetric tensor) of continuum mechanics. Once a metric g_{ij} is given, its curvature is expressed by the Riemann curvature tensor:

$$R_{ijh}{}^{k} = \partial_j \Gamma^k_{ih} - \partial_i \Gamma^k_{jh} + \Gamma^l_{ij}\Gamma^k_{lh} - \Gamma^l_{hj}\Gamma^k_{li}, \tag{2.2}$$

where the Γ^h_{ij} are the Christoffel symbols associated with the metric g_{ij}, while the Ricci tensor its contraction:

$$R_{ijh}{}^{j} = R_{ij}, \tag{2.3}$$

while, with another contraction obtain the Ricci or curvature scalar of g_{ij}:

$$R = R^h_h = g^{hk}R_{hk}. \tag{2.4}$$

Considering the matter distribution like a perfect fluid, the stress-energy ten-

sor is:

$$\Sigma_{ij} = (\rho + p)u_i u_j - p g_{ij}, \tag{2.5}$$

where u^i is the 4-velocity of the fluid particles and p and ρ are the pressure and energy density of the fluid, respectively. The stress-tensor energy Σ_{ij} must satisfy the conservation law:

$$\nabla^i \Sigma_{ij} = 0 \tag{2.6}$$

where ∇_i is the covariant derivative operator of the metric g_{ij}. The continuity equation requires Σ_{ij} to be covariantly constant.

Then, the field equations are (in order to $G = 1 = c$):

$$G_{ij} = 8\pi \Sigma_{ij}, \tag{2.7}$$

where

$$G_{ij} = R_{ij} - \frac{1}{2} g_{ij} R, \tag{2.8}$$

is the Einstein tensor of g_{ij}. These equations can be derived by minimizing an action and satisfy the conservation law (2.6) since the relation

$$\nabla^i G_{ij} = 0 \tag{2.9}$$

holds as a contraction of the Bianchi identities that the curvature tensor of g_{ij} has to satisfy [81].

The Lagrangian that, when varied, produces the field equations (2.7) is the sum of a "matter" Lagrangian density $\mathcal{L}_m$ the variational derivative of which is:

$$\Sigma_{ij} = \frac{-2}{\sqrt{-g}} \frac{\delta \left(\sqrt{-g}\mathcal{L}_m\right)}{\delta g^{ij}}, \tag{2.10}$$

and of the gravitational *(Hilbert-Einstein) Lagrangian*

$$\sqrt{-g}\mathcal{L}_{HE} = \sqrt{-g}R, \tag{2.11}$$

where g is the determinant of g_{ij}.

In literature it has been shown that curvature is not a purely metric notion but is also related to the linear connection defining parallel transport and covariant differentiation [148] and that the three principles of relativity, equivalence, and covariance, together with causality, require only that the spacetime structure be determined by either one or both of two fields, a Lorentzian metric g_{ij} and a linear connection Γ^h_{ij}. The metric g_{ij} fixes the causal structure of spacetime (the light cones) as well as its metric relations measured by clocks and rods and the lengths of four-vectors. The connection Γ^h_{ij} determines the laws of free fall, the four-dimensional spacetime trajectories followed by locally inertial observers.

On the basis of all this, it is possible, therefore, to obtain a class of new gravitational theories, called Extended Theories, because their basic assumptions are the same as those used by Einstein and Hilbert in the General Relativity formulation. These are theories in which gravitation is described by either a metric (*purely metric theories*), or by a linear connection (*purely affine theories*), or by both fields (*metric-affine theories*). In these theories, the Lagrangian is a scalar density of the curvature invariants constructed out of both g_{ij} and Γ^h_{ij}.

From recent astrophysical observations and from cosmological investigations, is legitimate to doubt the paradigmatic role played by the Einstein equations at various scales or to bypass the problem by assuming that the stress-energy tensor contains matter constituents of exotic nature, namely the dark matter and the dark energy of our universe. The extended theories, instead, allows us to take a different path, i.e. modify the geometry of the universe because is a priori simpler and more convenient to change the geometric/gravitational sector of these

equations by inserting non-linear corrections to the Lagrangian. In principle, the action belongs to a vast class of possible actions and, phenomenologically, this freedom allows it to be chosen on the basis of its best-fit with the available observational data at all astrophysical and cosmological scales. The fundamental problem of these theories comes from the fact that there are too many models that fit well the observations. This depends on the fact that there are a very large number of free functions and parameters so, consequently, there is a high risk of losing predictive efficiency. From the theoretical point of view, it makes perfect sense to give serious consideration to rather well-motivated non-linear theories of gravity based on non-singular Lagrangians. Instead, the ΛCDM model is accompanied by exotic matter completely different from the known baryons, never detected in our laboratories, and segregated at astrophysical scales.

2.4 Mach's principle and other fundamental issues

Extended theories are originally developed to better understand the concept of inertia, the most peculiar property of mass and today are used to answer unresolved questions of standard cosmology in order to explain the large-scale distribution of matter observed in the universe especially when trying to understand what is the dark matter problem. This motivation allow us to discuss some of the older features of extended theories where, for example, the scalar-tensor theory contained a new important feature, the variability of the gravitational "constant".

When Einstein formulated his theory in 1916, the technological shortcomings of the period did not allow it to be tested efficiently. With the development of new technologies, around the 60s, this theory began to have a new interest thanks above all to some astronomical discoveries that indicated in the relativistic

theory of gravity an important role in astrophysics and in cosmology. Moreover, a more advanced instrumentation in the laboratory, has allowed to have some more precise tests.

Compared to a slower experimental progress, the theoretical research in General Relativity continued more quickly, obtaining good results that allowed to understand some crucial aspects of Einstein's theory such as, for example, the Kerr-Newman metric, the thermodynamics of black holes and the discovery of the singularity theorem. In addition to this, new theories were formulated as Brans-Dicke theory, i.e. the scalar-tensor theory in 1961 [85]. The main motivations driving the formulation of alternative theories were, mainly, the attempt to obtain a quantum theory of gravity and the introduction and development of inflationary scenarios.

2.4.1 Mach's principle and the variation of G

The problem of Mach's principle states that the local inertial frame is determined by some average motion of distant astronomical objects [84; 87]. This principle was incorporated into a metric theory, the scalar-tensor theory, by constructing an alternative theory to that of Einstein [85]. Taking into account the influence that the total matter has at each point (constructing the "inertia"), was introduced, together with the standard metric tensor, a new scalar field of gravitational origin as the effective gravitational coupling where the gravitational "constant" is a function of the total mass distribution and of the scalar field, and is variable. Then, gravity is described by the Lagrangian density

$$\sqrt{-g}\mathcal{L}_{BD} = \sqrt{-g}\left[\phi R - \frac{\omega}{\phi}\nabla^i\phi\nabla_i\phi + \mathcal{L}_m\right], \tag{2.12}$$

where ω is the dimensionless Brans-Dicke parameter and $\mathcal{L}_m$ is the matter Lagrangian including all the non-gravitational fields. Furthermore, there are two different groups called conformal transformations, i.e. Weyl transformations, which allow a local rescaling of the metric tensor. Extended theories can be conformally transformed in an Einstein theory with one or more scalar fields. Like in the context of higher order gravity, as emphasized by Dicke [149], the Lagrangian (2.12), under the conformal transformations

$$g_{ij} \to \tilde{g}_{ij} = \Omega^2 g_{ij}, \qquad \Omega^2 = G_0\varphi, \tag{2.13}$$

become:

$$\sqrt{-g}\mathcal{L} = \sqrt{-\tilde{g}}\left(\tilde{R} + G_0\tilde{\mathcal{L}}_m + G_0\tilde{\mathcal{L}}_\Omega\right), \tag{2.14}$$

where

$$\tilde{\mathcal{L}}_\Omega = -\frac{(2\omega+3)}{4\pi G_0\Omega}\nabla^h(\sqrt{\Omega})\nabla_h(\sqrt{\Omega}), \tag{2.15}$$

and $\tilde{\mathcal{L}}_m$ is the conformally transformed Lagrangian density of matter where the total matter Lagrangian density $\tilde{\mathcal{L}}_{tot} = \tilde{\mathcal{L}}_m + \tilde{\mathcal{L}}_\Omega$ has been introduced. The field equations are now written in the form of Einstein-like equations as

$$\tilde{G}_{ij} = G_0\tilde{\tau}_{ij}, \tag{2.16}$$

where

$$\tilde{G}_{ij} = \tilde{R}_{ij} - \frac{1}{2}\tilde{g}_{ij}\tilde{R}, \qquad \tilde{\tau}_{ij} = \Sigma_{ij} + \Lambda_{ij}(\Omega), \tag{2.17}$$

are the Einstein and the stress-tensor energy under conformal transformations (2.13), while $\Lambda_{ij}(\Omega)$ is the curvature term. Therefore, "any" equation linear in Ricci can be recast in Einstein form including the ones in Jordan frame.

This new (tilded, or Einstein frame) form of the scalar-tensor theory has certain advantages over the theory non-tilded, or Jordan frame form; the Einstein

frame representation, being similar to the Einstein standard description, is familiar and easier to handle in some aspects as, for instance, for simulating dynamical space-time scenarios. But, in this new form, Brans-Dicke theory also shows problems. In fact, if we consider the motion of a spinless, electrically neutral, massive particle, its trajectory is no longer a geodesic in the conformally rescaled world. Only null rays are left unchanged because the rest mass is not constant in the conformally transformed world and the equation of motion of massive particles is modified by the addition of an extra force proportional to $\nabla^i\Omega$ [149]. Photon trajectories, on the other hand, are not modified because the vanishing of the photon mass implies the absence of a preferred physical scale and photons stay massless under the conformal rescaling, therefore their trajectories are unaffected.

This new approach is of particular interest in cosmology, since they have the potential to bypass many lacks of the standard cosmological model. These theories exhibit a non-constant gravitational coupling. The Newton constant G_N is replaced by the effective gravitational coupling

$$G_{eff} = \frac{1}{f(\phi)}. \tag{2.18}$$

In particular, in spatially homogeneous and isotropic cosmology, the coupling (2.18) can only be a function of the epoch, *i.e.*, of the cosmological era.

The variation of G_{eff} implies that local gravitational physics depends on the scalar field via ϕ. Therefore, we have then motivated the introduction of a stronger version of the Equivalence Principle, the *Strong Equivalence Principle*. These theories, with such a particular aspect, are called *Non-Minimally Coupled theories*.

In these theories, concerning standard matter, everything goes as in General Relativity *(i.e., $\eta_{ij} \to g_{ij}$, $\partial_i \to \nabla_i$)* following the minimal coupling prescription, but now there is a direct coupling between the scalar degree of freedom and a

function of the tensor degree of freedom (the metric) and its derivatives. Then, from the cosmological point of view, we are presented with two possibilities. The first is

$$\lim_{t\to\infty} G_{eff}(\phi(t)) = G_N, \tag{2.19}$$

where standard cosmology is recovered at the present time in the history of the universe. The second possibility occurs if the gravitational coupling is not constant today, i.e., G_{eff} is still varying with the epoch and $\frac{\dot{G}_{eff}}{G_{eff}}$ is non-vanishing.

Finally, in many theories of gravity, then, it is perfectly conceivable that G_{eff} varies with time: in some solutions G_{eff} does not even converge to the value observed today. In fact, for example, to analyze the variability of G_{eff}, its possible to use *lunar laser ranging* that monitoring the Earth-Moon distance, or obtain information from solar astronomy and, finally use data from binary pulsars. In [150; 151], the ratio $\frac{\dot{G}_{eff}}{G_{eff}}$ was measured obtaining a very small quantity.

2.4.2 Non-minimally coupled theories and the Equivalence Principle

In order to formulate a non-minimal coupling theory, we must to discuss definitely of the *Equivalence Principle* [124]. The first step is the equivalence between inertial and gravitational mass found already in Galilei's experiments and in Newton's work, which implies that all uncharged bodies fall with the same acceleration independent of their mass and internal structure, in a given gravitational field. This statement is called *Weak Equivalence Principle*:

"If an uncharged body is placed at an initial event in spacetime and given an initial velocity there, then its subsequent trajectory will be independent of its internal structure and composition"[124].

In his formulation, Einstein, using as an example the famous freely falling

elevator, said that not only the laws of mechanics behave in it as if gravity were absent, but all physical laws (except those of gravitational physics) have the same behavior. Following current terminology, we refer to this principle as the Einstein Equivalence Principle:

"the outcome of any local non-gravitational test experiment is independent of the velocity of the (free falling) apparatus and the outcome of any local non-gravitational test experiment is independent of where and when in the universe it is performed" [124].

A "local non-gravitational experiment" is defined as an experiment performed in a small size freely falling laboratory, in order to avoid the inhomogeneities of the external gravitational field, and in which any gravitational self-interaction can be ignored.

Therefore, the gravitational interaction must be described in terms of a curved spacetime, that is, the postulates of the so-called metric theories of gravity have to be satisfied [124]

1. Spacetime is described with a metric g_{ij};
2. The world lines of test particles are geodesics of that metric;
3. In local freely falling frames, i.e. *local Lorentz frames*, the non-gravitational laws of physics are those of Special Relativity.

Obviously, point 3 refers to non-gravitational physical laws. Both General Relativity and Brans-Dicke-like theories are metric-theories. However, in the extended theories context, these definitions meant to characterize the Equivalence Principle, and the physical properties discriminating between General Relativity and other metric theories of gravity turn out to depend on the conformal representation of the theory adopted. More precisely, in scalar-tensor gravity, massive test particles follow geodesics in the Jordan frame, satisfying the *Weak Equivalence*

Principle, but the same particles deviate from geodesic motion in the Einstein frame. This difference shows that the Equivalence Principle is formulated in a representation-dependent way [152] and to this day it has not yet been solved.

At this point, it is reasonable to ask which extended theories satisfy the *Einstein Equivalence Principle* given that the non-minimal coupling prescriptions given in our previous discussion are connected precisely with the mathematical formulation of the *Einstein Equivalence Principle*. In order to address this question we must introduce new concepts and generalize the two principles reported above. In [124], where the equivalence between inertial and gravitational masses is strongly confirmed, introduces the notion of "purely dynamical metric theory"; i.e. "the behaviour of each field is influenced to some extent by a coupling to at least one of the other fields in the theory" [124].

Let us consider then an experimental situation such as the Einstein freely falling elevator. We require that the frame used be sufficiently large to include a gravitational system. When calculating the metric, we have to assign boundary conditions "Far" from the local system, then solve the equations for the fields generated by the local system. Since the metric couples to the other fields, then it will be influenced from this fields, i.e. the metric will be related to the boundary values assumed "far away" by these fields. But local non-gravitational experiments are unaffected by such a behavior because they couple only with the metric which is locally Minkowskian. Of course, in a purely metric theory the only field coupling the local system with the environment is the metric tensor and it is always possible to find a Minkowskian coordinate system at the boundary between the local system and the external world. In this way the asymptotic behavior of the metric is Lorentz invariant, i.e., independent of the velocity and flat, i.e., independent of the location. The status of Brans-Dicke-like theories is different: in this case it is still possible to choose an asymptotically Minkowskian

(Lorentz-invariant) metric which is independent of the velocity and of the scalar field(s), but now the asymptotic value of these scalar(s) can give rise to a dependence on the location of the laboratory. An example of this situation is given by Brans-Dicke-like theories in which the gravitational coupling "constant" actually depends on the asymptotic value assumed by the scalar field.

All these considerations can be summarized in the *Strong Equivalence Principle*:

1. *"Weak Equivalence Principle is valid for self-gravitating bodies as well for test bodies*;

2. *The outcome of any local test experiment is independent of the velocity of the (freely falling) apparatus*;

3. *The outcome of any local test experiment is independent on where and when in the universe it is performed"* [124].

The *Strong Equivalence Principle* differs from the *Einstein Equivalence Principle* because of the inclusion of bodies with self-gravitating interactions, such as planets or stars, and because of experiments involving gravitational forces. If gravitational forces are ignored, the *Strong Equivalence Principle* reduces to the *Einstein Equivalence Principle*.

2.4.3 Higher order corrections to General Relativity

This type of approach is necessary when quantization is performed on a curved space-time and is directed at the problem of renormalization [88]. This class of theories is also present in the studies of inflation in the early universe [93]. The scalar-tensor theories, on the other hand, have had a growing interest because they could provide a fairly coherent description of the inflationary paradigm in

cosmology because the inflation provides very reasonable answers to the puzzles of Standard Big Bang cosmology as well as providing a physical mechanism for the generation of large scale structures in the universe.

Now we will see how we will try to connect a higher order and the scalar-tensor gravities. We begin with the particular case of fourth order theories described by the Lagrangian density:

$$\sqrt{-g}\mathcal{L} = \sqrt{-g}f(R), \tag{2.20}$$

where, in this case, the Lagrangian is a generic function of Ricci scalar. The variation of this Lagrangian with respect to g^{ij} give the 4th-order field equations

$$f'(R)R_{ij} - \frac{1}{2}f(R)g_{ij} - (\nabla_i\nabla_j - g_{ij}\Box)f'(R) = 0, \tag{2.21}$$

with $f'(R) = \frac{df(R)}{dR}$. The formal equivalence between models with variable gravitational coupling and Einstein gravity via conformal transformations has also been known for a long time [149; 153]. This has given rise to a debate, still continuing, on whether the mathematical equivalence between different conformal representations of the theory (called Jordan and Einstein conformal frames) is also a physical equivalence [154]. Taking this into account, the new set of variables

$$q = f'(R) = f'(g_{ij}, \partial_h g_{ij}, \partial_h\partial_k g_{ij}), \qquad \tilde{g}_{ij} = qg_{ij}, \tag{2.22}$$

links the *Jordan frame* variable g_{ij} to the *Einstein frame* variables (q, g_{ij}) where q is positive. In the vacuum, the Einstein frame equations are

$$\tilde{G}_{ij} = \frac{1}{2q^2}\left[3\partial_i q\partial_j q - \frac{3}{2}\tilde{g}_{ij}\tilde{g}^{hk}\partial_h q\partial_k q + \tilde{g}_{ij}(f(R) - Rq)\right]. \tag{2.23}$$

It is possible to rewrite the (2.23) as:

$$\tilde{G}_{ij} = (\nabla_i \nabla_j - \frac{1}{2}\tilde{g}_{ij}\nabla_h \nabla^h)\varphi - \tilde{g}_{ij}V(\varphi), \tag{2.24}$$

where

$$\varphi = \sqrt{3/2} lnq, \qquad V(\varphi) = \frac{Rf'(R) - f(R)}{2f'^2(R)}, \qquad R = R(q(\varphi)). \tag{2.25}$$

The (2.24) can be obtained from the Lagrangian written in terms of φ, where the sign of φ can be negative, and the tilded geometrical quantities

$$\sqrt{-g}\mathcal{L} = \sqrt{-\tilde{g}}\left[\frac{\tilde{R}}{2} - \frac{1}{2}\tilde{g}^{ij}\nabla_i\varphi\nabla_j\varphi - V(\varphi)\right], \tag{2.26}$$

which has the same form as that of Einstein gravity coupled to a self-interacting non-minimally coupled scalar field. So far we have seen how to go from the Jordan to the Einstein frame but, in principle, it is possible to do the reverse path, i.e., beginning with the Einstein frame, is in principle possible to go to a Jordan-type Lagrangian and when standard matter is present in these models, it is important to look at its dynamics. For example, the photon worldlines are geodesics in the Jordan frame as well as in the Einstein frame, but the case of massive particles is different: their Jordan frame geodesics are no longer transformed into Einstein frame geodesics, and *vice-versa*. In this regard, the two frames are not equivalent [129].

We conclude noticing that: in this chapter we have seen how it seems reasonable to extend General Relativity to more general schemes because in this way it is possible to explain several theoretical and observational facts where cosmology is a field which has seen many fruitful applications of these generalizations of Einstein gravity. Nowadays, we have not yet reached any definitive conclusion on

what is the "correct" theory of gravity but here we identify the search for "the theory of gravity" as a urgent problem of theoretical and experimental physics. The theories developed thus far, and those currently under development, are useful at least as toy models to learn how gravity could be different from Einstein's theory and to get a glimpse of the difficulties and phenomena one could expect in a more advanced theory.

Chapter 3

Scenarios beyond Einstein gravity

Summary

In this chapter we will discuss the two main class of the *Extended Theories of Gravity*, i.e. *scalar-tensor* and $f(R)$ gravity. We will see the action and field equations of *Brans-Dicke* theory and, more generally, the *scalar-tensor* theories and the action and field equations of metric $f(R)$ gravity general. The $f(R)$ gravity is described from classes of Lagrangians written as a generic function of Ricci scalar and includes higher order corrective terms in curvature invariants. Scalar-tensor gravity include a scalar field as an extra field mediating the gravitational interaction. We present the derivation of the field equations through the application of a variational principle and analyse the basic characteristics of the theories. As is the case for General Relativity, these theories are best expressed using actions and variational principles for the degrees of freedom that they contain [155].

3.1 The field equations of Brans-Dicke gravity

The Brans-Dicke theory of gravity [85; 156; 157; 158] is the prototype of gravitational theories alternative to General Relativity. The action in the Jordan frame (the set of variables (g_{ij}, ϕ)) is (for $G = 1 = c$)

$$\mathcal{A}_{(BD)} = \frac{1}{16\pi} \int d^4x \sqrt{-g} \left[\phi R - \frac{\omega}{\phi} g^{ij} \nabla_i \phi \nabla_j \phi - V(\phi) \right] + A_m \,, \tag{3.1}$$

where

$$\mathcal{A}_m = \int d^4x \sqrt{-g} \, \mathcal{L}_m, \tag{3.2}$$

is the action of ordinary matter and ω is the dimensionless Brans-Dicke parameter. The factor ϕ in the denominator of the kinetic term of ϕ in the action (3.1) is purely conventional and has the only purpose of making ω dimensionless. Matter does not couple directly to ϕ, *i.e.*, the Lagrangian density $\mathcal{L}_m$ is independent of ϕ. However, ϕ couples directly to the Ricci scalar. The gravitational field is described by both the metric tensor g_{ij} and the Brans-Dicke scalar ϕ which, together with the matter variables, constitute the degrees of freedom of the theory. The potential $V(\phi)$ generalizes the cosmological constant and may reduce to a constant, or to a mass term.[1].

As mentioned in chapter 2, the original motivation for introducing Brans-Dicke theory was the implementation of Mach's Principle. This is achieved in Brans-Dicke theory by making the effective gravitational coupling strength $G_{eff} \sim \phi^{-1}$ depend on the space-time position and being governed by distant matter sources, as in Eq. (3.9) below. The variation of the action (3.1) with

[1]Due to the particular equation (3.9) satisfied by the Brans-Dicke field ϕ, its mass is not the coefficient of the quadratic term in the expansion of $V(\phi)$, as for minimally coupled scalar fields, but rather the quantity m defined by $m^2 = \frac{1}{2\omega + 3} \left(\phi \frac{d^2V}{d\phi^2} - \frac{dV}{d\phi} \right)$ [159]

respect to g^{ij} and the well known properties [160]

$$\delta\left(\sqrt{-g}\right) = -\frac{1}{2}\sqrt{-g}\, g_{ij}\, \delta g^{ij}\,, \tag{3.3}$$

$$\delta\left(\sqrt{-g}\, R\right) = \sqrt{-g}\left(R_{ij} - \frac{1}{2}\, g_{ij} R\right) \delta g^{ij} \equiv \sqrt{-g}\, G_{ij}\, \delta g^{ij}\,, \tag{3.4}$$

yield the field equation

$$G_{ij} = \frac{1}{\phi}\left[8\pi\, \Sigma_{ij} + \frac{\omega}{\phi}\left(\nabla_i\, \nabla_j - \frac{1}{2} g_{ij} \nabla^h \nabla_h\right) \phi + \left(\nabla_i \nabla_j - g_{ij}\, \Box\right) \phi - \frac{V}{2}\, g_{ij}\right] \tag{3.5}$$

where

$$\Sigma_{ij} \equiv \frac{-2}{\sqrt{-g}}\, \frac{\delta}{\delta g^{ij}} \left(\sqrt{-g}\, \mathcal{L}_m\right), \tag{3.6}$$

is the energy-momentum tensor of ordinary matter. By varying the action with respect to ϕ, one obtains

$$\frac{2\omega}{\phi}\, \Box\phi + R - \frac{\omega}{\phi^2}\, \nabla^h \phi \nabla_h \phi - \frac{dV}{d\phi} = 0\,. \tag{3.7}$$

Taking now the trace of Eq. (3.5),

$$R = \frac{-8\pi\, \Sigma}{\phi} + \frac{\omega}{\phi^2}\, \nabla^h \phi \nabla_h \phi + \frac{3\Box\phi}{\phi} + \frac{2V}{\phi}\,, \tag{3.8}$$

and using the resulting Eq. (3.8) to eliminate R from Eq. (3.7) leads to

$$\Box\phi = \frac{1}{2\omega + 3}\left(8\pi\, \Sigma + \phi\, \frac{dV}{d\phi} - 2V\right). \tag{3.9}$$

Therefore, the scalar ϕ is sourced by non-conformal matter (*i.e.*, by matter with trace $\Sigma \neq 0$), however the scalar does not couple directly to $\mathcal{L}_m$: the Brans-Dicke

scalar ϕ reacts on ordinary matter only indirectly through the metric tensor g_{ij}, as dictated by Eq. (3.5). The term proportional to $\phi\, dV/d\phi - 2V$ on the right hand side of Eq. (3.9) vanishes if the potential has the form $V(\phi) = m^2\phi^2/2$ familiar from the Klein-Gordon equation and from particle physics. The (3.1) and the (3.5) suggest that the field ϕ be identified with the inverse of the effective gravitational coupling

$$G_{eff}\,(\phi) = \frac{1}{\phi}\,, \tag{3.10}$$

a function of the space-time location. In order to guarantee a positive gravitational coupling, only the range of values $\phi > 0$ corresponding to attractive gravity is considered. The dimensionless Brans-Dicke parameter ω is a free parameter of the theory: a value of ω of order unity would be natural in principle. However, values of ω of this order of magnitude are excluded by Solar System experiments, for a massless or light field ϕ (*i.e.*, one that has a range larger than the size of the Solar System).

The larger the value of ω, the closer Brans-Dicke gravity is to GR [81]; there are, however, exceptions such as vacuum Brans-Dicke solutions, and solutions sourced by conformal matter [161; 162; 163; 164; 165; 166; 167; 168; 169; 170]. The most stringent experimental limit, $\omega > 40,000$, was set by the Cassini probe in 2003 [171].

Brans-Dicke theory with a free or light scalar field is viable in the limit of large ω, but the large value of this parameter required to satisfy the experimental bounds is certainly fine-tuned and makes Brans-Dicke theory unappealing. However, this fine-tuning becomes unnecessary if the scalar field is given a sufficiently large mass and, therefore, a short range. This means that a self-interaction potential $V(\phi)$ has to be considered in discussing the limits on ω adjusting the original Brans-Dicke theory [85].

The Brans-Dicke theory or, more generally, scalar-tensor theories, are non-

minimally coupled theories, which are very useful for problems on a cosmological scale. In fact, the problem of accelerated expansion of the universe, called dark energy, has not yet been solved. Without requiring any dark component or considering non-baryonic matter that has not yet been found, in the following chapters we will see how, for some cosmological models, the dark energy component is modeled as a non-minimally coupled fermionic condensate with the gravitational field. We will compare the theoretical predictions with the observations and, then, with the analysis of the phase space, we will deduce the characteristics of the entire cosmic history of the considered models.

3.2 The field equations of metric $f(R)$-gravity

We now examine the variational principle and the field equations of another class of Extended Theories of Gravity, $f(R)$-gravity in the metric formalism. The salient feature of these theories is that the field equations are, "generilcally", of fourth order and, therefore, more complicated than those of General Relativity (which is recovered as the special case $f(R) = R$). Due to their higher order, these field equations admit a much richer variety of solutions than the Einstein equations. We discuss now a generic analytical function $f(R)$ in the metric formalism, beginning with the vacuum case, as described by the Lagrangian density

$$\sqrt{-g}\,\mathcal{L} = \sqrt{-g}\,f(R), \tag{3.11}$$

obeying the variational principle

$$\delta \int d^4x \sqrt{-g}\,f(R) = 0. \tag{3.12}$$

We have

$$\delta \int d^4x\sqrt{-g}\, f(R) = \int d^4x \left[\delta\left(\sqrt{-g}\, f(R)\right) + \sqrt{-g}\,\delta\left(f(R)\right)\right]$$

$$= \int d^4x\sqrt{-g}\left[f'(R)R_{ij} - \tfrac{1}{2}g_{ij}f(R)\right]\delta g^{ij} + \int d^4x\sqrt{-g}\, f'(R)g^{ij}\delta R_{ij}\,, \tag{3.13}$$

where the prime denotes differentiation with respect to R. We now compute these integrals in the local inertial frame. By using

$$g^{ij}\delta R_{ij} = g^{ij}\partial_h\left(\delta G^h_{ij}\right) - g^{ih}\partial_h\left(\delta G^j_{ij}\right) \equiv \partial_h W^h \tag{3.14}$$

where

$$W^h \equiv g^{ij}\delta G^h_{ij} - g^{ih}\delta G^j_{ij}\,, \tag{3.15}$$

the second integral in Eq. (3.13) can be written as

$$\int d^4x\sqrt{-g}\, f'(R)g^{ij}\delta R_{ij} = \int d^4x\sqrt{-g}\, f'(R)\partial_h W^h\,. \tag{3.16}$$

Integration by parts yields

$$\begin{aligned}\int d^4x\sqrt{-g}\, f'(R)g^{ij}\delta R_{ij} = \quad & \int d^4x\partial_h\left[\sqrt{-g}\, f'(R)W^h\right] - \\ & \int d^4x\partial_h\left[\sqrt{-g}f'(R)\right]W^h\,.\end{aligned} \tag{3.17}$$

The first integrand is a total divergence and can be discarded by assuming that the fields vanish at infinity, obtaining

$$\int d^4x\sqrt{-g}\, f'(R) g^{ij}\delta R_{ij} = -\int d^4x \partial_h \left[\sqrt{-g}\, f'(R)\right] W^h \,. \tag{3.18}$$

Let us calculate now the term W^h appearing in Eq. (3.18). We have

$$\begin{aligned} \delta G^h_{ij} = \quad & \delta\left[\frac{1}{2} g^{hk}\left(\partial_i g_{kj} + \partial_j g_{ik} - \partial_k g_{ij}\right)\right] = \\ & \frac{1}{2} g^{hk}\left[\partial_i\left(\delta g_{kj}\right) + \partial_j\left(\delta g_{ik}\right) - \partial_k\left(\delta g_{ij}\right)\right], \end{aligned} \tag{3.19}$$

since in the locally inertial frame considered here it is

$$\partial_k g_{ij} = \nabla_k g_{ij} = 0 \,. \tag{3.20}$$

Similarly, it is

$$\delta G^j_{ij} = \frac{1}{2}\, g^{jk}\partial_i\left(\delta g_{jk}\right) \,. \tag{3.21}$$

By combining Eqs. (3.20) and (3.21), one obtains

$$g^{ij}\delta G^h_{ij} = \frac{1}{2}\,\partial^h\left(g_{ij}\delta g^{ij}\right) - \partial^i\left(g_{ki}\delta g^{jk}\right) \,, \tag{3.22}$$

$$g^{ih}\delta G^j_{ij} = -\frac{1}{2}\,\partial^h\left(g_{jk}\delta g^{jk}\right) \,, \tag{3.23}$$

from which it follows immediately that

$$W^h = \partial^h\left(g_{ij}\delta g^{ij}\right) - \partial^i\left(g_{ij}\delta g^{hj}\right) \,. \tag{3.24}$$

Using this equation one can write

$$\int d^4x\sqrt{-g}\, f'(R)g^{ij}\delta R_{ij} = \int d^4x\partial_h \left[\sqrt{-g}\, f'(R)\right] \left[\partial^i \left(g_{ij}\delta g^{hj}\right) - \partial^h \left(g_{ij}\delta g^{ij}\right)\right] \tag{3.25}$$

Integrating by parts and discarding total divergences, one obtains

$$\begin{aligned} \int d^4x\sqrt{-g}\, f'(R)g^{ij}\delta R_{ij} &= \int d^4x g_{ij}\partial^h\partial_h[\sqrt{-g}f'(R)]\delta g^{ij} \\ &- \int d^4x g_{ij}\partial^i\partial_h \left[\sqrt{-g}\, f'(R)\right] \delta g^{hj}\,. \end{aligned} \tag{3.26}$$

The variation of the action is then

$$\begin{aligned} \delta \int d^4x\sqrt{-g}\, f(R) &= \int d^4x\sqrt{-g}\left[f'(R)R_{ij} - \tfrac{1}{2}f(R)g_{ij}\right]\delta g^{ij} \\ &+ \int d^4x \left[g_{ij}\partial^h\partial_h \left(\sqrt{-g}\, f'(R)\right) - g_{hj}\partial^i\partial_h \left(\sqrt{-g}f'(R)\right)\right] \delta g^{ij}\,. \end{aligned} \tag{3.27}$$

The vanishing of the variation implies the fourth order vacuum field equations

$$f'(R)R_{ij} - \frac{f(R)}{2}\, g_{ij} = \nabla_i\nabla_j f'(R) - g_{ij}\Box f'(R)\,. \tag{3.28}$$

These equations can be re-arranged in the Einstein-like form

$$f'(R)R_{ij} - \frac{f'(R)}{2}\, g_{ij}R + \frac{f'(R)}{2}\, g_{ij}R - \frac{f(R)}{2}\, g_{ij} = \nabla_i\nabla_j f'(R) - g_{ij}\Box f'(R) \tag{3.29}$$

and then

$$G_{ij} = \frac{1}{f'(R)} \left\{\nabla_i\nabla_j f'(R) - g_{ij}\Box f'(R) + g_{ij}\frac{[f(R) - f'(R)R]}{2}\right\}. \tag{3.30}$$

The right hand side of Eq. (3.30) is then regarded as an effective stress-energy tensor, which we call *curvature fluid* energy-momentum tensor $\Sigma_{ij}^{(curv)}$ sourcing the effective Einstein equations. Although this interpretation is questionable in principle because the field equations describe a theory different from General Relativity, and one is forcing upon them the interpretation as effective Einstein equations, this approach is quite useful in practice.

3.3 Extended Theories with torsion

In this section, we want to face the problem to study $f(R)$-gravity considering also torsion. Torsion theories have been taken into account firstly by Cartan and then were introduced by Sciama and Kibble in order to deal with spin in General Relativity (see [172] for a review). Being the spin as fundamental as the mass of the particles, torsion was introduced in order to complete the following scheme: the mass (energy) as the source of curvature and the spin as the source of torsion.

Up to some time ago, torsion did not seem to produce models with observable effects since phenomena implying spin and gravity were considered to be significant only in the very early Universe.

In principle, torsion could be constrained at every astrophysical scale and, as recently discussed, data coming from Gravity Probe B could contribute to this goal also at Solar System level [173].

In above section, a systematic discussion of metric-affine $f(R)$-gravity has been pursued. Here, following the same philosophy, we want to show that, starting from a generic $f(R)$ theory, the curvature and the torsion can give rise to an effective curvature-torsion stress-energy tensor capable, in principle, to address the problem of the Dark Side of the Universe in a very general geometric scheme [174].

3.3.1 The field equations of $f(R)$ gravity with torsion

Let us discuss the main features of a $f(R)$-gravity considering the most general case in which torsion is present in a $\mathcal{U}_4$ manifold [1] [175]. In a metric-affine formulation, the metric g and the connection Γ can be, in general, considered independent fields. More precisely, the dynamical fields are pairs (g, Γ) consisting of a pseudo-Riemannian metric g and a metric compatible linear connection Γ on the space–time manifold M. The corresponding field equations are derived by varying separately with respect to the metric and the connection the action functional

$$\mathcal{A}(g, \Gamma) = \int \sqrt{-g} f(R)\, ds\,, \tag{3.31}$$

where f is a real function, $R = R(g, \Gamma) = g^{ij} R_{ij}$ (with $R_{ij} := R^h{}_{ihj}$) is the scalar curvature associated with the dynamical connection Γ and $ds := dx^1 \wedge \cdots \wedge dx^4$. We use the index notation

$$R^h{}_{kij} = \frac{\partial \Gamma_{jk}{}^h}{\partial x^i} - \frac{\partial \Gamma_{ik}{}^h}{\partial x^j} + \Gamma_{il}{}^h \Gamma_{jk}{}^l - \Gamma_{jl}{}^h \Gamma_{ik}{}^l\,, \tag{3.32}$$

for the curvature tensor and

$$\nabla_{\frac{\partial}{\partial x^i}} \frac{\partial}{\partial x^j} = \Gamma_{ij}{}^h \frac{\partial}{\partial x^h}\,, \tag{3.33}$$

for the connection coefficients. In order to evaluate the variation $\delta\mathcal{A}$ under arbitrary deformations of the connection, we recall that, given a metric tensor g_{ij}, every metric connection Γ may be expressed as

$$\Gamma_{ij}{}^h = \tilde{\Gamma}_{ij}{}^h - K_{ij}{}^h\,, \tag{3.34}$$

[1] We indicate with $\mathcal{V}_4$ a $4D$ pseudo-Riemaniann manifold without torsion and with $\mathcal{U}_4$ a $4D$ manifold with torsion.

where (in the holonomic basis $\left\{\frac{\partial}{\partial x^i}, dx^i\right\}$) $\tilde{\Gamma}_{ij}{}^{h}$ denote the coefficients of the Levi-Civita connection associated with the metric g_{ij}, while $K_{ij}{}^{h}$ indicate the components of a tensor satisfying the antisymmetry property $K_{i}{}^{jh} = -K_{i}{}^{hj}$. This last condition ensures the metric compatibility of the connection Γ. In view of this, we can identify the actual degrees of freedom of the theory with the (independent) components of the metric g and the tensor K. Moreover, it is easily seen that the curvature and the contracted curvature tensors associated with every connection (3.34) can be expressed respectively as

$$R^{h}{}_{imj} = \tilde{R}^{h}{}_{imj} + \tilde{\nabla}_j K_{mi}{}^{h} - \tilde{\nabla}_m K_{ji}{}^{h} + K_{ji}{}^{l} K_{ml}{}^{h} - K_{mi}{}^{l} K_{jl}{}^{h}\,, \tag{3.35a}$$

and

$$R_{ij} = R^{h}{}_{ihj} = \tilde{R}_{ij} + \tilde{\nabla}_j K_{hi}{}^{h} - \tilde{\nabla}_h K_{ji}{}^{h} + K_{ji}{}^{l} K_{hl}{}^{h} - K_{hi}{}^{l} K_{jl}{}^{h}\,, \tag{3.35b}$$

where $\tilde{R}^{h}{}_{imj}$ and $\tilde{R}_{ij} = \tilde{R}^{h}{}_{ihj}$ are respectively the Riemann and the Ricci tensors of the Levi–Civita connection $\tilde{\Gamma}$ associated with the given metric g, and $\tilde{\nabla}$ indicates the Levi-Civita covariant derivative.

Making use of the identities (3.35b), the action functional (3.31) can be written in the equivalent form

$$\mathcal{A}(g,\Gamma) = \int \sqrt{-g} f [g^{ij}(\tilde{R}_{ij} + \tilde{\nabla}_j K_{hi}{}^{h} - \tilde{\nabla}_h K_{ij}{}^{h} + K_{ji}{}^{l} K_{hl}{}^{h} - K_{hi}{}^{l} K_{jl}{}^{h})]\, ds\,, \tag{3.36}$$

more suitable for variations in the connection. Taking the metric g fixed, we have

the identifications $\delta\Gamma_{ij}{}^{h} = \delta K_{ij}{}^{h}$ and then the variation

$$\begin{aligned}\delta\mathcal{A} = \quad & \int \sqrt{-g} f'(R) g^{ij} (\tilde{\nabla}_j \delta K_{hi}{}^{h} - \tilde{\nabla}_h \delta K_{ji}{}^{h} + \delta K_{ji}{}^{l} K_{hl}{}^{h} + K_{ji}{}^{l} \delta K_{hl}{}^{h}) ds + \\ & \int \sqrt{-g} f'(R) g^{ij} (-\delta K_{hi}{}^{l} K_{jl}{}^{h} - K_{hi}{}^{l} \delta K_{jl}{}^{h}) ds \,.\end{aligned} \tag{3.37}$$

Using the divergence theorem, taking the antisymmetry properties of K into account and renaming finally some indexes, we get the expression

$$\delta\mathcal{A} = \int \sqrt{-g} \left[-\frac{\partial f'}{\partial x^i} \delta^h_j + \frac{\partial f'}{\partial x^j} \delta^h_i + f' (K_{lj}{}^{l} \delta^h_i - K_{li}{}^{l} \delta^h_j - K_{ij}{}^{h} + K_{ji}{}^{h}) \right] \delta K_h{}^{ij} \, ds \,. \tag{3.38}$$

The requirement $\delta\mathcal{A} = 0$ yields therefore a first set of field equations given by

$$K_{lj}{}^{l} \delta^h_i - K_{li}{}^{l} \delta^h_j - K_{ij}{}^{h} + K_{ji}{}^{h} = \frac{1}{f'} \frac{\partial f'}{\partial x^l} \left(\delta^l_i \delta^h_j - \delta^l_j \delta^h_i \right) , \tag{3.39}$$

where $\mathcal{L}_m$ is independent of K. Considering that the torsion coefficients of the connection Γ are $T_{ij}{}^{h} := \Gamma_{ij}{}^{h} - \Gamma_{ji}{}^{h} = -K_{ij}{}^{h} + K_{ji}{}^{h}$ and thus (due to antisymmetry) $T_{li}{}^{l} = -K_{li}{}^{l}$, eqs. (3.39) can be rewritten as

$$T_{ij}{}^{h} + T_{jl}{}^{l} \delta^h_i - T_{il}{}^{l} \delta^h_j = \frac{1}{f'} \frac{\partial f'}{\partial x^l} \left(\delta^l_i \delta^h_j - \delta^l_j \delta^h_i \right) , \tag{3.40}$$

or, equivalently, as

$$T_{ij}{}^{h} = -\frac{1}{2f'} \frac{\partial f'}{\partial x^l} \left(\delta^l_i \delta^h_j - \delta^l_j \delta^h_i \right) , \tag{3.41}$$

because $T_{jl}{}^{l} \delta^h_i - T_{il}{}^{l} \delta^h_j = \frac{3}{2f'} \frac{\partial f'}{\partial x^l} \left(\delta^l_i \delta^h_j - \delta^l_j \delta^h_i \right)$.

In order to study the variation $\delta\mathcal{A}$ under arbitrary deformations of the metric, it is convenient to resort to the representation (3.31). Indeed, from the latter, we

have directly

$$\delta\mathcal{A} = \int \sqrt{-g}\left[f'(R)R_{ij} - \frac{1}{2}f(R)g_{ij}\right]\delta g^{ij}\,ds\,, \tag{3.42}$$

thus getting the second set of field equations

$$f'(R)R_{(ij)} - \frac{1}{2}f(R)g_{ij} = 0\,. \tag{3.43}$$

Of course, one can obtain the same equations (3.43) starting from the representation (3.36) instead of (3.31). In that case, the calculations are just longer. As a remark concerning Eqs. (3.43), it is worth noticing that any connection satisfying Eqs. (3.34) and (3.41) gives rise to a contracted curvature tensor R_{ij} automatically symmetric. Indeed, since the tensor K coincides necessarily with the contorsion tensor, namely

$$K_{ij}{}^{h} = \frac{1}{2}\left(-T_{ij}{}^{h} + T_{j}{}^{h}{}_{i} - T^{h}{}_{ij}\right)\,, \tag{3.44}$$

and since in (3.39) we already had $K = -T$, from Eqs. (3.41) we have

$$K_{ij}{}^{h} = \frac{1}{3}\left(T_j\delta^h_i - T_l g^{lh} g_{ij}\right)\,, \tag{3.45}$$

being

$$T_i := T_{ih}{}^{h} = -\frac{3}{2f'}\frac{\partial f'}{\partial x^i}\,. \tag{3.46}$$

Inserting Eq. (3.45) in Eq (3.35b), the contracted curvature tensor can be represented as

$$R_{ij} = \tilde{R}_{ij} + \frac{2}{3}\tilde{\nabla}_j T_i + \frac{1}{3}\tilde{\nabla}_h T^h g_{ij} + \frac{2}{9}T_i T_j - \frac{2}{9}T_h T^h g_{ij}\,. \tag{3.47}$$

The last expression, together with Eqs. (3.46), entails the symmetry of the indexes i and j. Therefore, in Eq. (3.43) we can omit the symmetrization symbol and write

$$f'(R)R_{ij} - \frac{1}{2}f(R)g_{ij} = 0\,. \tag{3.48}$$

Now, considering the trace of the equation (3.48), we get

$$f'(R)R - 2f(R) = 0\,. \tag{3.49}$$

The latter is an identity automatically satisfied by all possible values of R only in the special case $f(R) = \alpha R^2$. In all other cases, Eq.(3.49) represents a constraint on the scalar curvature R. As a conclusion follows that, if $f(R) \neq \alpha R^2$, the scalar curvature R has to be constant (at least on connected domains) and coincides with a given solution value of (3.49). In such a circumstance, Eqs.(3.41) imply that the torsion $T_{ij}{}^{h}$ has to be zero and the theory reduces to a $f(R)$-theory without torsion. In particular, we notice that in the case $f(R) = R$, eq. (3.49) yields $R = 0$ and therefore Eqs. (3.48) are equivalent to Einstein's equations in empty space $R_{ij} = 0$. On the other hand, if we assume $f(R) = \alpha R^2$, we can have non–vanishing torsion. In this case, by replacing Eq. (3.49) in Eqs. (3.41) and (3.48), we obtain field equations of the form

$$R_{ij} - \frac{1}{4}Rg_{ij} = 0\,, \tag{3.50a}$$

$$T_{ij}{}^{h} = -\frac{1}{2R}\frac{\partial R}{\partial x^i}\delta^h_j + \frac{1}{2R}\frac{\partial R}{\partial x^j}\delta^h_i\,. \tag{3.50b}$$

Finally, making use of Eq. (3.47) and the consequent relation

$$R = \tilde{R} + 2\tilde{\nabla}_h T^h - \frac{2}{3}T_h T^h\,, \tag{3.51}$$

in Eqs. (3.50), we can separately point out the contribution due to the metric and that due to the torsion. In fact, directly from eqs. (3.50a) we have

$$\tilde{R}_{ij} - \frac{1}{4}\tilde{R}g_{ij} = -\frac{2}{3}\tilde{\nabla}_j T_i + \frac{1}{6}\tilde{\nabla}_h T^h g_{ij} - \frac{2}{9}T_i T_j + \frac{1}{18}T_h T^h g_{ij}\,, \tag{3.52}$$

while from the "trace" $T_i := T_{jh}{}^h = -\dfrac{3}{2R}\dfrac{\partial R}{\partial x^i}$ of Eqs. (3.50b), we derive

$$\frac{\partial}{\partial x^i}\left(\tilde{R} + 2\tilde{\nabla}_h T^h - \frac{2}{3}T_h T^h\right) = -\frac{2}{3}\left(\tilde{R} + 2\tilde{\nabla}_h T^h - \frac{2}{3}T_h T^h\right) T_i\,, \tag{3.53}$$

Eqs. (3.52) and (3.53) are the coupled field equations in vacuum for metric and torsion in the $f(R) = \alpha R^2$ gravitational theory.

The presence of matter is embodied in the action functional (3.31) by adding to the gravitational Lagrangian a suitable material Lagrangian density $\mathcal{L}_m$, which can depend on a perfect fluid or on a generic Lagrangian scalar field, namely

$$\mathcal{A}(g,\Gamma) = \int \left(\sqrt{-g}f(R) + \mathcal{L}_m\right)\, ds\,. \tag{3.54}$$

In this case, the field equations take the form

$$f'(R)R_{ij} - \frac{1}{2}f(R)g_{ij} = \Sigma_{ij}\,, \tag{3.55a}$$

$$T_{ij}{}^h = -\frac{1}{2f'(R)}\frac{\partial f'(R)}{\partial x^l}\left(\delta^l_i\delta^h_j - \delta^l_j\delta^h_i\right)\,, \tag{3.55b}$$

where $\Sigma_{ij} := -\dfrac{1}{\sqrt{-g}}\dfrac{\delta\mathcal{L}_m}{\delta g^{ij}}$ plays the role of the energy–momentum tensor. From the trace of Eq. (3.55a), we obtain a fundamental relation between the curvature scalar R and the trace $\Sigma := g^{ij}\Sigma_{ij}$, which is

$$f'(R)R - 2f(R) = \Sigma\,, \tag{3.56}$$

(see also [176] and references therein). In what follows, there a lot of model in which (3.56) is locally invertible where you get branches and phase transitions and that $\Sigma \neq const$, thus allowing to express the curvature scalar R as a suitable function of Σ, namely

$$R = F(\Sigma)\,. \tag{3.57}$$

With this assumption in mind, using Eqs. (3.56) and (3.57) we can rewrite equations (3.55a) and (3.55b) in the form

$$R_{ij} - \frac{1}{2}Rg_{ij} = \frac{1}{f'(F(\Sigma))}\left(\Sigma_{ij} - \frac{1}{4}\Sigma g_{ij}\right) - \frac{1}{4}F(\Sigma)g_{ij}\,, \tag{3.58a}$$

$$T_{ij}{}^{h} = -\frac{1}{2f'(F(\Sigma))}\frac{\partial f'(F(\Sigma))}{\partial x^l}\left(\delta^l_i\delta^h_j - \delta^l_j\delta^h_i\right)\,. \tag{3.58b}$$

Moreover, making use of Eqs. (3.47) and (3.51), in Eq. (3.58a) we can decompose the contracted curvature tensor and the curvature scalar in their Christoffel and torsion dependent terms, thus getting an Einstein-like equation of the form

$$\begin{aligned}\tilde{R}_{ij} - \frac{1}{2}\tilde{R}g_{ij} = \quad & \frac{1}{f'(F(\Sigma))}\left(\Sigma_{ij} - \frac{1}{4}\Sigma g_{ij}\right) - \frac{1}{4}F(\Sigma)g_{ij} - \frac{2}{3}\tilde{\nabla}_j T_j + \\ & \frac{2}{3}\tilde{\nabla}_h T^h g_{ij} - \frac{2}{9}T_i T_j - \frac{1}{9}T_h T^h g_{ij}\,.\end{aligned} \tag{3.59}$$

Now, setting

$$\varphi := f'(F(\Sigma))\,, \tag{3.60}$$

from the trace of Eqs. (3.58b), we obtain

$$T_i := T_{ih}{}^{h} = -\frac{3}{2\varphi}\frac{\partial\varphi}{\partial x^i}\,. \tag{3.61}$$

Therefore, substituting in Eqs. (3.59), we end up with the final equations

$$\begin{aligned}\tilde{R}_{ij} - \frac{1}{2}\tilde{R}g_{ij} = \quad & \frac{1}{\varphi}\Sigma_{ij} + \frac{1}{\varphi^2}\left(-\frac{3}{2}\frac{\partial\varphi}{\partial x^i}\frac{\partial\varphi}{\partial x^j} + \varphi\tilde{\nabla}_i\frac{\partial\varphi}{\partial x^i}\right) + \\ & \frac{1}{\varphi^2}\left(\frac{3}{4}\frac{\partial\varphi}{\partial x^h}\frac{\partial\varphi}{\partial x^k}g^{hk}g_{ij} - \varphi\tilde{\nabla}^h\frac{\partial\varphi}{\partial x^h}g_{ij} - V(\varphi)g_{ij}\right),\end{aligned} \tag{3.62}$$

where we defined the effective potential

$$V(\varphi) := \frac{1}{4}\left[\varphi F^{-1}((f')^{-1}(\varphi)) + \varphi^2(f')^{-1}(\varphi)\right], \tag{3.63}$$

Eqs. (3.62) may be difficult to solve, neverthless we can simplify this task finding solutions for a conformally related metric. Indeed, performing a conformal transformation of the kind $\bar{g}_{ij} = \varphi g_{ij}$, eqs. (3.62) may be rewritten in the easier form (see, for example, [176; 177; 178])

$$\bar{R}_{ij} - \frac{1}{2}\bar{R}\bar{g}_{ij} = \frac{1}{\varphi}\Sigma_{ij} - \frac{1}{\varphi^3}V(\varphi)\bar{g}_{ij}\,, \tag{3.64}$$

where $\bar{R}_{ij}$ and $\bar{R}$ are respectively the Ricci tensor and the Ricci scalar curvature associated with the conformal metric $\bar{g}_{ij}$. Concerning the connection Γ, solution of the variational problem $\delta\mathcal{A} = 0$, from eqs. (3.34), (3.45) and (3.61), one gets the explicit expression

$$\Gamma_{ij}^{\ h} = \tilde{\Gamma}_{ij}^{\ h} + \frac{1}{2\varphi}\frac{\partial\varphi}{\partial x^j}\delta_i^h - \frac{1}{2\varphi}\frac{\partial\varphi}{\partial x^l}g^{lh}g_{ij}\,. \tag{3.65}$$

To conclude, we notice that Eqs. (3.64) are deducible from an Einstein-Hilbert like action functional only under restrictive conditions. More precisely, let us suppose that the material Lagrangian depends only on the components of the metric and not on its derivatives as well as that the trace $\Sigma = \Sigma_{ij}g^{ij}$ is

independent of the metric and its derivatives. Then, from the identities

$$\sqrt{-\bar{g}} = \varphi^2\sqrt{-g}, \quad \frac{\partial}{\partial g^{ij}} = \frac{1}{\varphi}\frac{\partial}{\partial \bar{g}^{ij}}, \quad \Sigma_{ij} = -\frac{1}{\sqrt{-g}}\frac{\delta \mathcal{L}_m}{\delta g^{ij}} = -\frac{1}{\sqrt{-g}}\frac{\partial \mathcal{L}_m}{\partial g^{ij}}\,, \quad (3.66)$$

we have the following relation

$$\Sigma_{ij} = -\varphi\frac{1}{\sqrt{-\bar{g}}}\frac{\partial \mathcal{L}_m}{\partial \bar{g}^{ij}} := \varphi\bar{\Sigma}_{ij}\,. \quad (3.67)$$

In view of this, and being $\varphi = \varphi(\Sigma)$, it is easily seen that Eqs. (3.64) may be derived by varying with respect to $\bar{g}^{ij}$ the action functional

$$\bar{\mathcal{A}}(\bar{g}) = \int\left[\sqrt{-\bar{g}}\left(\bar{R} - \frac{2}{\varphi^3}V(\varphi)\right) + \mathcal{L}_m\right] ds\,. \quad (3.68)$$

Therefore, under the stated assumptions, $f(R)$-gravity with torsion in the metric framework is conformally equivalent to an Einstein-Hilbert like theory.

The $f(R)$ theories are Extended Theories that include higher order corrective terms in curvature invariants. They are very useful theories to describe observational evidences both on astrophysical and on cosmological scale. In fact, in this thesis, these theories allowed us to describe Neutron Stars that, from their observations, would seem to exceed Chandrasekhar's limit. The problem that has emerged, on astrophysical scale, is that inn which pulsars have been discovered and measured that would seem to clearly violate this limit and these stable configurations are neither provided nor justified by General Relativity. What we will see, in the next chapters, is how to obtain stable configurations of Neutron Stars that go beyond this limit. We will proceed to derive the stellar structure equations, the Tolman-Oppenheimer-Volkoff equations, in the $f(R)$ theories in both cases. We will consider the Starobinsky model solving numerically these equations by considering appropriate equations of state for the dense matter.

We will plot the Mass-Radius diagrams for Neutron Stars, we will calculate the maximum value of Mass and Radius and we will make a comparison between the two theories. We will see how the two theories allow us to justify stable stellar configurations not provided by Einstein theory and, we will see how the metric theory can describe more compact objects than the metric-affine case where, the torsion, behaves like a repulsive field which tends to oppose the increase in the total mass of the star. All this happens when the quadratic corrective term added to the Lagrangian, tends to assume larger values when its parameter is chosen.

Chapter 4

Neutron Stars and Fermionic condensate

Summary

In this chapter, we will give a phenomenological overview of Neutron Stars, its physical properties, nuclear matter and its hadronic composition. We will see how one of its development sequences is correlated with the Mass-Radius relation. Finally we will make a brief description of a Fermionic condensate, highlighting its singular characteristics, i.e. the physical properties of matter in the superfluid state.

4.1 Compact objects: an overview

Compact objects are the remnants of bright stars [179]. At the end of its evolution, the stars, whatever their mass, go through a phase in which the matter that constitutes them assumes on a degenerate state.

During the stability phase of main sequence and the immediately following

phases, the star shines by losing energy. This loss, which the stars suffer, is compensated by the production of energy in the nucleus through nuclear fusion reactions.

When a star becomes unstable, the radiation pressure of the nucleus it is no longer able to oppose the gravity of the star outer layers. As a result, the core undergoes a collapse while the outer layers are expelled and what remains is a dense object, a compact star composed of matter in a highly degenerate state. They are classified like compact objects, White Dwarfs, Neutron Stars and Black Holes.

A White Dwarf is the final result of the low mass stars evolution (up to $8M_{\odot}$), where $M_{\odot}$ means one solar mass. After having converted all the hydrogen in helium and, subsequently, helium in all the other elements up to oxygen, the bright star no longer develops radiation pressure necessary to oppose the gravity that tends to make the star collapse on itself. In this way, there is a phase transition between the bright star and the White Dwarf freeing the gas cloud and dust residues in the form of a planetary nebula. The White Dwarf basically is a degenerate star where the nucleus is composed mainly of carbon and oxygen balanced thanks to the pressure of degenerate electrons which opposes the gravitational force. The dimensions of a White Dwarf are of the planet Earth order but with a mass that can reach a maximum of $1.44M_{\odot}$ value.

A Black Hole is probably the final evolutionary phase of the most massive stars ($> 25M_{\odot}$), one inaccessible space-time region in which the entire star, at the end of its luminous phase, including its remnants, is attracted within the very strong gravitational field of the Black Hole itself. In fact, all the objects that pass near the gravitational field of the Black Hole, will no longer be able to escape.

In the high mass stars evolution,($> 8M_{\odot}$), all the heavy elements are converted to iron thus forming a very high density iron core which, having an higher bond

energy than all the other elements, is no longer able to develop the radiation pressure that opposes the collapse of the star itself. What happens is that the star enters in the *type II Supernovae* phase, i.e. a highly energetic explosion that releases its gas residues and dusts, which are called *Supernovae Remnants*.

A Neutron Star, on the other hand, is the final evolutionary phase of stars that have a mass that falls in the range of $(8M_{\odot} < M < 25M_{\odot})$. The bright star that falls within this mass value, evolves like a high mass star, but the final result will not be a Black Hole but a Neutron Star.

Like White Dwarfs, Neutron Stars are degenerate stars where the matter state is characterized by an extremely high density, so that the greatest pressure contribution is given by the *Pauli Exclusion Principle*.

Neutron Stars are the smallest and most dense stars known. Like all stars, the Neutron Stars rotate around their own axis, but some even to do it a few hundred times per second. This type of rotating star will experience an enormous centrifugal force that must be balanced by gravity otherwise it would disintegrate. The equilibrium of the two forces gives information on the lower limit of stellar density. Neutron Stars are 10^{14} times more dense than the Earth.

Some Neutron Stars, together with a companion star, form a binary system and, in some cases, using the Kepler's III Law, it is possible to evaluate the mass by using mechanics classic. The mass of a Neutron Star is generally $1.44M_{\odot}$ and from this its possible to obtain their radius which are about $10km$.

The existence of Neutron Stars is deduced from the Supernovae explosion events and by observing the periodic emission of Pulsars at radio frequencies. In order to obtain the angular momentum conservation, the Neutron Stars acquire a very high angular velocity generating so strong magnetic fields through the magnetic flux conservation during bright star collapse. These are the two main physical properties that allow us to detect the Pulsars periodic signal. These

extreme characteristics distinguish Neutron Stars in physical principles from other classic stars and in-depth studies for their understanding are needed.

All other stars can be described very well with Newtonian gravity with low-energy atomic and nuclear energy physics in known laboratory conditions. Indeed the luminous stars evolve through thermonuclear reactions. These are nuclear reactions induced by high temperatures, but involve collision energies that are small on a nuclear scale. In some cases, the cross sections can be measured with nuclear accelerators and, in others, the cross sections measured, must be extrapolated to lower energies.

Neutron Stars, on the other hand, in their different forms push matter to such extremes density and, consequently, it is necessary to resort to nuclear and particle physics to describe them. Furthermore, the intense concentration of matter in Neutron Stars can only be described by General Relativity, the Einstein gravity theory which alone describes the way in which the weakest force of nature organizes the distribution of mass and the constituents of the densest objects of the universe.

4.2 Nuclear matter and adronic composition of Neutron Stars

The matter hypothesized within a stellar nucleus, compared with that of a Neutron Star, highlights similarities and differences. The similarities include the matter baryonic composition and have very similar nuclear densities. The differences instead arise from two important physical properties:

1. The nuclei are bound by the isospin symmetrical nuclear force but the Neutron Stars are bounded by gravity. This means that nuclei tend to be symmetrical in isospins while Neutron Stars are very asymmetrical.

2. There is another difference arising from the weak interaction timescale ($10^{10}s$). Because of the high density of matter in Neutron Stars and the fact that baryons obey the Pauli's principle, it is energetically favorable for nucleons at the top of the Fermi sea to convert to other baryons, including strange ones, (hyperons), so as to lower the Fermi energies. Strangeness is a quantum number that describes long-lived particles. The transformations do not violate the strangeness conservation of the strong interactions because strangeness is conserved only on the strong interaction timescale, not in the weak one.

In general the fundamental differences between nuclear matter and Neutron Stars are these, where the properties of such systems as symmetrical hot matter and the non-strangeness of matter produced in relativistic nuclear collisions are related in any matter theory.

Moreover, Neutron Stars are not composed only of neutrons. Charge neutrality is automatically satisfied by pure neutron matter, but this is not the lowest energy state of matter dense neutral. Some neutrons will decay in such a way as to reach the balance between protons, electrons and neutrons. Therefore, other thresholds populated by additional particle species are reached. The thresholds are simply, in a Fermi gas model, the masses of the particles. In general, particle thresholds depend on pure interactions.

The Neutron Stars therefore are not formed only by neutron matter, but of matter electronics at the lowest energy state consistent with neutrality of charge. In general, it could be a state that is very rich in baryonic species and is called *Neutron Star matter* and its baryonic composition constantly changes with the increase in baryonic density.

4.3 Development sequence and Mass-Radius relation of a Neutron Star

Neutron Stars are completely relativistic objects. Their structure can be derived only in the General Relativity context. When the problem solution of the Neutron Stars matter is obtained, we can use the equations of state. The Tolman-Oppenheimer-Volkoff equations provides a family with a parameter of stellar models that corresponds to a particular equation of state.

The Tolman-Oppenheimer-Volkoff equations are first order differential equations each with an initial condition. The equations must be integrated until the pressure becomes zero or until the pressure decreases rapidly as the star's radius increases, until it reaches the surface of the star itself. Then, for a fixed central density, both the radius and the mass are known, which is a function of the radius itself. The choice of one succession of increasing values for the central density corresponds to the development sequence of stars of increasing mass, until the mass limit is reached.

From Tolman-Oppenheimer-Volkoff equations solutions, for a given equation of state and central density chosen, we not only study the corresponding stellar mass and the radius but, as a result of the numerical integration of the equations, we obtain the mass-energy distribution for a particular star model.

All this allows us to plot the Mass-Radius diagram, i.e. the most important representation of a Neutron Star sequence, and is uniquely linked to the equation of state. While mass and radius are not quantities known so far for any Pulsar, its, in principle, possible to determine them in some cases. The mass can be determined by Binary Pulsars. In principle, the radius could be obtained by measuring the Doppler shift of known spectral transitions. The Doppler shift determines the Mass-Radius relation, which provides the radius if the mass is

known.

Neutron Stars are the Fermi degenerate systems: matter can be compressed without the heat generation. Instead, gravitational compression of pre-sequence and main sequence stars, which can be described by an equation of state of a perfect gas, raises the temperature to the combustion point of increasingly heavier elements in thermonuclear reactions. The degenerate stars, furthermore, have a generic relation between their mass and radius. Instead of being bigger, the degenerates high mass stars are smaller than low mass stars. The reason is simple. For low mass stars, the gravitational attraction is weak and the corresponding stars are large and widespread. Instead, for high mass stars, the gravitational attraction is stronger than all those in stable hydrostatic equilibrium. Correspondingly, the radius is smaller. For an object slightly more compact, the star becomes unstable, collapsing into a Black Hole. The general form of the Mass-Radius relation is generic for compact stars that are bound by gravitational force.

4.4 Fermionic condensate

A Fermionic condensate is a superfluid phase formed by Fermionic particles at low temperatures, then Fermionic condensates are a type of superfluid. A superfluid possesses fluid properties similar to those possessed by ordinary liquids and gases, such as the lack of a definite shape and the ability to flow in response to applied forces. However, superfluids possess some properties that do not appear in ordinary matter. For instance, they can flow at high velocities without dissipating any energy— i.e. zero viscosity. At lower velocities, energy is dissipated by the formation of quantized vortices, which act as "holes" in the medium where superfluidity breaks down. Superfluidity is the characteristic property of a fluid with zero viscosity which therefore flows without loss of kinetic energy. Superfluidity

occurs in two isotopes of helium (helium-3 and helium-4) when they are liquefied by cooling to cryogenic temperatures. The discovery of superfluidity of helium-3 [180; 181] was made by Lee, Richardson and Osheroff were jointly awarded the Nobel Prize in Physics in 1996 for this discovery. They discovered unexpected effects in their measurements, which they eventually explained as phase transitions to a superfluid phase of ^3He. Superfluidity is also a property of various other exotic states of matter theorized to exist in astrophysics, high-energy physics, and quantum gravity theories [180; 181]. The idea that superfluidity exists inside Neutron Stars was first proposed in [182], where it is expected that nucleons in a Neutron Star at sufficiently high density and low temperature can also form pairs of fermions bound together at low temperatures in a certain manner, also called Cooper pairs [183], where Cooper pairing is a quantum effect. The composition of the superdense matter in the core remains uncertain. One model describes the core as superfluid neutron-degenerate matter. More exotic forms of matter are possible, including degenerate strange matter, matter containing high-energy pions and kaons in addition to neutrons, [184] or ultra-dense quark-degenerate matter. Recent works, [see [185] and the references therein], have established that Neutron Stars have various emergent states in its interior in presence of a strongly interacting fermion system, i.e. the presence of a strongly interacting fermion system leads to emergence of various condensates and emergent states and their effects affect on the dynamics of the Neutron Star. Moreover, in [186], the structure of Neutron Star interiors has been proposed, and reproduced the theoretical arguments for the existence of superfluidity in Neutron Stars, discuting the implications of neutron superfluidity and proton superconductivity for the rotational dynamics of Pulsars. Finally, always in [186], arguments that has been proposed for observable effect of superfluidity on the timing history of Pulsars and perhaps other Neutron Stars have been revised.

Chapter 5

Stellar structure equations for Neutron Stars in $f(R)$ gravity

Summary

In this chapter, we will derive the stellar structure equations for Neutron Stars in $f(R)$ gravity both in metric and in metric-affine case where, in the metric-affine case, we will consider first the torsion with perfect fluids and, subsequently, the torsion with spin fluids. These equations, in the next chapter, will allow us to plot the Mass-Radius diagrams in both theories and derive the stellar parameters of Neutron Stars. Given the complexity of the equations, in this thesis, we will numerically solve them in the metric and in the torsion case considering matter composed of perfect fluids while, in the spin fluids case, they could be considered for future works, due to the strong non-linearity of the equations to be integrated.

5.1 Stellar structure equations in $f(R)$ gravity with perfect fluids

5.1.1 The purely metric theory

As mentioned in the third chapter and taken up here, in the purely metric formulation, the action for $f(R)$-gravity (in units for $G = 1 = c$) is given by

$$\mathcal{A} = \frac{1}{16\pi} \int d^4x \sqrt{-g}[f(R) + \mathcal{L}_m], \tag{5.1}$$

where $f(R)$ is a function of the scalar curvature R, g is determinant of the metric tensor g_{ij} and $\mathcal{L}_m$ is the matter Lagrangian. Varying the action (5.1) with respect to the metric tensor g_{ij}, one gets the field equations:

$$f'(R)R_{ij} - \frac{1}{2}f(R)g_{ij} - (\nabla_i\nabla_j - g_{ij}\Box)f'(R) = 8\pi\Sigma_{ij}. \tag{5.2}$$

In eqs. (5.2), R_{ij} is the Ricci tensor, $f'(R)$ denotes the derivative of $f(R)$ with respect to the scalar curvature, $\Sigma_{ij} = \dfrac{-2}{\sqrt{-g}} \dfrac{\delta\left(\sqrt{-g}\mathcal{L}_m\right)}{\delta g^{ij}}$ is the energy–momentum tensor of matter and $\Box = \frac{1}{\sqrt{-g}} \frac{\partial}{\partial x^j} \left(\sqrt{-g} g^{ij} \frac{\partial}{\partial x^i}\right)$ indicates the covariant d'Alembert operator. Here we adopt the signature $(+, -, -, -)$.

In order to describe stellar objects, we assume that the metric is static and spherically symmetric of the form:

$$ds^2 = e^{2\psi}dt^2 - e^{2\lambda}dr^2 - r^2(d\theta^2 + \sin^2\theta d\phi^2), \tag{5.3}$$

where ψ and λ are functions depending only on the radial coordinate r. Moreover, we also assume that inside the star matter is described as a perfect fluid, with energy–momentum tensor $\Sigma_{ij} = \mathrm{diag}(e^{2\psi}\rho, e^{2\lambda}p, r^2p, r^2p\sin^2\theta)$, where $\rho = \rho(r)$ and $p = p(r)$ are the matter density and pressure respectively.

By a direct calculation, it is possible to show that field equations (5.2), evaluated in the metric (5.3), are equivalent to the set of equations consisting of the Tolmann-Oppenheimer-Volkoff equations for $f(R)$ gravity and the continuity equation. In detail, the Tolmann-Oppenheimer-Volkoff equations for $f(R)$-gravity are expressed as

$$\begin{aligned}\frac{d\lambda}{dr} = & \frac{e^{2\lambda}[r^2(16\pi\rho + f(R)) - f'(R)(r^2R + 2)] + 2(2rf''(R)R_r + f'(R))}{2r\left[2f'(R) + rR_rf''(R)\right]} + \\ & \frac{2r^2\left[f'''(R)R_r^2 + f''(R)R_{rr}\right]}{2r\left[2f'(R) + rR_rf''(R)\right]},\end{aligned} \tag{5.4}$$

$$\frac{d\psi}{dr} = \frac{e^{2\lambda}[r^2(16\pi p - f(R)) + f'(R)(r^2R + 2)] - 2(2rf''(R)R_r + f'(R))}{2r\left[2f'(R) + rR_rf''(R)\right]}, \tag{5.5}$$

while the continuity equation is the usual one:

$$\frac{dp}{dr} = -(\rho + p)\frac{d\psi}{dr}. \tag{5.6}$$

Here R_r and $R_{r,r}$ denote respectively the first and second derivative of $R(r)$ with respect to r. In order to solve numerically the equations (5.4), (5.5) and (5.6), we can regard the scalar curvature R as an independent dynamical field. In doing this, we need an additional equation which is directly obtained form the very definition of scalar curvature:

$$R = 2e^{-2\lambda}\left[\psi_r^2 - \psi_r\lambda_r + \psi_{r,r} + \frac{2\psi_r}{r} - \frac{2\lambda_r}{r} + \frac{1}{r^2} - \frac{e^{2\lambda}}{r^2}\right], \tag{5.7}$$

Indeed, inserting the content of eqs. (5.4), (5.5) and (5.6) into (5.7), we get the

dynamical equation for R:

$$\begin{aligned}\frac{d^2R}{dr^2} = \quad & R_r\left(\lambda_r + \frac{1}{r}\right) + \frac{f'(R)}{f''(R)}\left[\frac{1}{r}\left(3\psi_r - \lambda_r + \frac{2}{r}\right) - e^{2\lambda}\left(\frac{R}{2} + \frac{2}{r^2}\right)\right] - \\ & R_r^2\left(\frac{f'''(R)}{f''(R)}\right),\end{aligned} \tag{5.8}$$

Finally, the numerical solution of the resulting dynamical equations relies on the assignment of a suitable Equation of State $p = p(\rho)$, relating pressure and density inside the star, as well as of initial data (values of the fields at the center of the star).

5.1.2 The torsion theory

Here too, as mentioned in the third chapter, we recall that in $f(R)$-gravity with torsion, the gravitational and dynamical fields are pairs $(g,\ \Gamma)$ consisting of a pseudo-Riemannian metric g and a metric compatible linear connection Γ with non–vanishing torsion.

The corresponding field equations are obtained by varying the action functional (5.1) independently with respect to the metric and the connection. It is worth noticing that now R refers to the scalar curvature associated with the dynamical connection Γ.

Moreover, we recall that any metric compatible linear connection Γ may be decomposed as the sum

$$\Gamma_{ij}{}^{h} = \tilde{\Gamma}_{ij}{}^{h} - K_{ij}{}^{h}, \tag{5.9}$$

where $\tilde{\Gamma}_{ij}{}^{h}$ is the Levi–Civita connection associated with the given metric g and $K_{ij}{}^{h}$ denotes the contorsion tensor, related to the torsion tensor $T_{ij}{}^{h} = \Gamma_{ij}{}^{h} - \Gamma_{ji}{}^{h}$

by the relation [187]:

$$K_{ij}{}^{h} = \frac{1}{2}\left(-T_{ij}{}^{h} + T_{j}{}^{h}{}_{i} - T^{h}{}_{ij}\right). \tag{5.10}$$

The contorsion tensor (5.10) verifies the antisymmetry property $K_{i}{}^{j\,h} = -K_{i}{}^{h\,j}$ and, together with the metric tensor g, identifies the actual degrees of freedom of the theory.

Making use of eqs. (5.9) and (5.10), we can decompose the Ricci and the scalar curvature of the dynamical connection respectively as:

$$R_{ij} = \tilde{R}_{ij} + \tilde{\nabla}_{j}K_{hi}{}^{h} - \tilde{\nabla}_{h}K_{ji}{}^{h} + K_{ji}{}^{p}K_{hp}{}^{h} - K_{hi}{}^{p}K_{jp}{}^{h}, \tag{5.11}$$

and

$$R = \tilde{R} + \tilde{\nabla}_{j}K_{h}{}^{jh} - \tilde{\nabla}_{h}K_{j}{}^{jh} + K_{j}{}^{jp}K_{hp}{}^{h} - K_{h}{}^{jp}K_{jp}{}^{h}, \tag{5.12}$$

where $\tilde{R}_{ij}$ and $\tilde{R}$ are the Ricci and the scalar curvature of the Levi–Civita connection induced by the metric g.

In the absence of matter spin density, variations of (5.1) yield the field equations [174; 175; 188; 189; 190]:

$$f'(R)R_{ij} - \frac{1}{2}f(R)g_{ij} = 8\pi\Sigma_{ij}, \tag{5.13}$$

and

$$T_{ij}{}^{h} = \frac{1}{2f'(R)}\frac{\partial f'(R)}{\partial x^{p}}(\delta^{p}_{j}\delta^{h}_{i} - \delta^{p}_{i}\delta^{h}_{j}), \tag{5.14}$$

where Σ_{ij} denotes again the energy-momentum tensor of matter, and the non–linearity of the gravitational Lagrangian function $f(R)$ becomes source of torsion.

Now, by inserting the content of equations (5.11) and (5.14) into equations (5.13), it is possible to show that the whole set of field equations evaluated in the

metric (5.3) is equivalent to the system formed by the following two Tolmann-Oppenheimer-Volkoff equations together with the continuity equation

$$\begin{aligned}\frac{d\lambda}{dr} = & \frac{e^{2\lambda}[r^2(16\pi\rho + f(R)) - f'(R)(r^2R+2)] + 2(2rf''(R)R_r + f'(R))}{2r\left[2f'(R) + rR_r f''(R)\right]} + \\ & \frac{2r^2\left[f'''(R)R_r^2 + f''(R)R_{rr} - \frac{3f''(R)^2R_r^2}{4f'(R)}\right]}{2r\left[2f'(R) + rR_r f''(R)\right]},\end{aligned} \tag{5.15}$$

$$\begin{aligned}\frac{d\psi}{dr} = & \frac{e^{2\lambda}[r^2(16\pi p - f(R)) + f'(R)(r^2R+2)] - 2rf''(R)R_r\left[2 + \frac{3f''(R)rR_r}{4f'(R)}\right]}{2r\left[2f'(R) + rR_r f''(R)\right]} \\ & - \frac{2f'(R)}{2r\left[2f'(R) + rR_r f''(R)\right]},\end{aligned} \tag{5.16}$$

$$\frac{dp}{dr} = -(\rho + p)\frac{d\psi}{dr}, \tag{5.17}$$

which also holds in the present case [137; 191; 192; 193; 194; 195].

Also in this torsional case, we consider the scalar curvature R as an independent dynamical variable, introducing a consequent additional equation derived from the very definition of R itself. In fact, inserting eqs. (5.10) and (5.14) into (5.12), evaluating all in the metric (5.3) and making use of eqs. (5.15) and (5.16), we obtain the evolution equation:

$$\begin{aligned}\frac{d^2R}{dr^2} = & R_r\left(\lambda_r + \frac{1}{r}\right) - \frac{2f'(R)}{f''(R)}\left[\frac{1}{r}\left(3\psi_r - \lambda_r + \frac{2}{r}\right) - e^{2\lambda}\left(\frac{R}{2} + \frac{2}{r^2}\right)\right] - \\ & R_r^2\left(\frac{f'''(R)}{f''(R)} + \frac{3f''(R)}{2f'(R)} + \frac{3\psi_r}{R_r} + \frac{9}{rR_r}\right),\end{aligned} \tag{5.18}$$

Again, in order to be solved, the set of dynamical equations (5.15), (5.16), (5.17) and (5.18) for the unknowns R, λ, ψ, p and ρ must be completed by an equation

of state and initial data.

5.2 Stellar structure equations in $f(R)$ gravity with spin fluids

As for the previous section, always using the Palatini's calculus, we now get the the Tolmann-Oppenheimer-Volkoff equations but considering a Weyssenhoff spin fluid. Using the above techiques, the field equations in this case are [174; 175; 188; 189; 190]:

$$f'(R)R_{ij} - \frac{1}{2}f(R)g_{ij} = 8\pi\Sigma_{ij}, \tag{5.19}$$

$$T_{ij}{}^{h} = \frac{1}{f'(R)}\left[\frac{1}{2}\left(\frac{\partial f'(R)}{\partial x^p} + S_{pq}{}^{q}\right)(\delta^p_j\delta^h_i - \delta^p_i\delta^h_j) + S_{ij}{}^{h}\right], \tag{5.20}$$

where R_{ij} and $T_{ij}{}^{h}$ are the Ricci and Torsion tensors associated with the dynamical connection Γ, Σ_{ij} and $S_{ij}{}^{h}$ are the energy-momentum and spin density tensors of the matter fields, while $S_{pq}{}^{q}$ is the antisymmetrized spin tensor. We note that, in these field equations, the energy-momentum tensor, the tensor and Ricci scalar have, in their internal definition, some additives terms due to the spin (see for more details [196; 197; 198]). From (5.20), one realizes that it is possible to have non-vanishing torsion even in absence of spin density. We now consider a Weyssenhoff spin fluid, characterized by an energy-momentum tensor of a perfect fluid and a spin density tensor given by

$$S_{ij}{}^{h} = S_{ij}U^h, \tag{5.21}$$

where U^h ($U^hU_h = 1$) denote the 4-velocity of energy-momentum, while S_{ij} the spin density of the fluid (see, for example, [199; 200] and references therein). The

4-velocity and the spin density satisfy the convective condition

$$S_{ij}U^j = 0. \tag{5.22}$$

Like for the previous section, by considering the trace equation and excluding the case $f(R) = k\,R^2$, we get that $R = R(r)$.

Now, by choosing the reference frame where

$$U_1 = 0, U_2 = 0, U_3 = 0, U_4 = e^{-\psi(r)},$$

we substitute the equations (5.20) in the system (5.19). By taking into account equations (5.21), (5.22), we get that the components of field equations $(1,3), (2,3), (1,2)$ imply $S_{ih,4} = 0$. On the other hand, the components of field equations $(2,4)$ and $(3,4)$ give

$$S_{13}\ (2\psi_r f'(R) + f''(R)\,R_r) = 0, \quad S_{12}\ (2\psi_r f'(R) + f''(R)\,R_r) = 0. \tag{5.23}$$

We distinguish now a first case, that we call the *regular one*, in which

$$2\psi_r\, f'(R) + f''(R)\,R_r \neq 0,$$

and so, consequently $S_{12} = 0, S_{13} = 0$. The second case, that we call the *singular one*, is verified when

$$2\psi_r\, f'(R) + f''(R)\,R_r = 0.$$

This last case, implying

$$f'(R) = C\ e^{-2\,\psi(r)},$$

for some costant C, will be not discussed here. By limiting our study to the

regular case, it is possible to show that the field equations imply

$$S_{12} = 0, S_{13} = 0, S_{23} = \sigma(r)\, r^2\, \sin(\theta),$$

where $\sigma^2 = \sigma^2(r) = \frac{1}{2} S_{ij} S^{ij}$ is the square of the spin density.

Further, we show that the remaining field equations are equivalent to the Tolmann-Oppenheimer-Volkoff equations

$$\begin{aligned} \frac{d\lambda}{dr} = & \frac{e^{2\lambda}\left[r^2(16\pi\rho + f(R)) - f'(R)\left(r^2 R + 2 + \frac{\sigma^2 r^2}{2f'(R)^2}\right)\right]}{2r\left[2f'(R) + rR_r f''(R)\right]} + \\ & \frac{2[2rf''(R)R_r + f'(R)] + 2r^2\left[f'''(R)R_r^2 + f''(R)R_{rr} - \frac{3f''(R)^2 R_r^2}{4f'(R)}\right]}{2r\left[2f'(R) + rR_r f''(R)\right]}, \end{aligned} \tag{5.24}$$

$$\begin{aligned} \frac{d\psi}{dr} = & \frac{e^{2\lambda}\left[r^2(16\pi p - f(R)) + f'(R)\left(r^2 R + 2 - \frac{\sigma^2 r^2}{2f'(R)^2}\right)\right]}{2r\left[2f'(R) + rR_r f''(R)\right]} - \\ & - \frac{2rf''(R)R_r\left[2 + \frac{3f''(R) r R_r}{4f'(R)}\right] + 2f'(R)}{2r\left[2f'(R) + rR_r f''(R)\right]}, \end{aligned} \tag{5.25}$$

together with the continuity equation

$$\frac{dp}{dr} = -(\rho + p)\,\frac{d\psi}{dr} + \frac{\left[f'(R)\,(\sigma\,\psi_r + \sigma_r) - \sigma\, f''(R)\; R_r\right]\sigma}{16\pi f'(R)^2}. \tag{5.26}$$

The calculation of the Ricci scalar is similar to the one of the previous section. By substituting the contorsion tensor in eq. (5.12) and using the field equations

we obtain:

$$\begin{aligned}\frac{d^2R}{dr^2} = \quad & R_r\left(\lambda_r+\frac{1}{r}\right)-\frac{2f'(R)}{f''(R)}\left[\frac{1}{r}\left(3\psi_r-\lambda_r+\frac{2}{r}\right)-e^{2\lambda}\left(\frac{R}{2}+\frac{2}{r^2}-\frac{\sigma^2}{4f'(R)^2}\right)\right] \\ & -R_r^2\left(\frac{f'''(R)}{f''(R)}+\frac{3f''(R)}{2f'(R)}+\frac{3\psi_r}{R_r}+\frac{9}{rR_r}\right),\end{aligned} \tag{5.27}$$

where λ_r and ψ_r are the (5.24) and (5.25), respectively.

Moreover, if we define the *effective density and pressure* $\rho^\star$, $p^\star$ as :

$$\rho^\star=\rho-\frac{\sigma^2}{32\pi f'(R)},\quad p^\star=p-\frac{\sigma^2}{32\pi f'(R)} \tag{5.28}$$

the Tolmann-Oppenheimer-Volkoff equations (5.24), (5.25) become the equations (5.15), (5.16) with respect to the effective density and pressure:

$$\begin{aligned}\frac{d\lambda}{dr} = \quad & \frac{e^{2\lambda}[r^2(16\pi\rho^\star+f(R))-f'(R)(r^2R+2)]+2[2rf''(R)R_r+f'(R)]}{2r\left[2f'(R)+rR_rf''(R)\right]}+ \\ & \frac{2r^2\left[f'''(R)R_r^2+f''(R)R_{rr}-\frac{3f''(R)^2R_r^2}{4f'(R)}\right]}{2r\left[2f'(R)+rR_rf''(R)\right]},\end{aligned} \tag{5.29}$$

$$\begin{aligned}\frac{d\psi}{dr} = \quad & \frac{e^{2\lambda}[r^2(16\pi p^\star-f(R))+f'(R)(r^2R+2)]-2rf''(R)R_r\left[2+\frac{3f''(R)rR_r}{4f'(R)}\right]}{2r\left[2f'(R)+rR_rf''(R)\right]} \\ & -\frac{2f'(R)}{2r\left[2f'(R)+rR_rf''(R)\right]}.\end{aligned} \tag{5.30}$$

We observe that the effect of the square of the spin in Tolmann-Oppenheimer-Volkoff equations behaves like a type of repulsive force for the density and pressure. The continuity equation will become

$$\frac{dp^\star}{dr}=-(\rho^\star+p^\star)\frac{d\psi}{dr}-\frac{\tilde{\sigma^2}\,f''(R)\,R_r}{16\pi\,f'(R)^2}. \tag{5.31}$$

In absence of spin it is easy to show that the (5.31) become the classic (5.6). The trace equation, dependent from the previous equations, is

$$f'(R)R - 2f(R) = \Sigma, \tag{5.32}$$

where $\Sigma = g^{ij}\Sigma_{ij}$ is the trace of energy-momentum tensor.

With the presence of the spin, inside the star the Eqs. (5.24), (5.25),(5.26), (5.27) can be solved for the equation of state $p = p(\rho)$ for pressure and $\sigma = \sigma(\rho)$ for spin.

5.3 The case $f(R) = R$

In order to apply the Tolmann-Oppenheimer-Volkoff equations to study stellar structures, Neutron Stars in primis, they must be equivalent to the classic Tolmann-Oppenheimer-Volkoff equations in General Relativity limit. Therefore, in the limit $f(R) = R$, we have $f'(R) = 1$ and $f''(R) = f'''(R) = 0$. Substituting in (5.4)(5.5) and (5.15)(5.16) we have

$$\frac{d\lambda}{dr} = \frac{e^{2\lambda}(8\pi r^2\rho - 1) + 1}{2r}, \tag{5.33}$$

$$\frac{d\psi}{dr} = \frac{e^{2\lambda}(8\pi r^2 p + 1) - 1}{2r}. \tag{5.34}$$

We known that a mass parameter $m(r)$ can be defined according to the relation:

$$e^{-2\lambda} = 1 - \frac{2m}{r}, \tag{5.35}$$

therefore substituting in (5.34) we have

$$\frac{d\psi}{dr} = \frac{1}{r^2}\left(m + 4\pi r^3 p\right)\left(1 - \frac{2m}{r}\right)^{-1}. \tag{5.36}$$

Substituting (5.36) in (5.6) we get the classic Tolmann-Oppenheimer-Volkoff equations written as in [52]

$$\frac{dp}{dr} = -\frac{1}{r^2}\left(\rho + p\right)\left(m + 4\pi r^3 p\right)\left(1 - \frac{2m}{r}\right)^{-1}, \tag{5.37}$$

in units where $G = 1 = c$. It can be easily checked that, for $f(R) = R$, eq. (5.13) reduces to the trace of General Relativity, i.e.

$$R = -8\pi(\rho - 3p). \tag{5.38}$$

Considering instead the (5.24)(5.25)(5.26), in the limit $f(R) = R$, there will be additive terms due to the presence of the spin. Therefore we have

$$\frac{d\lambda}{dr} = \frac{e^{2\lambda}\left[8\pi r^2\rho - 1 - \frac{r^2\sigma^2}{4}\right] + 1}{2r}, \tag{5.39}$$

$$\frac{d\psi}{dr} = \frac{e^{2\lambda}\left[8\pi r^2 p + 1 - \frac{r^2\sigma^2}{4}\right] - 1}{2r}, \tag{5.40}$$

$$\frac{dp}{dr} = -\left(\rho + p - \frac{\sigma^2}{16\pi}\right)\frac{d\psi}{dr} + \frac{\sigma^2\sigma_r}{16\pi\sigma}. \tag{5.41}$$

Using (5.35) in (5.40) we have

$$\frac{d\psi}{dr} = \frac{1}{r^2}\left(m + 4\pi r^3 p - \frac{r^3\sigma^2}{8}\right)\left(1 - \frac{2m}{r}\right)^{-1}, \tag{5.42}$$

where obviously, a further term due to the spin appears. Substituting (5.42) in (5.41) we get the generalized Tolmann-Oppenheimer-Volkoff equations with spin in the General Relativity limit:

$$\frac{dp}{dr} = -\frac{1}{r^2}\left(\rho + p - \frac{\sigma^2}{16\pi}\right)\left(m + 4\pi r^3 p - \frac{r^3\sigma^2}{8}\right)\left(1 - \frac{2m}{r}\right)^{-1} + \frac{\sigma^2\sigma_r}{16\pi\sigma}. \tag{5.43}$$

If the spin is zero, then the (5.43) is equivalent to (5.37). Now we consider the effective quantities for density and pressure defined in (5.28). In this case we have

$$\rho^* = \rho - \frac{\sigma^2}{32\pi}, \quad p^* = p - \frac{\sigma^2}{32\pi} \tag{5.44}$$

and we obtain the Tolmann-Oppenheimer-Volkoff equations and the conservation equation of the (5.33)(5.34), for $f(R) = R$, in the form

$$\frac{d\lambda}{dr} = \frac{e^{2\lambda}[8\pi r^2\rho^* - 1] + 1}{2r}, \tag{5.45}$$

$$\frac{d\psi}{dr} = \frac{e^{2\lambda}[8\pi r^2 p^* + 1] - 1}{2r}, \tag{5.46}$$

$$\frac{dp^\star}{dr} = -(\rho^* + p^*)\frac{d\psi}{dr}. \tag{5.47}$$

Using (5.35) in (5.46) we have

$$\frac{d\psi}{dr} = \frac{1}{r^2}\left(m + 4\pi r^3 p^*\right)\left(1 - \frac{2m}{r}\right)^{-1}. \tag{5.48}$$

Substituting (5.48) in (5.47) the classic Tolmann-Oppenheimer-Volkoff equations written as in [52] but with the effective quantities, i.e.

$$\frac{dp^\star}{dr} = -\frac{1}{r^2}\left(\rho^* + p^*\right)\left(m + 4\pi r^3 p^*\right)\left(1 - \frac{2m}{r}\right)^{-1}, \tag{5.49}$$

always in units where $G = 1 = c$. Hence, the equations written in the previous sections are valid to describe any stellar structure in the extreme field regimes choosing the appropriate boundary conditions and suitable equations of state [31; 193; 201].

In the next chapter, we solve numerically the Tolman-Oppenheimer-Volkoff equations, for the Starobinsky model considering both theories and perfect fluids with a suitable choice of the equations of state of dense matter. We will plot the Mass-Radius diagrams for a Neutron Star and calculate its stellar parameters. We will make a comparison between the theories and we will see how, in both cases, it is possible to obtain stable stellar configurations, not justified by General Relativity, that are compatible with the recent observations of Neutron Stars that exceed the Chandrasekhar's limit, i.e. $1.44 M_\odot$. Since the Tolman-Oppenheimer-Volkoff equations are strongly non-linear, the case with spin fluids will be studied in future works because, with a further degree of freedom due to spin, the non-linearity is even stronger.

Chapter 6

The Mass-Radius relation for Neutron Stars in $(R + \alpha R^2)$-gravity: a comparison between the purely metric and the torsion theory.

Summary

In this chapter, within the framework of the Starobinsky model, we study realistic models of Neutron Stars. By numerically solving modified Tolman-Oppenheimer-Volkoff equations, we investigate the Mass–Radius relation in both purely metric and the torsion theory. In particular, we observe that the torsion effects are seen to decrease the compactness and total mass of the Neutron Stars, therefore mimicking the effects of a repulsive massive field. The opposite occurs in the metric theory, where mass and compactness tends to increase, thus inducing, in

both theories, an excess of mass that overtakes the standard General Relativity limit.

6.1 The $f(R) = R + \alpha R^2$ model

We consider here the specific form of $f(R)$:

$$f(R) = R + \alpha R^2, \tag{6.1}$$

where α is the coupling parameter of the quadratic curvature correction. This model is specially suitable to account for cosmological inflation, where higher-order curvature terms naturally lead to cosmic accelerated expansion. The quadratic term emerges in strong gravity regimes, while on Solar System scales and more in general in the weak field regime, the linear term predominates.

This statement can be easily demonstrated because any analytic $f(R)$ model, in the weak field limit, presents a Yukawa-like correction in the gravitational potential except $f(R) = R$. As shown in [202; 203], such a correction is relevant at very large scales (e.g. at galactic scales and beyond [36]) with respect to Solar System and does not affect classical experimental constraints of General Relativity. As a consequence, R^2 terms are relevant only in the strong field regime.

Since the interior of a Neutron Star presents very similar conditions to those that an early universe could have had, the model (6.1) is particularly suited to our considerations. In this model, eqs. (5.4), (5.5) and (5.8) take the explicit form:

$$\frac{d\lambda}{dr} = \frac{e^{2\lambda}[16\pi r^2\rho - 2 - \alpha R(r^2R + 4)] + 4\alpha(r^2R_{,r} + 2rR_r + R) + 2}{4r\left[1 + \alpha(2R + rR_r)\right]}, \tag{6.2}$$

$$\frac{d\psi}{dr} = \frac{e^{2\lambda}[16\pi r^2 p + 2 + \alpha R(r^2 R + 4)] - 4\alpha(2rR_r + R) - 2}{4r\left[1 + \alpha(2R + rR_r)\right]}, \tag{6.3}$$

$$\frac{d^2R}{dr^2} = R_r\left(\lambda_r + \frac{1}{r}\right) + \frac{1 + 2\alpha R}{2\alpha}\left[\frac{1}{r}\left(3\psi_r - \lambda_r + \frac{2}{r}\right) - e^{2\lambda}\left(\frac{R}{2} + \frac{2}{r^2}\right)\right], \tag{6.4}$$

while eqs. (5.15), (5.16) and (5.18) become respectively:

$$\frac{d\lambda}{dr} = \frac{e^{2\lambda}[16\pi r^2\rho - 2 - \alpha R(r^2R + 4)] + 4\alpha r^2\left[R_{,r} + \frac{2R_r}{r} + \frac{R}{r^2} - \frac{3\alpha R_r^2}{2(1+2\alpha R)}\right] + 2}{4r\left[1 + \alpha(2R + rR_r)\right]} \tag{6.5}$$

$$\frac{d\psi}{dr} = \frac{e^{2\lambda}[16\pi r^2 p + 2 + \alpha R(r^2R + 4)] - 4\alpha r^2\left[\frac{2R_r}{r} + \frac{R}{r^2} + \frac{3\alpha R_r^2}{2(1+2\alpha R)}\right] - 2}{4r\left[1 + \alpha(2R + rR_r)\right]}, \tag{6.6}$$

$$\begin{aligned}\frac{d^2R}{dr^2} = \quad & R_r\left(\lambda_r + \frac{1}{r}\right) - \frac{1 + 2\alpha R}{\alpha}\left[\frac{1}{r}\left(3\psi_r - \lambda_r + \frac{2}{r}\right) - e^{2\lambda}\left(\frac{R}{2} + \frac{2}{r^2}\right)\right] - \\ & R_r^2\left(\frac{3\alpha}{1 + 2\alpha R} + \frac{3\psi_r}{R_r} + \frac{9}{rR_r}\right).\end{aligned} \tag{6.7}$$

In the next section, we shall discuss numerical solutions for the interior space–time of spherically symmetric Neutron Stars in both purely metric and torsional $f(R) = R + \alpha R^2$-gravity. Our intent is to propose a comparison between the solutions of the above differential equations that emerge from the two different theories.

In view of this, it is worth noticing that, in vacuo, $(R + \alpha R^2)$-gravity with torsion amounts to General Relativity [175; 190]. Therefore, under the assumption of spherical symmetry, in the case with torsion the space–time outside the

star must necessarily coincide with the Schwarzschild one. In order to better perform the comparison between the two theories, it seems then reasonable and consistent assuming Schwarzschild as the space–time outside the star also in the purely metric theory. Note that Schwarzschild space–time is actually a vacuum solution for purely metric $(R+\alpha R^2)$-gravity [204; 205].

Therefore, in order for given interior solutions be viable, at their boundary they have to match with the exterior Schwarzschild space–time. In this regard, we recall that junction conditions for $f(R)$-gravity have been studied in [206] for the purely metric formulation, and in [207] for the theory with torsion. Referring the reader to [206; 207] for more details, in the present context the junction conditions at the stellar radius result to be:

$$\lambda \in C^0, \quad \psi \in C^1, \quad R \in C^1 \qquad \text{in the purely metric theory} \tag{6.8}$$

$$\lambda \in C^0, \quad \psi \in C^1, \quad \frac{dR}{dr} \in C^0 \qquad \text{in the torsional theory} \tag{6.9}$$

where outside the star λ, ψ and R refer to the corresponding Schwarzschild quantities. Eqs. (6.8) and (6.9) are the conditions at the stellar radius to be satisfied by the numerical solutions we shall investigate in the next sections.

6.2 Numerical aspects of the stellar structure equations in $(R+\alpha R^2)$-gravity

The Tolman-Oppenheimer-Volkoff equations presented in Sec. 5.1 together with an equation of state form a closed system of equations that can be solved numerically once a suitable set of initial conditions are provided. The equations of state accounts for the behavior of the matter fields in the Neutron Star at nuclear level

but also dominating the Neutron Star macroscopic properties as the total mass $\mathcal{M}$, radius $\mathcal{R}_S$ and compactness $\mathcal{C} = \mathcal{M}/\mathcal{R}_S$. The total mass $\mathcal{M}$ and the radius $\mathcal{R}_S$ may vary significantly depending on the state of the matter at the Neutron Star interior where $C \approx [0.02, 0.25]$, being $C = 0.5$ the black hole solution. On the other hand, the knowledge of the macroscopic properties provides a direct insight to understand the particle interactions, energy transport and state of the matter in the Neutron Star core. Until recently, there were placed only vague constraints on the equations of state of Neutron Stars from electromagnetic observations [208]. The recent LIGO-Virgo Binary Neutron Star observation has significantly clarified the state of the art concerning the equations of state physics. The largest accuracy of the Gravitational Waves channel in relation to the electromagnetic observations, has allowed to rule out stiffer solutions (less compact) thus reducing significantly the number of astrophysically relevant equation of state. In this section we discuss some aspects of the numerical solution of the The Tolman-Oppenheimer-Volkoff equations in the metric and torsional $f(R)$ formulations described above, for four equations of state compatible with the recent LIGO constraints: APR4, MPA1, SLy, WFF1 [209; 210; 211; 212], accurately described the piecewise polytropic fits provided in [213].

Then, to solve numerically the The Tolman-Oppenheimer-Volkoff equations, we use a dimensionless version of the them by re-scaling our physical variables as

$$r \to r/r_g, \qquad R \to R/r_g^2, \qquad p \to P/P_0, \qquad \rho \to \rho/\rho_0\,, \tag{6.10}$$

where

$$r_g = GM_\odot/c^2, \qquad P_0 = M_\odot c^2/r_g^3, \qquad \rho_0 = M_\odot/r_g^3\,, \tag{6.11}$$

and $M_\odot$ is the mass of the sun, r_g is the gravitational radius ($\simeq 1.5km$), G Newton's Gravitational constant and c the speed of light. The two systems of

differential equations shown in Subsection 6.1 take the following form,

$$p' = f_1(\rho, p, \psi', r), \quad \lambda' = f_2(\lambda, R, R', R'', \rho, r), \quad \psi' = f_3(\lambda, R, R', p, r) \tag{6.12}$$

and

$$R'' = f_4(\lambda, \lambda', \psi', R, R', \rho, r), \quad p = f_5(\rho)\,, \tag{6.13}$$

where the *primed* variables denote radial derivatives. Therefore, we are left to setup five initial conditions for the variables $\{p(0), \lambda(0), \psi(0), R(0), R'(0)\}$ to complete the numerical scheme. Initial conditions are chosen at the center of the star $r = 0$ in order to preserve regularity, thus preventing the generation of large gradients that may lead to numerical instabilities. Mathematically this involves that any expansion around the Neutron Star center must have a zero first derivative. In particular, the scalar curvature at the Neutron Star center may be expanded as,

$$R(r \to 0) \approx R(0) + R'(0)r + \frac{1}{2}R''(0)r^2\,, \tag{6.14}$$

where regularity involves $R'(0) = 0$. Pressure and density at the center $\rho(0) = \rho_c$ and $p(0) = p_c$ are given by the equation of state so they only depend on the type of fluid under consideration. For the metric potential λ is natural to fix $\lambda(0) = 0$, analogously to what happens in Newtonian gravity, where the $\lambda(r)$ and $\psi(r)$ variables are matched to the $m(r)$ mass of the system by,

$$e^{2\lambda(r)} = \left(1 - 2\frac{m(r)}{r}\right)^{-1}, \qquad e^{2\psi(r)} = \left(1 - 2\frac{m(r)}{r}\right). \tag{6.15}$$

Notice that the variable $\psi(r)$ does not enter directly in our system of differential equations which implies that $\psi(0)$ can be defined up to any arbitrary constant. Therefore we adjust $\psi(0)$ conveniently to match (i) the internal solu-

tions with the external Schwarzschild solution at the stellar radius $\mathcal{R}_S$ and (ii) to obtain asymptotically the $\mathcal{O}(r^{-1})$ profile as,

$$\lambda(r\to\infty)\approx\frac{M}{r},\qquad \psi(r\to\infty)\approx-\frac{M}{r},\qquad \rho(r\to\infty)=0,\qquad p(r\to\infty)=0\,. \tag{6.16}$$

The star radius is ideally defined where the pressure $p(\mathcal{R}_S)\approx 0$ though, in practice, and for numerical reasons, is sufficient to set a ground value ϵ as $p(\mathcal{R}_S)/p_c\leq\epsilon\sim 10^{-10}$.

The fulfillment of eqs. (6.16) require to find an optimal choice for the Ricci scalar $R_c=R(0)$. In general, this is achieved by shooting the central value R_c within some sufficiently large range $[R_c^{min},R_c^{max}]$, containing the true value R_c. Then R_c is found by applying bijection root-finding methods until eqs. (6.16) are satisfied up to numerical tolerance. Unfortunately, the existence of such R_c strongly depends on the particular form of the $f(R)$ model, giving rise to ghosts in case of ill-defined configuration of the model parameters. This is true for both metric and torsional $R+\alpha R^2$-theories, matter of study of this thesis. Then we choose the sign of α to be the one that better matches the junction conditions at the surface of the star (6.8)(6.9) for the metric and torsional theory respectively. As we evince in the following sections, the only choices that reproduce not blowing up solutions are $\alpha>0$ for the metric case and $\alpha<0$ for the torsion one. Unfortunately, these choices generate of some typical tachyonic oscillations due to the fact of a bad behaved $f''(R)$ [214] and that we could not remove numerically. This effect was also reported in [215], thus also showing an oscillatory behavior in a form of a damped-sinusoid outside the star even in the minimally perturbed scenario with $\alpha\ll 1$. These oscillations grow as the value of α increases and they are as well propagated to our metric potentials $\lambda(r)$ and $\psi(r)$. This inserts some ambiguity in defining the asymptotic conditions (6.16) at large r since the oscil-

lations are not totally vanished when the numerical noise begins to dominate the solution (at $r \sim 100$). To overcome this issue and to reduce the amplitude of the oscillations, we restrict our analysis to small values of $\alpha \in [0.001, 0.1]$. As this is anyway consistent with current observational tests, doing so we are not discarding any relevant astrophysical scenario and that also allow us to set $R_c \approx R_{GR}$. This hypothesis is shown to have a minimal impact in the $\mathcal{M} - \mathcal{R}$ diagrams as we discuss throughout next sections. Moreover, the assumption of a Schwarzschild-type solution outside the star allows us to smooth out these oscillations and to recover a good fulfillment of the junction conditions. Given all that, we justify the choice of $\alpha > 0$ for the metric theory and $\alpha < 0$ for the torsional one.

Finally, the two systems of ordinary differential equations are solved by using a $8th$-order Runge-Kutta with adaptive step-size and high-stiffness control methods implemented in the `Wolfram Mathematica` package [216]. These methods regulate the discretization step-size by estimating the error of the Runge-Kutta method point by point ensuring the numerical convergence of the solution step by step. The stiffness control methods use polynomial extrapolation on the short regimes where the gradients get too large. We have found these methods essential to ensure the accuracy of the solutions in the torsional formulation.

6.3 Numerical solutions

We compute the $\mathcal{M} - \mathcal{R}$ diagrams for metric and torsional formulations of $R+\alpha R^2$ gravity. Due to the numerical limitations found throghout our analysis, we restrict $|\alpha| \in [0, 0.1]$ where α is required to be positive for the purely metric theory and negative in the theory with torsion to avoid blowing up solutions [215]. These values are anyway consistent with solar system tests of General Relativity [215; 217]. Such tests fix light constraints on the form $f(R) \lesssim 10^{-6}$ rather than on the param-

eter α, thus being translated as $R+|\alpha|R^2 \lesssim 10^{-6}$. Bearing in mind that curvatures themselves are expected to be small, all this leaves the parameter α rather unconstrained. Other tests as Eöt-Wash laboratory experiment set $\alpha \lesssim 10^{-10}m^2$. On the contrary, there exist alternative observational space-based constraints coming from the Gravity Probe B experiment [218] or the observation of the binary pulsar PSR J0737-3039 [219; 220] that set $\alpha \lesssim [5 \times 10^{11}, 2.3 \times 10^{15}]m^2$. Therefore, the discrepancies among the several experiments do not set tight bounds on the value of α, and our choice seems to be compatible with existing data.

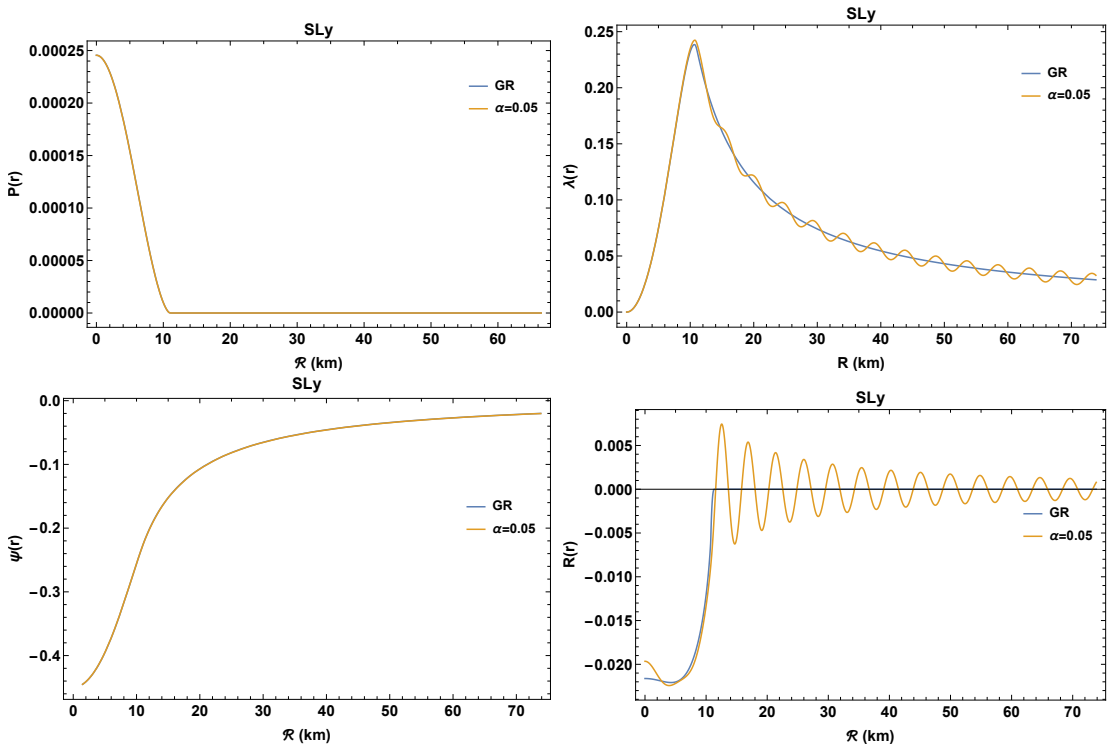

Figure 6.1: Solutions of The Tolman-Oppenheimer-Volkoff equations for General Relativity (blue) and purely metric $R + \alpha R^2$ with $\alpha = 0.05$ (orange), using the SLy equation of state. All the plotted quantities show small deviations with respect to General Relativity. Note the asymptotic decay of the metric potentials λ and ψ as $r \to \infty$. Our choice of α explains the oscillatory behavior as reported in [215].

6.3.1 Purely metric theory

The solutions of the Tolman-Oppenheimer-Volkoff equations for the purely metric $f(R) = R + \alpha R^2$ model are illustrated in Fig. 6.1. The pressure at the center of the star p_c drops quickly until it eventually gets equal to zero, thus defining the radius of the star $\mathcal{R}_S$. This radius is used as our reference point to compute the total mass $\mathcal{M}$ by means of eq. (6.15). The numerical system exhibits

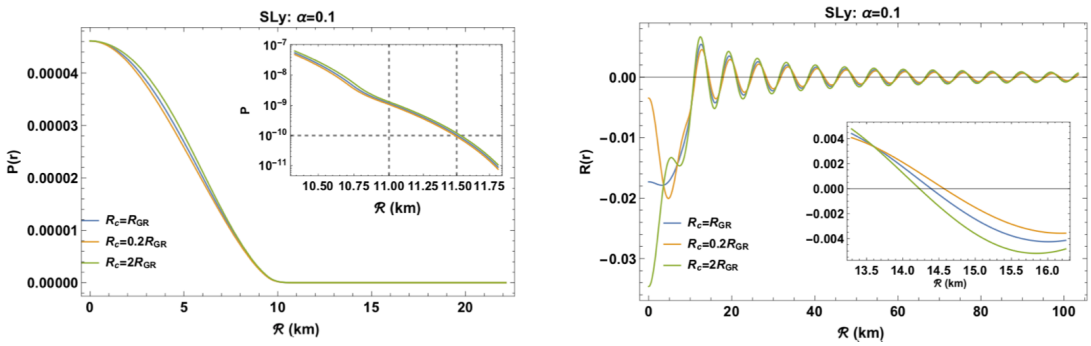

Figure 6.2: Profiles for the pressure P (left) and the Ricci scalar R (right) corresponding to $R_c = \{R_{GR_c}, 0.2R_{GR_c}, 2R_{GR_c}\}$ for the $f(R) = R + \alpha R^2$ model with $\alpha = 0.1$. In the zoomed-in plot for the pressure, the grid lines fix two possible values for the radius of the star $\mathcal{R}_S$ that depend on to the accuracy chosen in defining its position as: $p(\mathcal{R}_S)/pc \leq \{10^{-9}, 10^{-10}\}$ providing a relative difference of about 4%. Complementary, on the right hand side plot we show the $R = 0$ point for different choices of the central value R_c. Notice that on the latter the effects of choosing one or another R_c contribute in total about the $\sim 2\%$ between $0.2R_{GR_c}$ and $2R_{GR_c}$ choices thus this error being smaller than the our error estimate in defining $\mathcal{R}_S$.

some dissipative oscillations about the Ricci scalar R and the metric potential λ. These oscillations naturally arise from the harmonic-form of the Ricci scalar $R(r)$ equation in vacuum [215], for a non optimal choice of the Ricci scalar R_c at the center of the star, and where optimal choice is here defined as that matching the Schwarzschild junction conditions at the stellar radius. Unfortunately, such a choice becomes increasingly difficult as α tends to zero since the system

of equations become also stiffer [221]. Generally speaking, this may appear to be counterintuitive, since $\alpha \to 0$ should exactly recover the General Relativity space-time. However the asymptotic approach to $\alpha \to 0$ of the Ricci scalar equations (6.4)(6.7) are ill-defined. This is clear if, for instance, one re-expresses (6.4) as,

$$R'' = -\frac{e^{2\lambda}\left(8\pi(\rho - 3p) + R\right)}{6\alpha} - R'\left(-\lambda' + \psi' + \frac{2}{r}\right) . \tag{6.17}$$

Notice that the numerator of the first term is exactly zero in General Relativity and that ideally approaches to zero faster than to linear order in α. However, this is not so exact when dealing with numerical uncertainties, where the same factor may behave as a $\sim 0/0$ solution for $\alpha << 1$ thus requiring much more precision on the estimation central value R_c. To overcome this issue, we have set $R(0) = R_{GR} = 8\pi(3p_c - \rho_c)$ to the General Relativity value. Though this seems apparently an arbitrary choice, we notice that for $\alpha \lesssim< 1$ the solution must be close to that of General Relativity so the value can not be further to that of General Relativity. This is self-evident from Fig. 6.2, where in the right plot we illustrate the variations on the pressure $p(r)$ and the Ricci scalar $R(r)$ for different choices of the central value $R_c = \{R_{GR_c}, 0.2R_{GR_c}, 2R_{GR_c}\}$. Then, notice than the effect of varying R_c on the radius $\mathcal{R}$ for such small values of α is about $\sim 2\%$ considering the maximum and minimum choices of R_c. This variation is then compared with the uncertainty arising from the definition of the star radius $\mathcal{R}_{\rm s}$ to be the place where the pressure drops by a factor ϵ. Then, in the left plot we show that the impact of relaxing this value to $\epsilon \sim 10^{-9}$ would generate an uncertainty of about the 4%, thus larger than the one from varying R_c.

In Fig. 6.3, we show the behavior of the metric potentials $\lambda(r)$ and $\psi(r)$ and the derivatives $R'(r)$ and $\psi'(r)$ paying special attention to: (i) the junction conditions at the Neutron Star boundary and (ii) their profiles as $r \to \infty$. We show the full numerical solution (blue line), its corresponding Schwarzschild solution

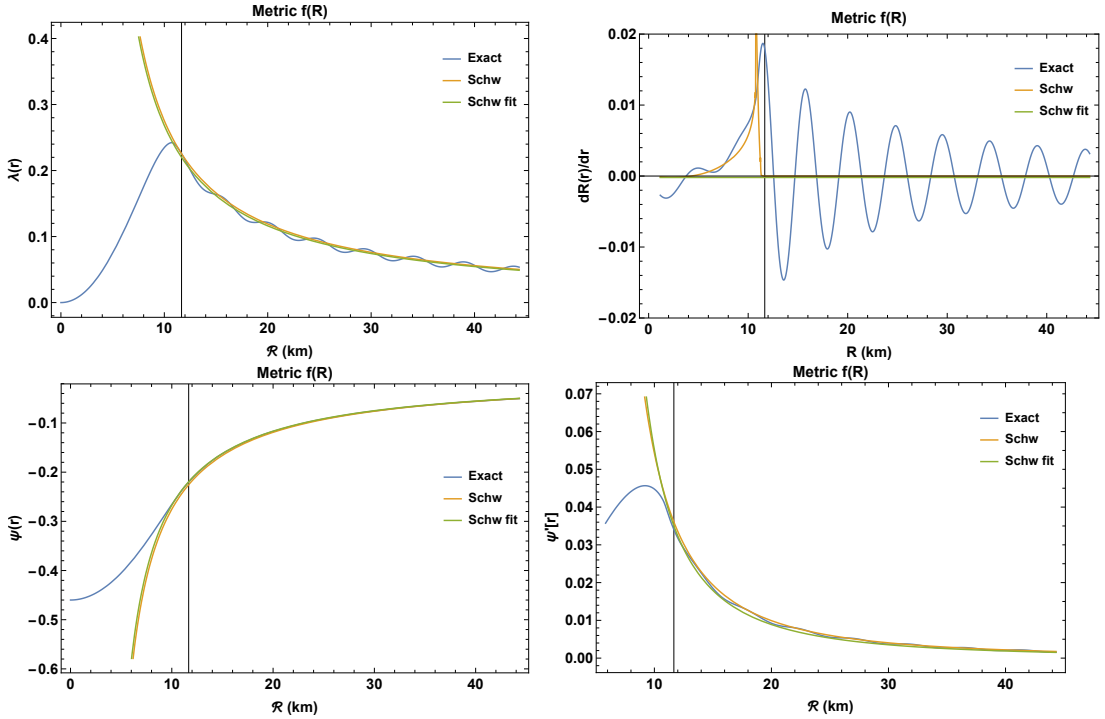

Figure 6.3: Results of our analysis with $\alpha = 0.05$ for λ and ψ (left plots) and the derivatives for R' and ψ' (right plots) for the exact numerical solution (blue line); the Schwarzschild solution (orange line) with mass $\mathcal{M} = 1.43\mathcal{M}_\odot$; a Schwarzschild fit (green line) to the numerical data outside the star, that is, with $\mathcal{R} > 11.6km$. We note that, for α small and averaging out all the oscillations, all physical quantities reproduce rather well the Schwarzschild solution outside the star, while matching as well the junction conditions (6.8). From the fitted results we get $\mathcal{M} = 1.40\mathcal{M}_\odot$, thus very close to the theoretical one.

(orange line) given by eqs. (6.15) with $M = 1.43M_\odot$ and the result of fitting the exterior data to the same Schwarzschild-like ansatz in order to quantify the agreement with the Schwarzschild space-time outside the star and which results in a Neutron Star with total mass $M = 1.40M_\odot$. The good agreement between the three lines confirms that the solution is well approximated by the Schwarzschild solution right outside the star radius by better than $\sim 2\%$. This good match is also extended to their derivatives thus globally satisfying the necessary junction conditions of eqs. (6.8) once the oscillations are averaged out. On the other

hand, since the oscillations do not appear on $\psi(r)$, we choose this quantity more appropriated to define the Neutron Star mass $\mathcal{M}$.

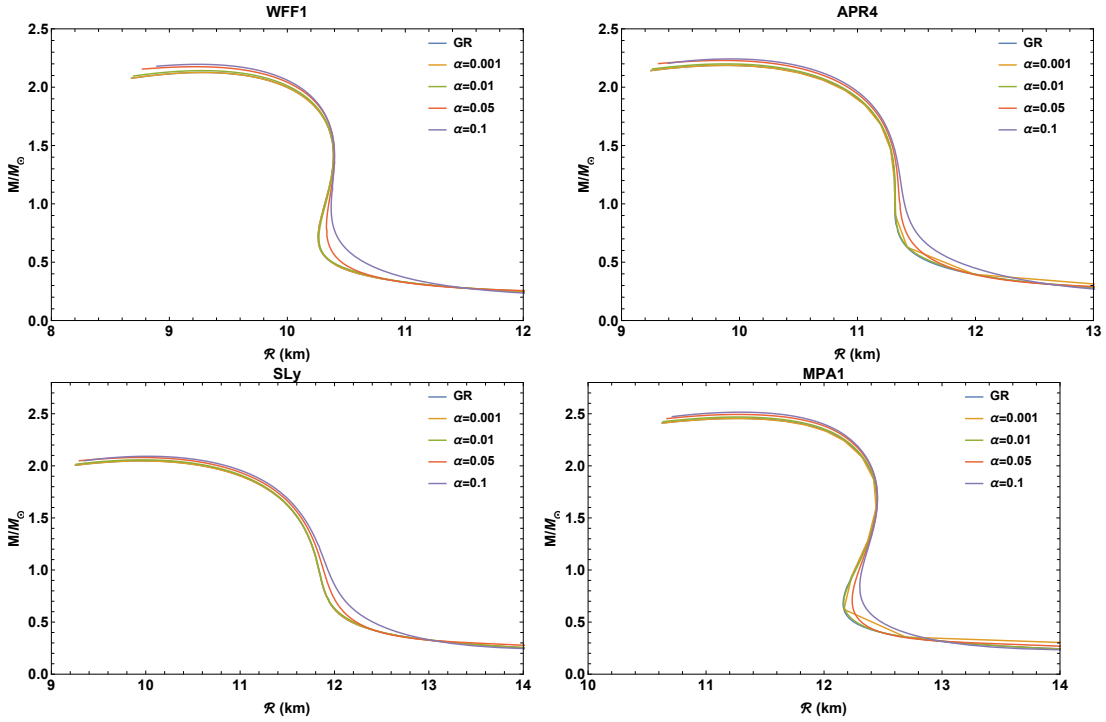

Figure 6.4: $\mathcal{M}-\mathcal{R}$ relations obtained within the purely metric formalism with $\alpha = \{0, 0.001, 0.01, 0.05, 0.1\}$ for the four equations of state considered in this thesis. Note the general increase of the total mass as the quadratic term takes larger values, thus favoring the formation of more massive objects than in standard General Relativity.

Finally, in Fig. 6.4, we show the $\mathcal{M}-\mathcal{R}$ diagrams for the four equations of state considered in this thesis. For each choice of the central density ρ_c we get a different estimate of the radius $\mathcal{R}_S$ and the total mass $\mathcal{M}$. We loop over ρ_c until $d\mathcal{M}/d\mathcal{R} = 0$ which defines the unstable branch, i.e. the point at which the Neutron Star is expected to collapse to a Black Hole and that provides the maximum allowed mass $\mathcal{M}_{max}$ for the given equation of state. Note that for all the equations of state considered, the total mass tends to increase with respect to General Relativity as in [17; 221]. This is because gravity becomes stronger,

thus allowing more massive systems. Indeed, in the $R + \alpha R^2$ scenario, Newton's gravitational constant G is replaced by

$$G \to G_{eff} = \frac{G}{f'(R)} = \frac{G}{1 + 2\alpha R}\,. \tag{6.18}$$

The combined conditions of $\alpha > 0$ and $R < 0$ imply then $G_{eff} > G$, thus generating a more *attractive* gravity.

6.3.2 Torsion Theory

We repeat the analysis for the torsional $f(R) = R+\alpha R^2$ theory. Although further models have been also considered in the literature, the numerical complexity of the torsional equations makes difficult a full exploration of other kinds of $f(R)$ functions. This issue becomes more relevant when considering the torsional theory with spin [188], where spin gradients add higher order derivatives to our system of equations that increase the stiffness of the numerical system. We plan to extend our study in the presence of spin matter in a forthcoming work.

In Fig. 6.5, we repeat the same Schwarzschild-based tests than for the metric formalism for $\alpha = 0.05$. In this case, the total mass $\mathcal{M} = 1.37\mathcal{M}_\odot$ is slightly diminished with respect to the metric case. Notice that the Schwarzschild solution is as well verified at the star radius $\mathcal{R}_s$, where the metric $\lambda(r)$ is clearly C^0 and $\psi(r)$ still preserves the C^1 condition. Outside the star, and once the oscillations are vanished, the metric functions λ and ψ still preserve the $1/r$ decay.

In Fig. 6.6, we show the results we obtained for the theory with torsion, using the same range for $|\alpha|$ as in the metric case but choosing $\alpha < 0$. In this scenario, we see that the general trend predicts a decreasing of the total mass of the Neutron Star, independently of the equations of state considered. This could be related with the fact that the stable branch of the solutions given by

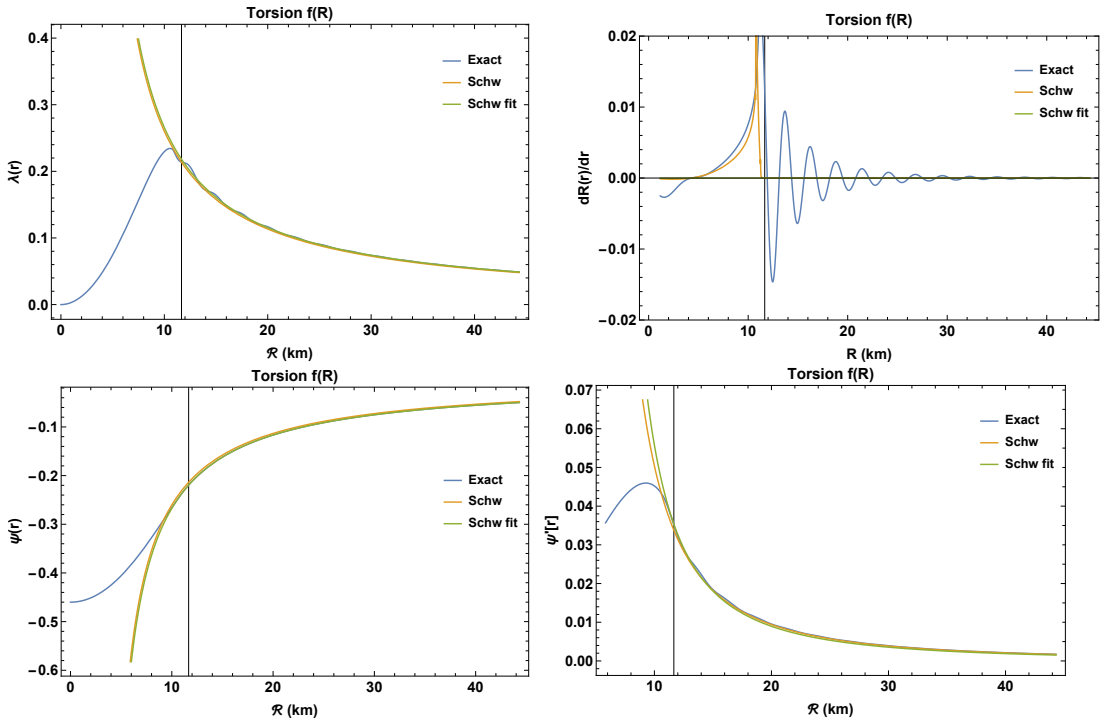

Figure 6.5: Results of the analysis in the torsional case with $\alpha = 0.05$. We show the metric potentials λ and ψ (left plots) and the derivatives for ψ' and R' (right plots) for the exact numerical solution (blue line), the Schwarzschild solution (orange line) and a Schwarzschild fit (green line) to the numerical data outside the star, that is with $\mathcal{R} > 11.6km$. Notice that once the oscillations are averaged out, all the distributions satisfy (up to numerical accuracy) the junction conditions.

the signature of α is reversed with respect to the purely metric case, in order to avoid for ghosts. However, the estimates for the total mass and radius are still compatible with the astrophysical observations [4], thus not allowing us to rule out any of the models studied here. On the other hand, if we further increase $|\alpha|$ the errors generated by eq. (6.7) and propagated to the total mass $\mathcal{M}$ and the total radius $\mathcal{R}_S$ become too large. Therefore, we restrict the our analysis to $|\alpha| \leq 0.1$.

Finally, in Fig. 6.7, we compare the different predictions obtained in the purely metric and the torsional formulation respectively, for $\alpha = 0.1$. Note that,

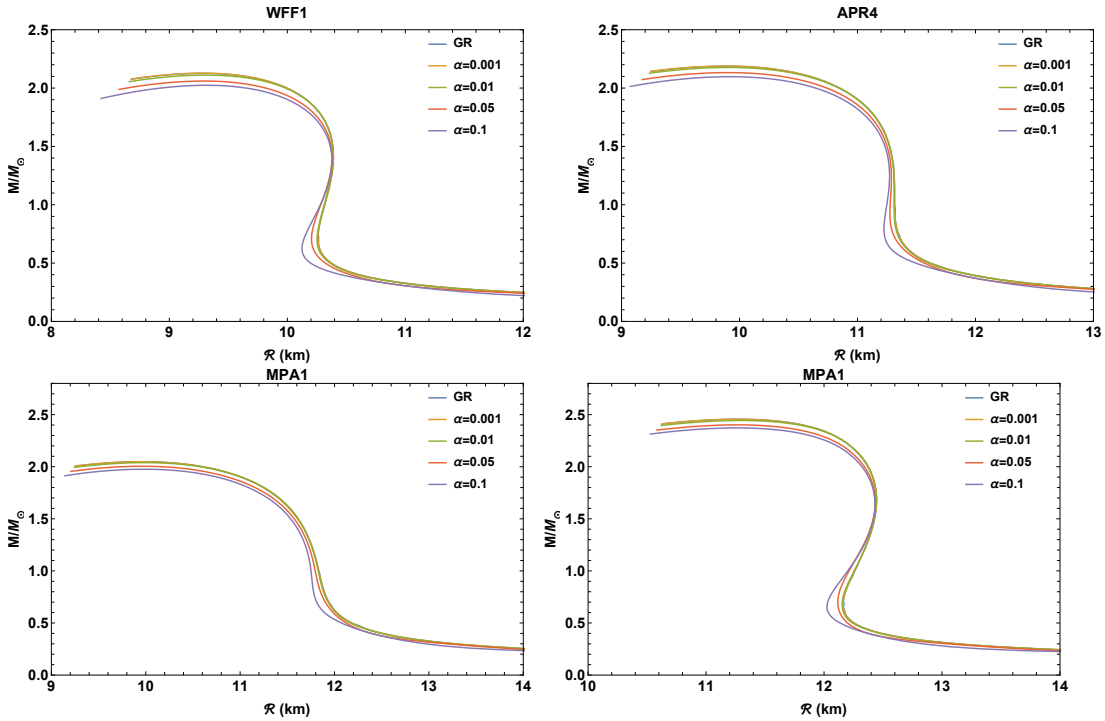

Figure 6.6: Analogous $\mathcal{M}-\mathcal{R}$ relations to those of Fig. 6.4 but here obtained within the torsional formalism. The effect of the torsion tends to decrease the total mass of the Neutron Star, contrary to what occurs in the purely metric case. This is dominantly caused by sign flip on the α-dependent part of eq. (6.7) with respect to eq. (6.4), which actually acts as a repulsive term.

in the theory with torsion though the total mass of the Neutron Star decreases, while increases in relation to the metric case but, in torsion theory, the relative deviations, in absolute value, with respect to General Relativity seem to be larger respect to the metric case. This is caused by the effective repulsion generated by the extra torsional terms (see eq. (6.7)) which induce a partial screening of the gravitational field that prevents to reach Neutron Stars masses as large as in standard General Relativity. This is explicitly shown in Table 6.1, where we show the variation of the maximum mass $\mathcal{M}_{max}$, radius $\mathcal{R}_{max}$ and compactness C for the purely metric and torsional theories respectively, corresponding to the points in the $\mathcal{M}-\mathcal{R}$ diagrams where $dM/d\mathcal{R}=0$. Note that whereas the purely metric

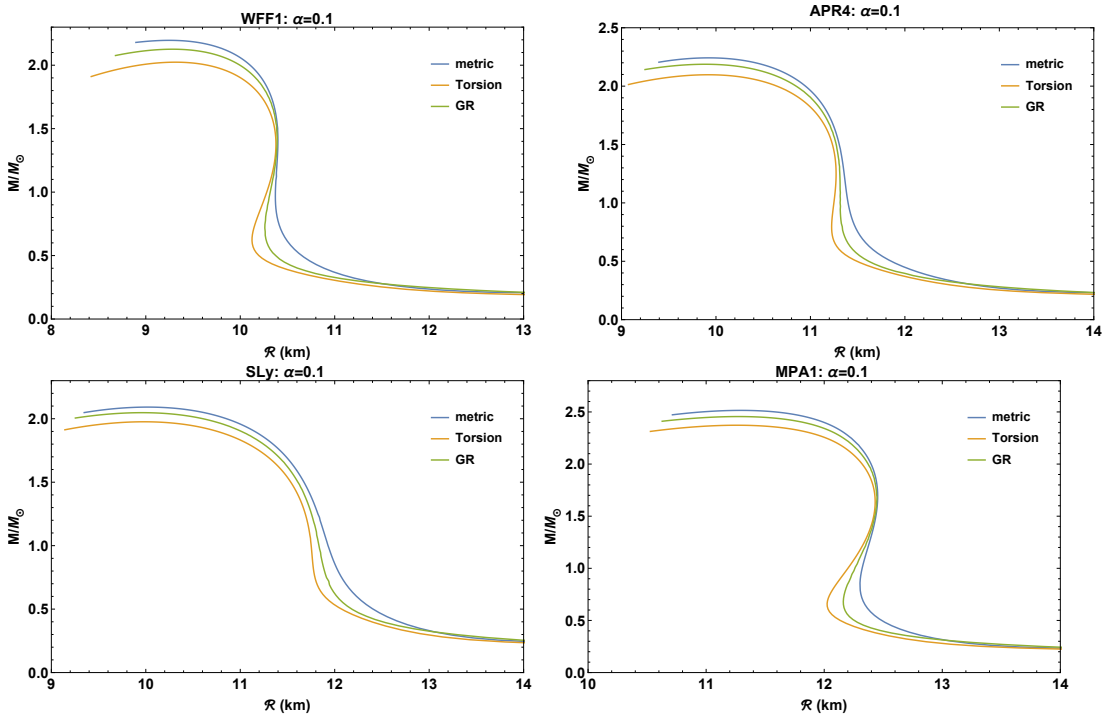

Figure 6.7: $\mathcal{M} - \mathcal{R}$ relations for $\alpha = 0.1$ in GR (blue), metric (green) and torsion (orange) for the four equations of state considered in this thesis. The torsion contributions tend to decrease the total mass of the system.

formulation tends to more massive and compact Neutron Stars, the opposite occurs when considering torsion. Indeed, as the quadratic term in the curvature increases, the effects of torsion counterbalance the increase of total mass. This can be intuitively derived by using the same reasoning as in (6.18) with $\alpha < 0$ and $R < 0$, implying $G_{eff} < G$ and thus generating a less *attractive* gravity.

EoS	$\|\alpha\|$	$M^{(M)}_{max}$ $M_\odot$	$R^{(M)}_{max}$ Km	$C^{(M)}$	$M^{(T)}_{max}$ $M_\odot$	$R^{(T)}_{max}$ Km	$C^{(T)}$
WWF1	0	2.13	9.29	0.23	2.13	9.29	0.23
	0.001	2.13	9.29	0.23	2.13	9.29	0.23
	0.01	2.14	9.28	0.23	2.11	9.30	0.23
	0.05	2.19	9.21	0.24	2.06	9.28	0.22
	0.1	2.20	9.24	0.24	2.02	9.31	0.21
APR4	0	2.19	9.88	0.22	2.19	9.88	0.22
	0.001	2.19	9.91	0.22	2.19	9.88	0.22
	0.01	2.20	9.88	0.22	2.18	9.91	0.22
	0.05	2.23	9.85	0.23	2.13	9.91	0.21
	0.1	2.24	9.92	0.23	2.10	9.91	0.21
SLy	0	2.05	9.97	0.20	2.05	9.97	0.20
	0.001	2.05	9.94	0.20	2.05	9.94	0.20
	0.01	2.06	9.97	0.21	2.04	9.98	0.20
	0.05	2.08	9.94	0.21	2.00	9.96	0.20
	0.1	2.10	10.02	0.21	1.98	9.98	0.20
MPA1	0	2.45	11.28	0.22	2.45	11.28	0.22
	0.001	2.45	11.30	0.22	2.45	11.26	0.22
	0.01	2.47	11.26	0.22	2.44	11.30	0.22
	0.05	2.50	11.28	0.22	2.40	11.26	0.21
	0.1	2.51	11.30	0.22	2.37	11.26	0.21

Table 6.1: Parameters of Neutron Stars for the equations of state considered in this thesis for the α values for the (6.1) models in the metric formalism and in a torsion theory. The case $\alpha = 0$ is the standard General Relativity. $\mathcal{M}_{max}$ and $\mathcal{R}_{max}$ are the maximum values of mass and radius, where $M_\odot$ is the Solar mass. The superscripts stand for the (M) metric formalism and (T) torsional formalism, where $C^{(M)}$ and $C^{(T)}$ refer to the compactness $\mathcal{M}_{max}/\mathcal{R}_{max}$ in units of $M_\odot/Km$.

Chapter 7

Non-minimally coupled condensate cosmologies: matching observational data with phase space

Summary

In this chapter, we compare theoretical predictions with observations for a class of cosmological models in which the dark energy component is modeled as a Fermionic condensate, non-minimally coupled with the gravitational field and characterized by some specific self-interaction potentials. Our analysis will be based on the Markov Chain Monte Carlo Method and employs different data sets. It turns out that, with an appropriate choice of parameters, our models will be fully compatible with several observed data. We will combine these parameter values with phase space analysis to deduce the features of the entire cosmic history of the considered models.

7.1 The $(1+\epsilon(\bar{\psi}\psi))R$-theory in a cosmological metric

For convenience of the reader, we briefly review the main features of the theory proposed in [76]. Making use of natural units ($\hbar = c = k_B = 8\pi G = 1$) for simplicity, let us consider the action functional

$$\mathcal{S} = \int \sqrt{|g|}\left[\left(1+\epsilon(\bar{\psi}\psi)\right)R - \mathcal{L}_D\right] ds, \tag{7.1}$$

in which the Einstein–Hilbert term is non–minimally coupled to the condensate $\bar{\psi}\psi$ associated with a Dirac field. The latter has a Lagrangian of the usual form

$$\mathcal{L}_D = \frac{i}{2}\left(\bar{\psi}\Gamma^i D_i\psi - D_i\bar{\psi}\Gamma^i\psi\right) - m\bar{\psi}\psi + V(\bar{\psi}\psi), \tag{7.2}$$

where a fermionic self–interaction potential $V(\bar{\psi}\psi)$ is present. In eq. (7.1) ϵ indicates a suitable constant parameter, while in eq. (7.2) we have $\Gamma^i := e^i_\mu\gamma^\mu$, γ^μ representing Dirac matrices and e^μ_i a tetrad field such that the metric tensor can be expressed as $g_{ij} = e^\mu_i e^\nu_j \eta_{\mu\nu}$ ($\eta_{\mu\nu} = \text{diag.}(1,-1,-1,-1)$); D_i denotes the covariant derivative of the spinor field

$$D_i\psi = \partial_i\psi - \Omega_i\psi, \qquad D_i\bar{\psi} = \partial_i\bar{\psi} + \bar{\psi}\Omega_i, \tag{7.3}$$

where

$$\Omega_i = -\frac{1}{4}g_{ij}\left(\Gamma_{pq}^{\ \ j} - e^j_\mu\partial_p e^\mu_q\right)\Gamma^p\Gamma^q, \tag{7.4}$$

are the spin covariant derivative coefficients associated with the Levi–Civita connection $\Gamma_{pq}^{\ \ j}$.

Some remarks are here in order on the nature of the fermion field we are considering [222; 223; 224]. Our approach is entirely classical, ψ denoting a set

of four complex–valued spacetime local functions which transform according to the spinor representation of the Lorentz group. This means that, rather than an actual fermion field, ψ can be though to represent macroscopic objects made of fermions (see e.g. [69]). Indeed, as we are considering cosmic eras in which particles are non-relativistic, a second quantization fermion field would not really be compatible with our assumptions. On top of this, we are restricting specifically to the case in which such fermion field is a condensate and it is known that in this case a classical description of the field is able to capture all the key properties of the quantum field [69].

As a consequence, our Dirac action and the resulting matter field equations do not necessarily have to satisfy the same properties as those in quantum field theory. This applies, for example to the issue of renormalizability. As a matter of fact, if we were to insist considering ψ a quantum field, we could ask if the presence of the self-interaction potential and even more the non-minimal coupling can make the Dirac equations non–renormalizable. In this regards, in Section 7.3 we shell consider three different potentials (see subsequent Eqs. (7.33), (7.34), (7.35)). In particular, in the minimal coupled theory the potentials (7.33) and (7.35) would be renormalizable respectively for $\alpha < \frac{4}{3}$ and $\gamma < \frac{2}{3}$, while potential (7.34) would be always renormalizable. Instead, the real problem lays, at least in the purely metric theory, in the non–renormalizable terms generated by the non-minimal coupling. A possible way out of this problem would be to introduce torsion. Indeed, following the procedure given in [225] and according to Wilson's analysis of renormalizability, it is easy to see that in the theory with torsion the presence of non-minimal coupling leads always to renormalizable actions, provided that the considered potentials have the values of α and γ in the intervals mentioned above. We will see that the values we will obtain for these parameters belong to these intervals.

Making use of the notation $\varphi := \bar{\psi}\psi$, from the the action (7.1) we derive Einstein–like and Dirac equations respectively of the form

$$(1+\epsilon\varphi)\left(R_{ij}-\frac{1}{2}Rg_{ij}\right)=\Sigma_{ij}+\epsilon\left(\nabla_i\nabla_j\varphi-g_{ij}g^{pq}\nabla_p\nabla_q\varphi\right), \tag{7.5}$$

and

$$i\Gamma^i D_i\psi - m\psi + V'(\varphi)\psi - \epsilon\psi R = 0, \tag{7.6a}$$

$$iD_i\bar{\psi}\Gamma^i + m\bar{\psi} - V'(\varphi)\bar{\psi} + \epsilon\bar{\psi}R = 0, \tag{7.6b}$$

where

$$\Sigma_{ij}=\frac{i}{4}\left(\bar{\psi}\Gamma_{(i}D_{j)}\psi-D_{(i}\bar{\psi}\Gamma_{j)}\psi\right)-\frac{1}{2}\mathcal{L}_D\, g_{ij}, \tag{7.7}$$

is the energy–momentum tensor of the Dirac field and $V' := \frac{dV}{d\varphi}$. For later use, inserting eqs. (7.6) into (7.7), we can express the energy–momentum tensor Σ_{ij} as

$$\Sigma_{ij}=+\frac{i}{4}\left(\bar{\psi}\Gamma_{(i}D_{j)}\psi-D_{(i}\bar{\psi}\Gamma_{j)}\psi\right)-\frac{\epsilon}{2}\varphi R\, g_{ij}-\frac{1}{2}V(\varphi)\, g_{ij}+\frac{1}{2}\varphi V'(\varphi)\, g_{ij}. \tag{7.8}$$

In order to discuss cosmological models arising from the above presented theory, let us consider a spatially flat Friedmann–Lemaître–Robertson–Walker metric tensor

$$ds^2=dt^2-a(t)^2\left(dx^2+dy^2+dz^2\right). \tag{7.9}$$

It is seen that the Einstein–like equations (7.5), evaluated in the metric (7.9), reduce to [76]

$$(1+\epsilon\varphi)3\left(\frac{\dot{a}}{a}\right)^2=\frac{m}{2}\varphi-3\epsilon\frac{\dot{a}}{a}\dot{\varphi}-\frac{1}{2}V(\varphi), \tag{7.10a}$$

$$(1+\epsilon\varphi)\left[2\frac{\ddot{a}}{a}+\left(\frac{\dot{a}}{a}\right)^2\right]=-\frac{\epsilon}{2}\varphi R-\epsilon\ddot{\varphi}-2\epsilon\frac{\dot{a}}{a}\dot{\varphi}-\frac{1}{2}V(\varphi)+\frac{1}{2}\varphi V'(\varphi). \quad (7.10b)$$

We can replace eq. (7.10b) by the equivalent Raychaudhuri equation

$$(1+\epsilon\varphi)6\frac{\ddot{a}}{a}=-\frac{3}{2}\epsilon\varphi R-3\epsilon\ddot{\varphi}-3\epsilon\frac{\dot{a}}{a}\dot{\varphi}-\frac{m}{2}\varphi-V(\varphi)+\frac{3}{2}\varphi V'(\varphi). \quad (7.11)$$

Analogously, in the metric (7.9) the Dirac equations (7.6) assume the expression

$$\dot{\psi}+\frac{3}{2}\frac{\dot{a}}{a}\psi+im\gamma^0\psi-V'(\varphi)\gamma^0\psi+i\epsilon R\gamma^0\psi=0, \quad (7.12a)$$

$$\dot{\bar{\psi}}+\frac{3}{2}\frac{\dot{a}}{a}\bar{\psi}-im\bar{\psi}\gamma^0+V'(\varphi)\bar{\psi}\gamma^0-i\epsilon R\bar{\psi}\gamma^0=0. \quad (7.12b)$$

From eqs. (7.12) we immediately derive the evolution law for the scalar field $\varphi=\bar{\psi}\psi$

$$\dot{\varphi}+3\frac{\dot{a}}{a}\varphi=0, \quad (7.13)$$

yielding the final relation

$$\varphi=\frac{\varphi_0}{a^3}. \quad (7.14)$$

Since $\varphi\to 0$ when the scale factor grows, it is expected that the non-minimal coupling contributions tend to disappear at cosmological late time. For sake of completeness, we can add a perfect fluid to our cosmological model. To this end, we suppose a barotropic perfect fluid assigned, with equation of state $p=w\rho$ ($w\in[0,1[$) and standard conservation law

$$\dot{\rho}+3\frac{\dot{a}}{a}(\rho+p)=0. \quad (7.15)$$

In such a circumstance, the field equations (7.10) and (7.11) become respectively

$$(1+\epsilon\varphi)3\left(\frac{\dot{a}}{a}\right)^2 = \rho + \frac{m}{2}\varphi - \frac{1}{2}V(\varphi) - 3\epsilon\frac{\dot{a}}{a}\dot{\varphi}, \tag{7.16a}$$

$$(1+\epsilon\varphi)\left[2\frac{\ddot{a}}{a} + \left(\frac{\dot{a}}{a}\right)^2\right] = -p - \frac{\epsilon}{2}\varphi R - \frac{1}{2}V(\varphi) + \frac{1}{2}\varphi V'(\varphi) - \epsilon\ddot{\varphi} - 2\epsilon\frac{\dot{a}}{a}\dot{\varphi}, \tag{7.16b}$$

and

$$(1+\epsilon\varphi)6\frac{\ddot{a}}{a} = -(\rho+3p) - \frac{3}{2}\epsilon\varphi R - 3\epsilon\ddot{\varphi} - 3\epsilon\frac{\dot{a}}{a}\dot{\varphi} - \frac{m}{2}\varphi - V(\varphi) + \frac{3}{2}\varphi V'(\varphi). \tag{7.17}$$

Inserting the evolution equation (7.13) for the scalar field and the expression of the Ricci scalar in flat Friedmann–Lemaître–Robertson–Walker spacetime $R = -6\left(\frac{\ddot{a}}{a} + \frac{\dot{a}^2}{a^2}\right)$ into eqs. (7.16) and (7.17), we get the final system of equations

$$3(1-2\epsilon\varphi)\left(\frac{\dot{a}}{a}\right)^2 = \rho + \frac{m}{2}\varphi - \frac{1}{2}V(\varphi), \tag{7.18a}$$

$$6(1-2\epsilon\varphi)\frac{\ddot{a}}{a} = -(\rho+3p) - 18\epsilon\varphi\left(\frac{\dot{a}}{a}\right)^2 - \frac{m}{2}\varphi - V(\varphi) + \frac{3}{2}\varphi V'(\varphi), \tag{7.18b}$$

$$\dot{\varphi} + 3\frac{\dot{a}}{a}\varphi = 0, \tag{7.18c}$$

$$\dot{\rho} + 3\frac{\dot{a}}{a}(1+w)\rho = 0, \tag{7.18d}$$

which represent the starting point of our subsequent analysis.

7.2 Redshift cosmological equations

In this section we rewrite the system of equations (7.18) in terms of redshift z. To start with, let us take the identities $a = \frac{a_0}{1+z}$ and $H = \frac{\dot{a}}{a}$ into account, so that the system (7.18) assumes the form

$$3(1-2\epsilon\varphi)H^2 = \rho + \frac{m}{2}\varphi - \frac{1}{2}V(\varphi), \tag{7.19a}$$

$$6(1-2\epsilon\varphi)(H^2+\dot{H}) = -(\rho+3p) - 18\epsilon\varphi H^2 - \frac{m}{2}\varphi - V(\varphi) + \frac{3}{2}\varphi V'(\varphi), \tag{7.19b}$$

$$\dot{\varphi} + 3H\varphi = 0, \tag{7.19c}$$

$$\dot{\rho} + 3H\,(1+w)\,\rho = 0. \tag{7.19d}$$

From now on we restrict ourselves to a dust filled Universe with $w = 0$ and thus $p = 0$. In this case, the last two equations have exact solutions

$$\varphi(z) = \frac{\varphi_0}{a^3} = \varphi_0(1+z)^3, \tag{7.20}$$

$$\rho(z) = \frac{\rho_0}{a^3} = \rho_0(1+z)^3\,, \tag{7.21}$$

thus implying that the fermion condensate evolves as the dark matter energy density composed of dust fluid. The Eqs. (7.19a), and (7.19b) can be slightly manipulated in order to define the effective pressure and energy density of the

fermion field

$$p_\varphi = -\frac{\varphi\left[(1-2\epsilon\varphi)V'(\varphi) - 2\epsilon\varphi\left(m + \frac{2\rho_0}{\varphi_0}\right)\right] + V(\varphi)(4\epsilon\varphi - 1)}{2(1-2\epsilon\varphi)}, \quad (7.22)$$

$$\rho_\varphi = \frac{m\varphi}{2} - \frac{V(\varphi)}{2}. \quad (7.23)$$

These two expressions allow us to define an effective equation of state w_φ, which drives the behavior of the model in the dark energy dominated era:

$$w_\varphi = -\frac{\varphi\left[(\varphi_0 - 2\epsilon\varphi\varphi_0)\,V'(\varphi) - 2\epsilon\varphi\,(m\varphi_0 + 2\rho_0)\right] + \varphi_0 V(\varphi)(4\epsilon\varphi - 1)}{\varphi_0(1-2\epsilon\varphi)[m\varphi - V(\varphi)]}\,. \quad (7.24)$$

Now we can interpret the fermion condensate as the source of an effective Λ *term* Λ_{eff}, by defining $\Lambda_{eff} = \frac{\rho_\varphi}{F}$, being $F(\varphi) = (1-2\epsilon\varphi)$, and the effective gravitational constant as $G_{eff} = \frac{1}{F}$. With these definitions, the Eqs. (7.19a) and (7.19b) can be rewritten in terms of ρ_φ and p_φ as

$$3H^2 = G_{eff}\rho_m + \Lambda_{eff}\,, \quad (7.25)$$

$$2\dot{H} + 3H^2 = -G_{eff}p_\varphi\,. \quad (7.26)$$

Introducing the standard Ω parameters by [195; 226]

$$\Omega_m = \frac{\rho_m}{3H^2}, \quad \Omega_{\Lambda_{eff}} = \frac{\rho_\varphi}{3H^2}\,,$$

we get the relation

$$\Omega_m + \Omega_{\Lambda_{eff}} = F\,. \quad (7.27)$$

Note that in order to write the (7.25) and (7.26) we have defined

$$G_{eff} = \frac{1}{1-2\epsilon\varphi} = \frac{1}{1-2\epsilon\varphi_0(1+z)^3}, \tag{7.28}$$

and therefore we assumed that the denominator $1-2\epsilon\varphi_0(1+z)^3$ does not vanish. In order to analyze the cosmological solutions, we first formulate the Friedmann equation (7.25) in terms of the red-shift z, making use of the well known relations

$$1+z = \frac{a_0}{a}, \tag{7.29}$$

$$\frac{d}{dt} = -(1+z)H(z)\frac{d}{dz}, \tag{7.30}$$

where the Hubble function $H(z)$ is here expressed as

$$H(z) = \sqrt{\frac{m\varphi(z) - V(\varphi(z)) + 2\rho_0(z+1)^3}{6-12\epsilon\varphi(z)}}\,. \tag{7.31}$$

Let us subsitute $\rho_0 = 3H_0^2\Omega_m$, $\varphi(z) = \varphi_0(1+z)^3$, and $\varphi_0 = \beta\rho_0 = 3\beta H_0^2\Omega_m$, thus obtaning the expression

$$H(z) = \sqrt{\frac{3H_0^2(z+1)^3(\beta m+2)\Omega_m - V(z)}{6\left[1-6\beta H_0^2(z+1)^3\epsilon\Omega_m\right]}}\,, \tag{7.32}$$

In Eq. (7.32) the fermion condensate not only acts as dark energy, through its self-interaction potential, but it can also play the role of a dark matter term. In the following we will consider models for which ϵ and φ_0 have the same sign. This anzats can appear ill chosen as it allows the presence of divergences in the effective gravitational constant and in the Hubble term (7.28) and (7.32). The phase space analysis in Section (7.7) reveals, however, that these singular states are unstable and therefore never reachable dynamically. In addition, in order to avoid possible problems within the numerical codes used to process observational

data, we set for ϵ and φ_0 very small values, as, for instance, in Fig. (7.4). It is worth noting that the *critical* quantity is the product $\epsilon\,\varphi_0$; therefore we set $\epsilon = 10^{-7}$: in this way the evolution of the cosmology will be always far from the singular states.

7.3 Some cosmological models

So far we have made no assumptions about the form of the self-interaction potential $V(\varphi)$ appearing in the Eqs. (7.19a) and (7.19b). In this section we investigate three different forms of $V(\varphi)$:

$$V(\varphi) = V_0\varphi^\alpha, \tag{7.33}$$

$$V(\varphi) = V_0\exp(-\lambda\varphi), \tag{7.34}$$

$$V(\varphi) = V_0(\varphi^2 + V_1)^\gamma\,. \tag{7.35}$$

The potential $V(\varphi) = V_0\varphi^\alpha$ is largely used in the dark energy literature and also in the investigation of fermionic dark energy. Because of Eq. (7.14), for $a \to 0$ the potential can be, depending on the sign of the parameter α, negligible or dominant. The converse happens when $a \to \infty$. The exponential potentials of the kind (7.34) are very important to describe not only quintessence models of the dark energy, but also various scenarios of the inflationary expansion of the early universe. Actually, for a flat Friedmann universe filled with a minimally coupled exponential field, we know the general exact solution of the field equations [227]. Moreover, in the limit $\varphi \to 0$ exponential potentials become cosmological constant terms, introducing in this way a dynamical realization of the cosmological constant related to the scalar field. Finally, the potential $V = V_0(\varphi^2 + V_1)^\gamma$ is a simple generalization of the power law potential. It has been chosen because of

its relevance in inflationary scenarios in the presence of a scalar field. For $a \to 0$ this potential coincides with the pure power law one. However, for $a \to \infty$ it generates a cosmological term related to the value of the constant V_1. In the following discussion, we will compare theoretical predictions with observational data for each cosmological model arising from the above three different choices of potential. To accomplish this aim, we parametrize in a different way our models introducing in their analytical representation parameters for which we can *immagine* the proper ranges of variations: for each cosmological model, indeed, V_0 is not a fit parameters, but is expressed in terms of different observables, as shown in Eq. (7.36).

7.3.1 The case $V(\varphi) = V_0\varphi^\alpha$

In order to analyze the cosmological scenarios arising from this power law model, we start from the Eq. (7.31) which can be parametrized in a different way by requiring that $H(0) = H_0$, where $_0$ refers to today. It turns out that we can express V_0 in terms of H_0 and the other parameters:

$$V_0 = \varphi_0^{-\alpha}\left[6H_0^2\left(\Omega_m + 2\epsilon\varphi_0 - 1\right) + m\varphi_0\right] \tag{7.36}$$

so that the Hubble function H can be expressed as (with $u = z + 1$)

$$H = \sqrt{\frac{(u)^3\left(6H_0^2\Omega_m + m\varphi_0\right) - (u)^{3\alpha}\left[6H_0^2\left(\Omega_m + 2\varphi_0\epsilon - 1\right) + m\varphi_0\right]}{6 - 12\varphi_0(u)^3\epsilon}} \tag{7.37}$$

If we introduce the dimensionless Hubble parameter $E(z,\theta) = \frac{H(z)}{H_0}$, where θ indicates the set of parameters characterizing the cosmological model, then we can construct the luminosity distance and the modulus of distance according to

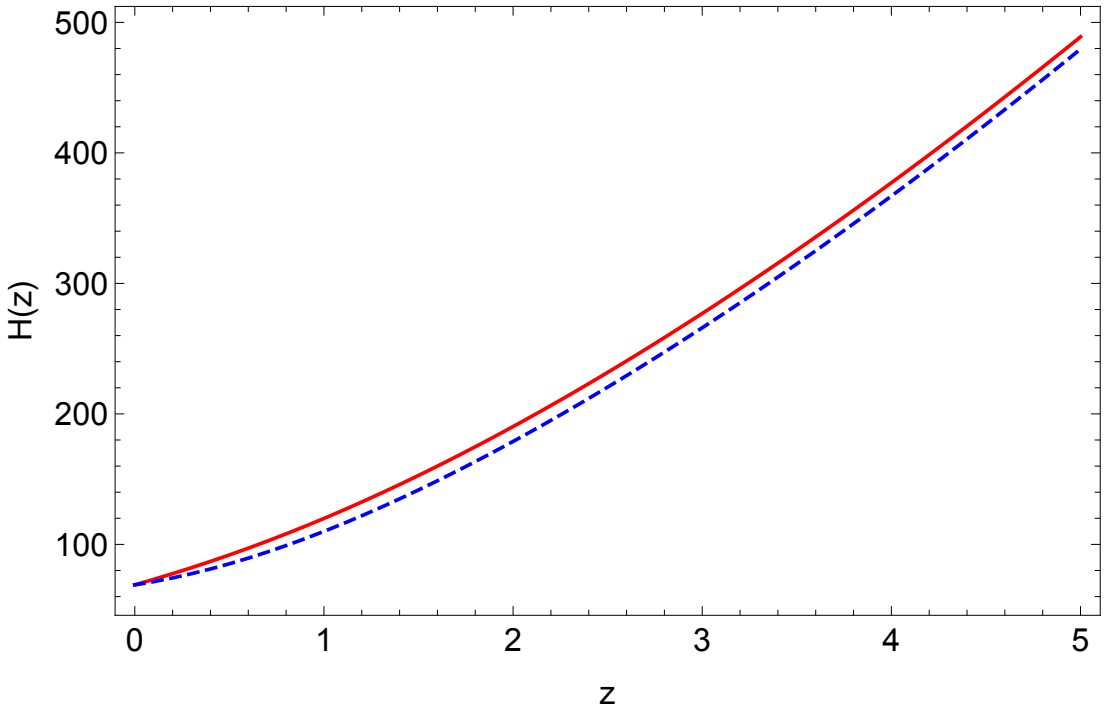

Figure 7.1: The behaviour in redshift of the function $H(z)$ (red solid line) for the power law potential $V(\varphi) = V_0\varphi^\alpha$, corresponding to the best fit values of the parameters as in Table (7.2) ($\epsilon = 10^{-7}$, $\varphi_0 = 0.006$, $\alpha = 0.23$, $m = 1.56$). It is compared with the standard ΛCDM model (blue dashed line): it turns out that, with an appropriate choice of the parameters these behaviours are comparable within a wide range of redshifts and will differ at very high redshift.

the following relations:

$$d_L(z,\theta) = \frac{c}{H_0}(1+z)\int_0^z \frac{d\zeta}{E(\zeta,\theta)}\,, \tag{7.38}$$

$$\mu_{th}(z,\theta) = 25 + 5\log d_L(z,\theta)\,. \tag{7.39}$$

In Fig. (7.1) we compare the evolution of the Hubble functions [226; 228] in our power law model and in the standard ΛCDM model.

7.3.2 The case $V(\varphi) = V_0 \exp(-\lambda\varphi)$

Following the same procedure implemented in the previous subsection, also in the case of the exponential potential we use the condition $H(0) = H_0$ to express V_0 in terms of H_0 and the other parameters:

$$V_0 = e^{\lambda\varphi_0}\left[6H_0^2\left(\Omega_m + 2\varphi_0\epsilon - 1\right) + m\varphi_0\right] \tag{7.40}$$

$$\tag{7.41}$$

so that the Hubble function H assumes the form (with $u = z + 1$ and $v = 6H_0^2$)

$$H = \sqrt{\frac{(u)^3\left(v\Omega_m + m\varphi_0\right) - e^{\lambda\varphi_0[1-(u)^3]}\left[v\left(\Omega_m + 2\varphi_0\epsilon - 1\right) + m\varphi_0\right]}{6 - 12\varphi_0(u)^3\epsilon}} \tag{7.42}$$

In Fig. (7.2) we compare the evolution of the Hubble function in our exponential model and in the standard ΛCDM model.

7.3.3 The case $V(\varphi) = V_0(\varphi^2 + V_1)^\gamma$

Owing to the presence of an additional parameter, in this case we include both H_0 and the deceleration parameter q_0 in the new parametrization and, consequently, we need more constraints. Actually, the conditions $H(0) = H_0$ allow us to express V_0 in terms of the other parameters:

$$V_0 = \left(V_1 + \varphi_0^2\right)^{-\gamma}\left[6H_0^2\left(\Omega_m + 2\epsilon\varphi_0 - 1\right) + m\varphi_0\right]\ . \tag{7.43}$$

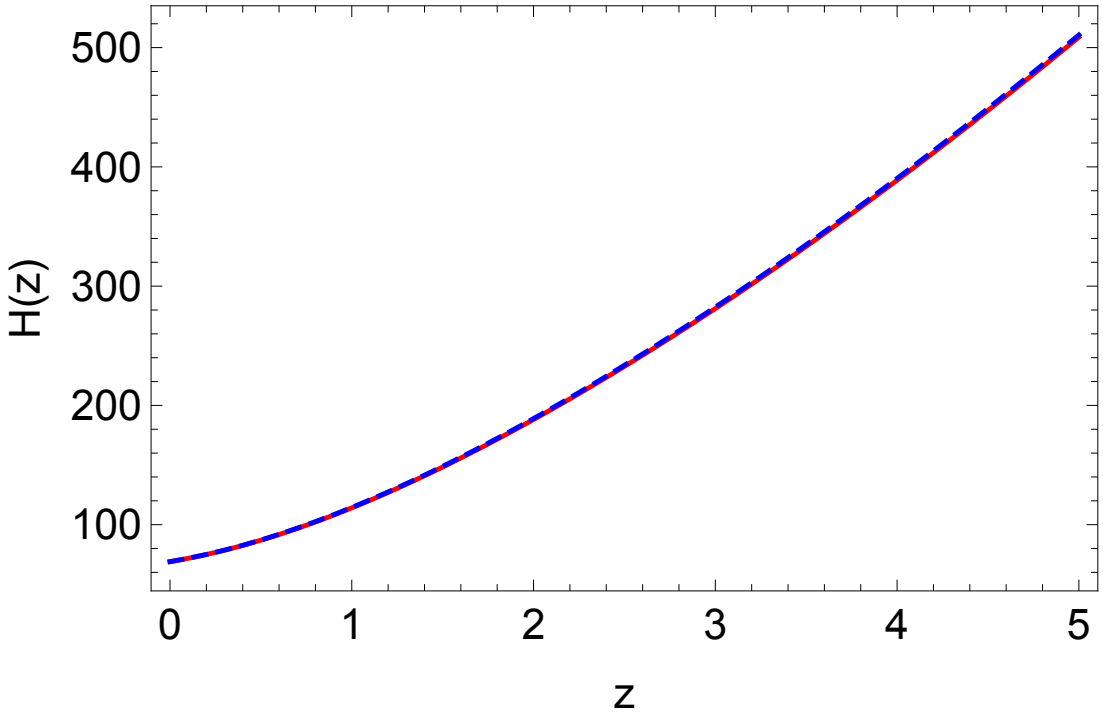

Figure 7.2: The behaviour in redshift of the function $H(z)$ (red solid line) for the exponential potential $V(\varphi) = V_0 \exp(-\lambda\varphi)$ corresponding to the best fit values of the parameters as in Table (7.2) ($\epsilon = 10^{-7}$, $\varphi_0 = 0.006$, $\lambda = 0.67$, $m = 0.33$). It is compared with the standard ΛCDM model (blue dashed line): it turns out that, with an appropriate choice of the parameters these behaviours are comparable within a wide range of redshifts and will differ at very high redshift.

With this substitution the Hubble function H takes the form: (always with $u = z + 1$ and $v = 6H_0^2$)

$$H(z) = \sqrt{\frac{\left[v\left(\Omega_m + \frac{\varphi_0}{5\cdot 10^6} - 1\right) + m\varphi_0\right]\left[V_1 + (u)^6\varphi_0^2\right]^\gamma - (u)^3\left(v\Omega_m + m\varphi_0\right)}{\left(V_1 + \varphi_0^2\right)^{-\gamma}\left[\frac{3(u)^3\varphi_0}{2{,}5\cdot 10^6} - 6\right]}}. \tag{7.44}$$

It is worth noting that, owing to the presence of an additional parameter, it is also possible include both H_0 and the deceleration parameter q_0 in the new parametrization so that the conditions $H(0) = H_0$ and $q_0 = -H_0\left(\lim_{z\to 0}\frac{dH(z)}{dz}\right)$ allow us to express V_0 and V_1 in terms of H_0, q_0 and the other parameters:

$$\begin{aligned} V_0 = \quad & 2^{-\gamma}\left[6H_0^2\left(\Omega_m + 2\varphi_0\epsilon - 1\right) + m\varphi_0\right] \times \\ & \left\{\frac{\gamma\varphi_0^2\left[6H_0^2\left(\Omega_m + 2\varphi_0\epsilon - 1\right) + m\varphi_0\right]}{H_0^2\left[6\Omega_m + q_0\left(8\varphi_0\epsilon - 4\right) + 20\varphi_0\epsilon - 4\right] + m\varphi_0}\right\}^{-\gamma}, \end{aligned} \tag{7.45}$$

and

$$\begin{aligned} V_1 = \quad & \frac{\varphi_0^2\left\{2H_0^2\left[6\gamma\left(\Omega_m + 2\varphi_0\epsilon - 1\right) - 3\Omega_m + q_0\left(2 - 4\varphi_0\epsilon\right) - 10\varphi_0\epsilon + 2\right]\right\}}{H_0^2\left[6\Omega_m + q_0\left(8\varphi_0\epsilon - 4\right) + 20\varphi_0\epsilon - 4\right] + m\varphi_0} + \\ & \frac{(2\gamma - 1)m\varphi_0^3}{H_0^2\left[6\Omega_m + q_0\left(8\varphi_0\epsilon - 4\right) + 20\varphi_0\epsilon - 4\right] + m\varphi_0}. \end{aligned} \tag{7.46}$$

With these substitutions the Hubble function H takes the form: ($\delta = 2\gamma - 1$, $u = z + 1$ and $v = 6H_0^2$)

$$H(z) = \Bigg\{ \frac{1}{12\varphi_0(u)^3\epsilon - 6} \left[2^{-\gamma}\gamma^{-\gamma} \left(v\Omega_m + 2v\varphi_0\epsilon - v + m\varphi_0 \right) \times \right. \tag{7.47}$$
$$\left[v\left(\Omega_m + 2\varphi_0\epsilon - 1\right) + m\varphi_0 \right]^{-\gamma} \left\{ \frac{2v}{3} \left[\frac{3\Omega_m}{2} + \varphi_0\epsilon\left(2q_0 + 5\right) - q_0 - 1 \right] + m\varphi_0 \right\}^{\gamma}$$
$$\left\{ \frac{\frac{v}{3}\left[3\delta\Omega_m + 2\left[-3\gamma + \varphi_0\epsilon\left(6\gamma - 2q_0 - 5\right) + q_0 + 1\right]\right] + \delta m\varphi_0}{\frac{2v}{3}\left[\frac{3\Omega_m}{2} + \varphi_0\epsilon\left(2q_0 + 5\right) - \left(q_0 + 1\right)\right] + m\varphi_0} + (u)^6 \right\}^{\gamma}$$
$$\left. -(u)^3\left(v\Omega_m + m\varphi_0\right)\right] \Bigg\}^{\frac{1}{2}} .$$

In Fig.(7.3) we compare the evolution of the Hubble function in our modified power law model and in the standard ΛCDM model. In Fig.(7.4) we compare the evolution of the Hubble functions the power law model and in the standard ΛCDM model. As we shall see, in order to carry out the comparison with the observational data, it turns out that the above parametrizations are more efficient in exploring the region of parameters.

7.3.4 The value of the parameter ϵ

The equations (7.13) is deduced from the Dirac equations (7.12) and, then, it is evident that it is the same that we would have in the minimally coupled theory ($\epsilon = 0$). This similarity, however, is only apparent. Equation (7.12) is coupled to Einstein's equations (7.10) where the non-minimal coupling manifests itself explicitly, showing that the minimally coupled theory and the non-minimally coupled one are very different, at least in terms of corresponding field equations. This corresponds effectively to the fact that the evolution of the condensate is different because the expansion of the universe, which appears in $\dot{a}/a$, is different. In spite of this fact, since $\varphi \to 0$ when the scale factor grows, it is expected that the non-minimal coupling contributions tend to disappear at cosmological late time and therefore, for redshifts not too large, both theories tend to coincide. It

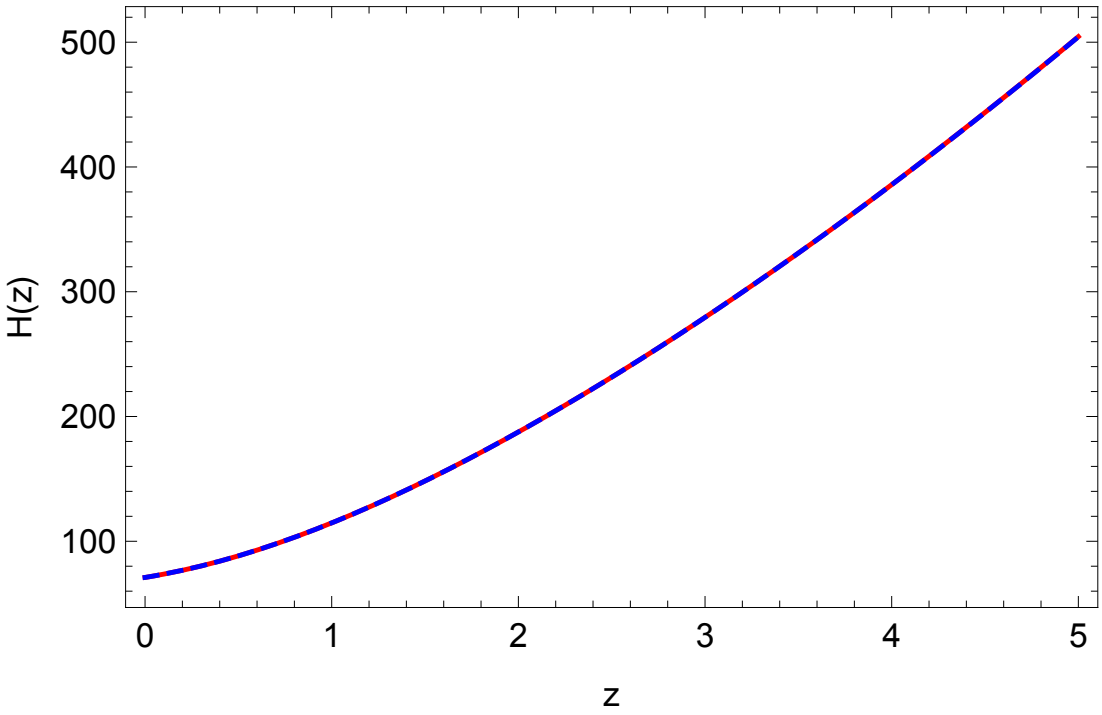

Figure 7.3: The behaviour in redshift of the function $H(z)$ (red solid line) for the extended power law potential $V(\varphi) = V_0(\varphi^2 + V_1)^\gamma$ corresponding to the best fit values of the parameters as in Table 7.2 ($\epsilon = 10^{-7}$, $\varphi_0 = 0.006$, $V_0 = -236$, $V_1 = 16.5$, $\gamma = 0.51$, $m = 0.87$). It is compared with the standard ΛCDM model (blue dashed line): it turns out that, with an appropriate choice of the parameters these behaviours are comparable within a wide range of redshifts and will differ at very high redshift.

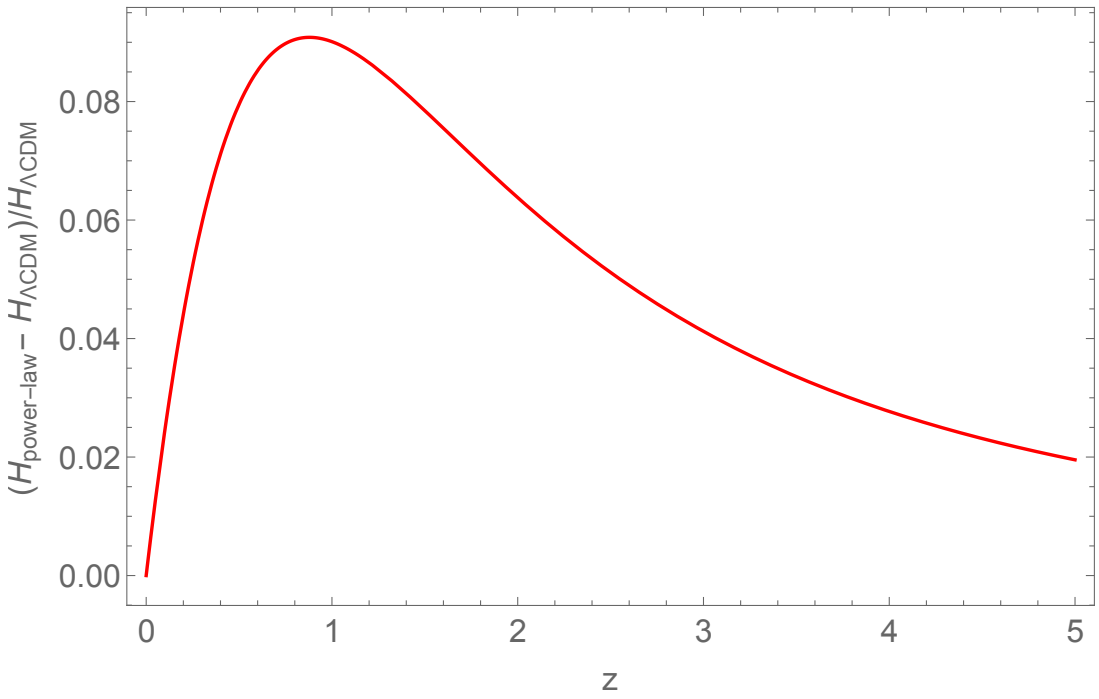

Figure 7.4: The behaviour in redshift of the relative variation of the Hubble function $H(z)$ for the power law potential $V(\varphi) = V_0\varphi^\alpha$, compared with the standard ΛCDM model. The parameters correspond to the best fit values, as in Table (7.2) ($\epsilon = 10^{-7}$, $\varphi_0 = 0.006$, $\alpha = 0.23$, $m = 1.56$). For this power law model we have the worst matching with the ΛCDM model.

would be an error to think, however, that they are exactly the same. In doing the fits, a (common) strategy that we have adopted is to gauge the initial data using the most precise information available, which concern only the cosmology of eras of dominance of the self-interaction potentials. Therefore, the two models are the same today by definition. Why then bothering considering a data analysis of this model with data at the present time? As mentioned repeatedly in the chapter, finding the values of the parameters today allows to reconstruct via the dynamical analysis the evolution at early times in which the effects of the condensate are more evident (as proved in a previous work [76]). Indeed, this is exactly the main purpose, i.e. matching observational data with a phase space analysis. In addition to that, the similarities of the model we considered with the standard model of cosmology quickly disappear when one considers other aspects of the cosmological model, like for example the matter perturbations. The determination of the value of the parameters, including ϵ, will have a much more relevant role in that case. In this perspective, our analysis and the result we find for the constant ϵ is very relevant and cannot be dismissed by arguing that ϵ very small is the same of $\epsilon = 0$.

As in all non-minimally coupled theories our model we do not have exactly $G_{eff} \equiv G_N \equiv G_{\text{Newton}}$ at a given time. This is directly due to the action of the condensate and therefore depends strictly on the value of ϵ. Recent data analysis indicates that the gravitational constant and its derivatives are slowly varying, *i.e.* $\left|\dot{G}/G\right| \propto 10^{-14}$ [229; 230]. However, a change in G_{eff} would affect observations on solar system dynamics, Big Bang Nucleosynthesis predictions, data concerning the growth rate of structures and the CMB (see e.g. [229; 231; 232]). Our analysis offers a way to probe these differences using measures performed today. In order to give an idea of the differences that our model could present with respect to the Standard cosmological model, in Figs. (7.5), we plot the be-

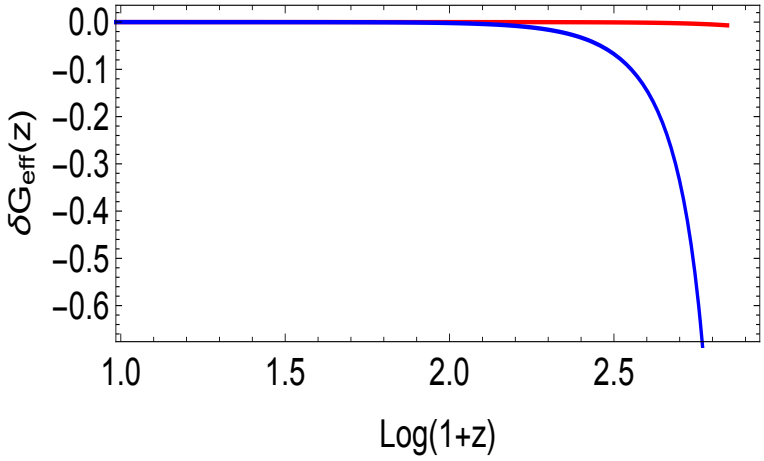

Figure 7.5: Time evolution for the relative variation δG for our model, with $\epsilon = 10^{-5}$ (blue line), and $\epsilon = 10^{-7}$ (red line). As we see, the evolution of G_{eff} is very different.

haviour of $\delta G = \frac{G_{eff} - G_N}{G_N}$ for two different values of ϵ while, in Figs. (7.6), we plot the behaviour of $\dot{G}_{eff}$ for two different values of ϵ. It turns out that the high-z behaviour of the the effective gravitational is different, showing that indeed an importa difference exists between different values of ϵ.

7.4 Observational data sets

In our investigation we use observational data sets on *Type Ia Supernovae* and *Gamma Ray Bursts* Hubble diagram, as well as some recent measurements of $H(z)$ from the differential age of passively evolving elliptical galaxies [80]. We set Gaussian priors on the distance data from the *Baryon Acoustic Oscillations* and the Hubble constant h. These priors were included to help break the degeneracies among the parameters of different cosmological models.

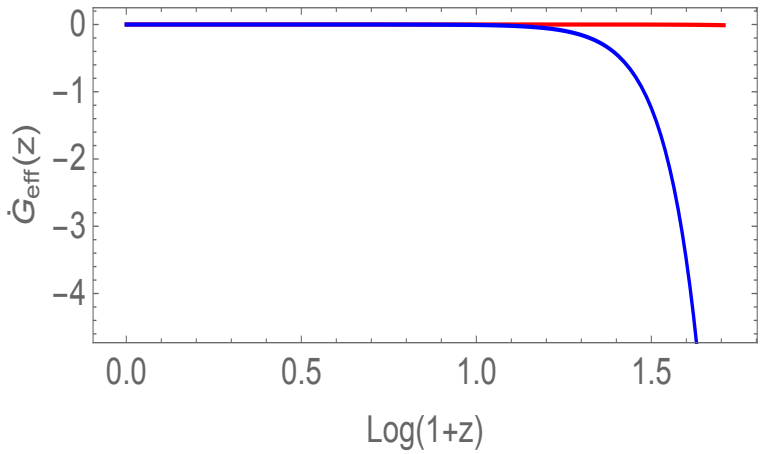

Figure 7.6: Time evolution for the derivate $\dot{G}_{eff}$ for our model, with $\epsilon = 10^{-5}$ (blue line), and $\epsilon = 10^{-7}$ (red line). As in the previous case, the evolution of $\dot{G}_{eff}$ is very different.

7.4.1 Supernovae and Gamma Ray Bursts Hubble diagram

Type Ia Supernovae observations gave the first strong evidence of the present accelerating expansion of the Universe [233; 234]. Here we consider the recently updated Supernovae Cosmology Project Union 2.1 compilation [61], which spans the redshift range $0.015 \leq z \leq 1.4$. We compare the theoretically predicted distance modulus $\mu(z)$ with the observed one through a Bayesian approach, based on the definition of the distance modulus for each of the different models described in the previous section

$$\mu(z_j) = 5\log_{10}(D_L(z_j, \{\theta_i\})) + \mu_0\,, \tag{7.48}$$

where $D_L(z_j, \{\theta_i\})$ is the Hubble free luminosity distance, expressed as a series depending on the cosmological parameters. The parameter μ_0 encodes the Hubble constant and the absolute magnitude M, and has to be marginalized over. In our

analysis we use the version of the χ^2 given by

$$\tilde{\chi}^2_{\rm SN}(\{\theta_i\}) = \sum_{j=1}^{\mathcal{N}_{SNIa}} \frac{(\mu(z_j;\mu_0=0,\{\theta_i\}) - \mu_{obs}(z_j))^2}{\sigma^2_{\mu,j}} - \frac{\sum_{j=1}^{\mathcal{N}_{SNIa}} \frac{(\mu(z_j;\mu_0=0,\{\theta_i\}) - \mu_{obs}(z_j))}{\sigma^2_{\mu,j}}}{\sum_{j=1}^{\mathcal{N}_{SNIa}} \frac{1}{\sigma^2_{\mu,j}}} \,. \tag{7.49}$$

Gamma-Ray Bursts are visible up to very high redshifts thanks to the enormous released amount of energy, and thus are good candidates for our high-redshift cosmological investigation. Since their peak luminosity spans a wide range, they are not standard candles; however it is possible to consider them as distance indicators calibrating some empirical correlations of distance-dependent quantities and rest-frame observables [235]. These empirical relations allow us to deduce the Gamma Ray Bursts rest-frame luminosity or energy from an observer-frame measured quantity, so that the distance modulus can be obtained with an error that depends essentially on the intrinsic scatter of the adopted correlation. We perform our analysis using a Gamma Ray Bursts Hubble diagram data set, built by calibrating the $E_{\rm p,i}$ – $E_{\rm iso}$ relation [236; 237], plotted in Fig. 7.7.

7.4.2 Baryon acoustic oscillations and H(z) measurements

Baryon acoustic oscillations data are standard rulers available to investigate several cosmological models; they are related to density fluctuations induced by acoustic waves due to primordial perturbations. Measurements of the Cosmic Microwave Background radiation provide the absolute scale for these peaks, and the observed position of the peaks of the two-point correlation function of the large scale matter distribution enables to measure distance scales, if it is compared with these absolute values. In order to use Baryon acoustic oscillations data, we define [238]

$$d_z = \frac{r_s(z_d)}{d_V(z)} \,, \tag{7.50}$$

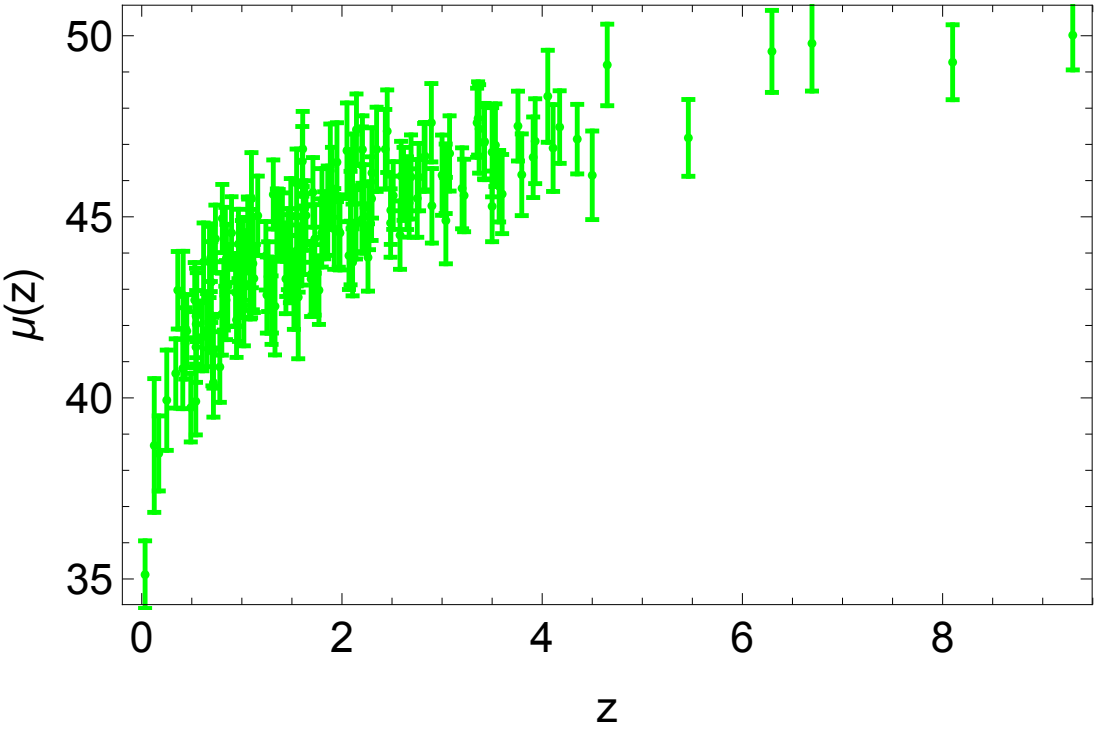

Figure 7.7: Gamma Ray Bursts Hubble diagram used in our analysis.

where z_d is the drag redshift computed in [239], $r_s(z)$ is the sound horizon

$$r_s(z) = \frac{c}{\sqrt{3}} \int_0^{(1+z)^{-1}} \frac{da}{a^2 H(a) \sqrt{1 + (3/4)\Omega_b/\Omega_\gamma}} \,, \tag{7.51}$$

and $d_V(z)$ is the volume distance:

$$d_V(z) = \left[(1+z)\, d_A(z)^2 \frac{cz}{H(z)} \right]^{\frac{1}{3}} . \tag{7.52}$$

Here $d_A(z)$ is the angular diameter distance. The data used in our analysis are from [240]. The measurements of Hubble parameters are a complementary probe to constrain the cosmological parameters and investigate dark energy effects [80; 241]. The Hubble parameter, defined as the logarithmic derivative of the scale factor $H(z) = \frac{\dot{a}}{a}$, depends on the differential age of the Universe as a function

of the redshift and can be measured using the so-called cosmic chronometers. From spectroscopic surveys we can measure the differential redshift interval dz with high accuracy and the differential evolution of the age of the Universe dt in the redshift interval dz can be measured too, provided that optimal probes of the aging of the Universe (that is cosmic chronometers) are identified [242]. The most reliable cosmic chronometers are old early-type galaxies that evolve passively on a timescale much longer than their age difference, which have formed the most part of their stars early and have not experienced further star formation events. Moreover, the Hubble parameter can also be obtained from the Baryon acoustic oscillations measurements [243]. We used a list of 28 $H(z)$ measurements, compiled in [80] and shown in Table (7.1).

7.5 Statistical analysis

To constrain the cosmological parameters which characterize the models described in Sect. 7.3, we performed a preliminary and standard fitting procedure to maximize a likelihood function $\mathcal{L}(\mathbf{p})$, in order to identify appropriate starting points for the statistical analysis. This required the knowledge of the precision matrix:

$$\begin{aligned}
\mathcal{L}(\mathbf{p}) \propto & \frac{\exp\left(-\chi^2_{SNIa/GRB}/2\right)}{(2\pi)^{\frac{\mathcal{N}_{SNIa/GRB}}{2}}|\mathbf{C}_{SNIa/GRB}|^{1/2}}\frac{\exp\left(-\chi^2_{BAO}/2\right)}{(2\pi)^{\mathcal{N}_{BAO}/2}|\mathbf{C}_{BAO}|^{1/2}} \\
\times & \frac{1}{\sqrt{2\pi\sigma^2_{\omega_m}}}\exp\left[-\frac{1}{2}\left(\frac{\omega_m-\omega_m^{obs}}{\sigma_{\omega_m}}\right)^2\right], \\
& \times\frac{1}{\sqrt{2\pi\sigma^2_h}}\exp\left[-\frac{1}{2}\left(\frac{h-h_{obs}}{\sigma_h}\right)^2\right]\frac{\exp\left(-\chi^2_H/2\right)}{(2\pi)^{\mathcal{N}_H/2}|\mathbf{C}_H|^{1/2}} \\
\times & \frac{1}{\sqrt{2\pi\sigma^2_{\mathcal{R}}}}\exp\left[-\frac{1}{2}\left(\frac{\mathcal{R}-\mathcal{R}_{obs}}{\sigma_{\mathcal{R}}}\right)^2\right]
\end{aligned} \tag{7.53}$$

z	$H(z)$ (km s^{-1} Mpc $^{-1}$)	σ_H (km s^{-1} Mpc $^{-1}$)
0.070	69	19.6
0.100	69	12
0.120	68.6	26.2
0.170	83	8
0.179	75	4
0.199	75	5
0.200	72.9	29.6
0.270	77	14
0.280	88.8	36.6
0.350	76.3	5.6
0.352	83	14
0.400	95	17
0.440	82.6	7.8
0.480	97	62
0.593	104	13
0.600	87.9	6.1
0.680	92	8
0.730	97.3	7.0
0.781	105	12
0.875	125	17
0.880	90	40
0.900	117	23
1.037	154	20
1.300	168	17
1.430	177	18
1.530	140	14
1.750	202	40
2.300	224	8

Table 7.1: Measurements of the Hubble parameter used in our analysis, as compiled in [80]

where

$$\chi^2(\mathbf{p}) = \sum_{\mathbf{i,j=1}}^{\mathbf{N}} \left(\mathbf{_i} - \mathbf{x_i^{th}}(\mathbf{p})\right) \mathbf{C_{ij}^{-1}} \left(\mathbf{_j} - \mathbf{x_j^{th}}(\mathbf{p})\right) . \tag{7.54}$$

$\omega_m = h^2\Omega_m$, $\mathbf{p}$ indicates the set of the cosmological parameters, N is the number of data, $\mathbf{_i}$ is the $i-th$ measurement; $\mathbf{x_i^{th}}(\mathbf{p})$ denote the theoretical predictions for these measurements and depend on the cosmological model and its own parameters $\mathbf{p}$; $\mathbf{C_{ij}}$ is the covariance matrix (specifically, $\mathbf{C}_{SNIa/GRB/H}$ indicates the SNIa/GRBs/H covariance matrix); $(h^{obs}, \sigma_h) = (0.742, 0.036)$ [244], and $(\omega_m^{obs}, \sigma_{\omega_m}) = (0.1356, 0.0034)$ [59]. We tested that our results are not biased by the choice of the prior on h. The term $\frac{1}{\sqrt{2\pi\sigma_{\mathcal{R}}^2}} \exp\left[-\frac{1}{2}\left(\frac{\mathcal{R}-\mathcal{R}_{obs}}{\sigma_{\mathcal{R}}}\right)^2\right]$ in the likelihood $\mathcal{L}(\mathbf{p})$ takes into account the so called shift parameter $\mathcal{R}$, defined as

$$\mathcal{R} = H_0\sqrt{\Omega_M}\int_0^{z_\star} \frac{dz'}{H(z')}\,, \tag{7.55}$$

with $z_\star = 1090.1$ [245], [246].

According to the Planck data, $(\mathcal{R}_{obs}, \sigma_{\mathcal{R}}) = (1.7407, 0.0094)$. To sample the $\mathcal{N}$ dimensional space of parameters corresponding to each of our models, we used the Markov Chain Monte Carlo Method and ran five parallel chains, the convergence of which has been tested using the reduction factor R^*, defined as the square root of the ratio of the variance extra-chain and the variance intra-chain. A large R^* indicates that the extra-chain variance is substantially greater than the intra-chain variance, so that a longer simulation is needed. We required that the convergence was reached if R^* approached 1 for each parameter: we set the precision of order 0.05. As first step, which allowed us to select the starting points of the full analysis, we ran our chains to compute the likelihood $\mathcal{L}(\mathbf{p})$ considering only the Type Ia Supernovae data. Therefore we applied the same Markov Chain Monte Carlo approach to evaluate the likelihood $\mathcal{L}(\mathbf{p})$, combining all the data, as described above. We discarded the first 30% of the point iterations at the

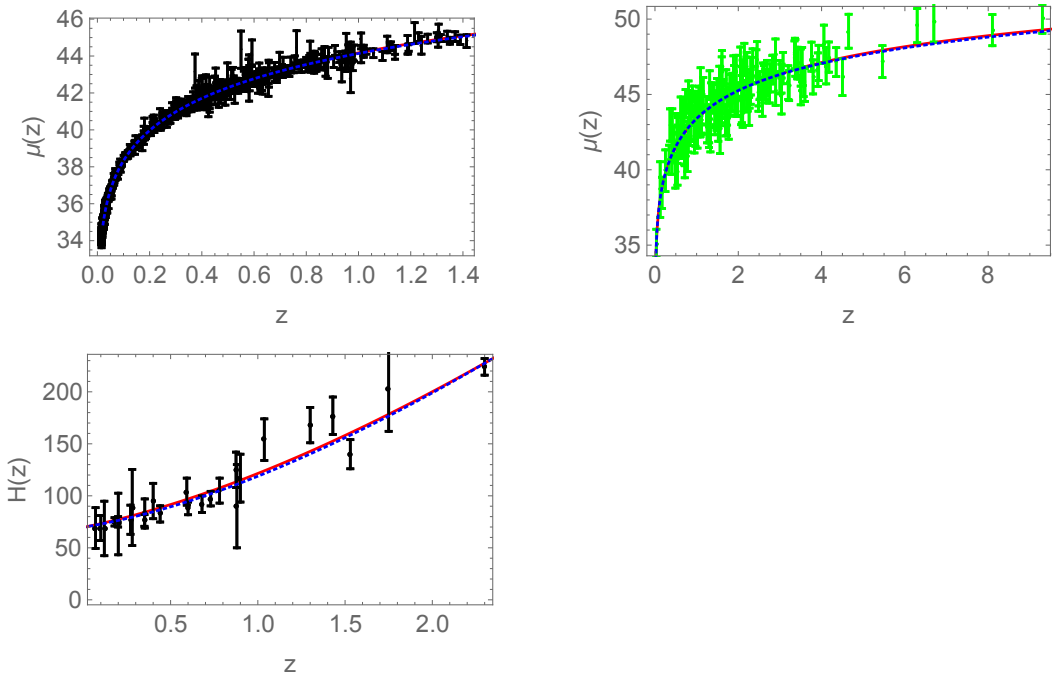

Figure 7.8: Comparison between the observational data and the theoretical predictions for the power law potential (red solid line), and the exponential potential, corresponding to their own best fit values for the parameters.

beginning of any Markov Chain Monte Carlo run, and thinned the chains that were run many times. We finally extracted the constraints on the parameters by coadding the thinned chains. The histograms of the parameters from the merged chains were then used to infer median values and confidence ranges: the 15.87th and 84.13th quantiles define the 68% confidence interval; the 2.28th and 97.72th quantiles define the 95% confidence interval; the 0.13th and 99.87th quantiles define the 99% confidence interval. In Table 7.2, we presented the results of our analysis: we indicated the mean, the median, the 1σ and 2σ regions of confidence for the main parameters of the different models. In Fig. (7.8) we plot the observational data with the best fit model relative to the power law and exponential potential.

Id	$\langle x \rangle$	$\tilde{x}$	68% CL	95% CL
		$V(\varphi) = V_0 \varphi^\alpha$		
Ω_m	0.21	0.22	(0.19, 0.24)	(0.17, 0.25)
h	0.69	0.70	(0.67, 0.71)	(0.66, 0.72)
α	0.23	0.21	(0.19, 0.24)	(0.15, 0.30)
m	1.56	1.60	(1.39, 1.7)	(1.31, 1.76)
		$V(\varphi) = V_0 \exp(-\lambda\varphi)$		
Ω_m	0.25	0.25	(0.23, 0.27)	(0.21, 0.29)
h	0.69	0.69	(0.69, 0.71)	(0.68, 0.72)
λ	0.67	0.68	(0.25, 1.1)	(0.21, 1.35)
m	0.33	0.24	(0.1, 0.78)	(0.06, 0.96)
		$V(\varphi) = V_0(\varphi^2 + V_1)^\gamma$		
Ω_m	0.21	0.23	(0.20, 0.24)	(0.16, 0.27)
h	0.70	0.71	(0.67, 0.73)	(0.65, 0.74)
q_0	-0.66	-0.63	(-0.65, -0.57)	(-0.67, -0.49)
γ	0.51	0.6	(0.47, 0.91)	(0.45, 1.05)
m	0.87	0.8	(0.66, 0.95)	(0.52, 1.17)

Table 7.2: Constraints on the main cosmological parameters which enter in the representation of the models described in Sect. 7.3. The likelihood has been marginalized with respect the others. Columns report the mean $\langle x \rangle$ and median $\tilde{x}$ values and the 68% and 95% confidence limits.

7.6 Comparison of our Fermionic models with the Chevallier-Polarski-Linder model

In this section we compare the different models presented in the previous sections and check if we can discriminate against them. We use the Akaike Information Criterion, AIC, [247; 248], and its indicator

$$AIC = -2\ln \mathcal{L}_{\mathbf{max}} + 2k_p + \frac{2k_p(k_p+1)}{N_{tot}-k_p-1}\,, \tag{7.56}$$

where N_{tot} is the total number of data and k_p the number of free parameters (of the cosmological model) . It turns out that the smaller is the value of AIC the better is the fit to the data. To compare different cosmological models we introduce the model difference $\Delta_{AIC} = AIC_{model} - AIC_{min}$. The relative difference corresponds to different cases: $4 < \Delta_{AIC} < 7$ indicates a positive evidence against the model with higher value of AIC_{model}, while $\Delta_{AIC} \geq 10$ indicates a strong evidence. $\Delta_{AIC} \leq 2$ is an indication that the two models are consistent. In our case we have found that the model with the lower AIC is the exponential potential model $V(\varphi) = V_0 \exp(-\lambda\varphi)$. It turns out that $\Delta_{AIC} = 4.3$ if we consider the exponential potential and $\Delta_{AIC} = 1.97$ for the the extended power law potential. We can use he same method to make a comparison of our model with the CPL parametrization for dark energy, which assumes a dark energy equation of state given by

$$w(z) = w_0 + w_1 z(1+z)^{-1}\,, \tag{7.57}$$

where w_0 and w_1 are real numbers that represent the equation of state present value and its overall time evolution, respectively [249; 250]. For high redshift we

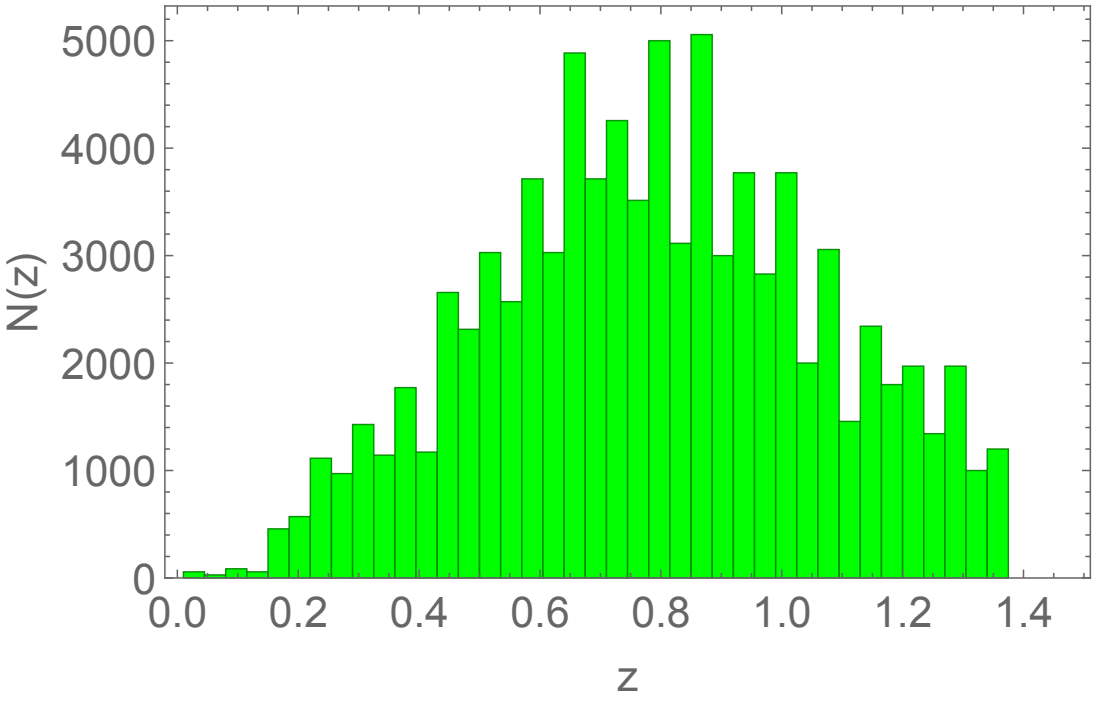

Figure 7.9: Simulated data for an Euclid-like mission: we plot the Type Ia Supernovae redshift distribution used in our analysis.

have the following behavior

$$\lim_{z\to\infty} w(z) = w_0 + w_1\,. \tag{7.58}$$

If we compare the exponential potential model with the CPL, it turns out that the exponential model has got the lower AIC, and $\Delta_{AIC} = 5.9$. This indicates a weak evidence against the CPL model. To confirm the results obtained above we rely on future data. Here we investigate the possibility to constrain our model using simulated data from an Euclid - like survey [251]. The number of Type Ia Supernovae which could be used for cosmology and their redshift distribution is plotted in Fig. 7.9. To each simulated Supernovae we estimate the error on the

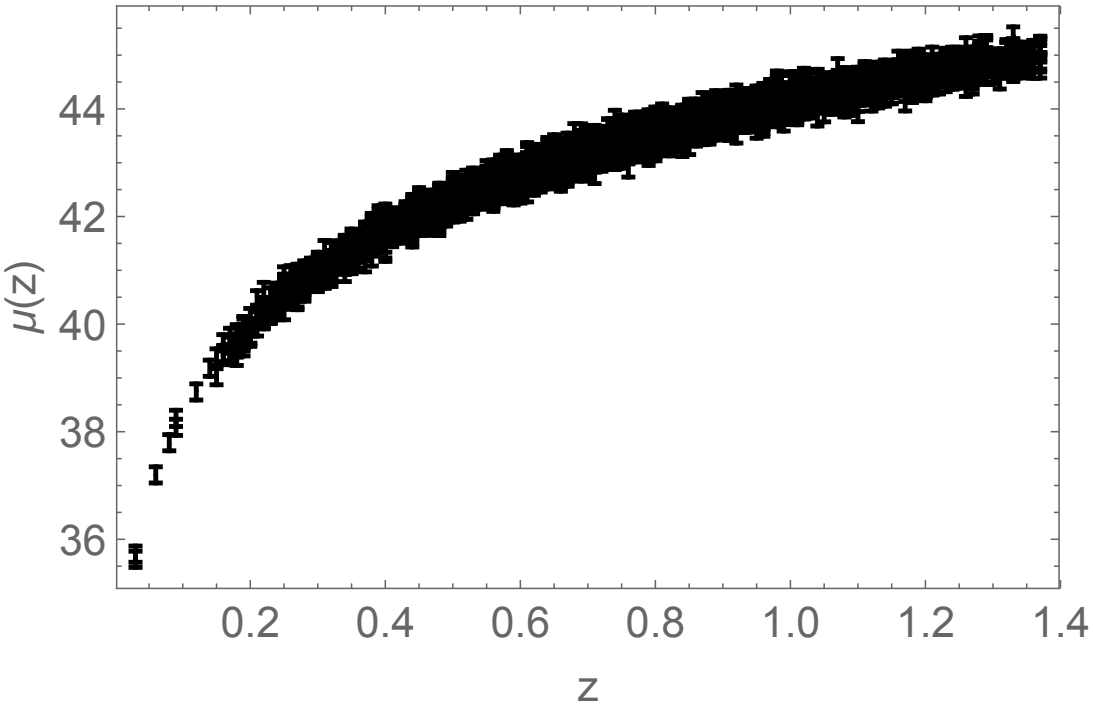

Figure 7.10: The mock dataset used in our analysis.

distance modulus as [252]:

$$\sigma_\mu(z) = \sqrt{\sigma_{sys}^2 + (z/z_{max})^2\sigma_m^2}\,. \tag{7.59}$$

Here z_{max} is the maximum redshift of the sample, σ_{sys} an instrinsic scatter and σ_m depends on the photometric accuracy. In our case $(z_{max}, \sigma_{sys}, \sigma_m) = (1.4, 0.15, 0.02)$. We then assign to each Supernovae a distance modulus randomly generated from a Gaussian distribution centered on a fiducial model $\mu_{fid}(z)$ and variance $\sigma_\mu(z)$. In this analysis we set the exponential potential model as the fiducial model. In Fig. 7.10 we plot the mock dataset. In Table 7.3 we summarized the results of the simulation, when we consider the simulated Type Ia Supernovae HD as cosmological probes: it turns out that the mock dataset is able to constraint much better our model.

Id	$\langle x \rangle$	$\tilde{x}$	68% CL	95% CL
Ω_m	0.27	0.27	(0.26, 0.27)	(0.25, 0.28)
H_0	70.1	70.1	(69.8, 70.5)	(69.5, 70.7)
φ_0	0.005	0.005	(0.004, 0.006)	(0.003, 0.007)
m	0.60	0.51	(0.39, 0.89)	(0.30, 0.99)
λ	2.45	2.50	(2.04, 2.87)	(1.54, 2.97)

Table 7.3: Results of our statistical analysis, when we consider the simulated Type Ia Supernovae HD as cosmological probes. Columns report the mean $\langle x \rangle$ and median $\tilde{x}$ values and the 68% and 95% confidence limits.

7.7 A new dynamical system formulation

We can combine the data analysis above with the dynamical system approach to infer further features of the cosmic history that corresponds to the observational results we have obtained.

Under the condition $\varepsilon > 0$ and $\varphi_0 > 0$, we can consider the dynamical system variables

$$\begin{aligned} \Omega &= \sqrt{\frac{\rho}{\mathcal{D}^2}}, \qquad Y = \sqrt{\frac{m\varphi}{2\mathcal{D}^2}}, \\ E &= \sqrt{\frac{2\epsilon\dot{\varphi}^2}{3\varphi\mathcal{D}^2}}, \qquad Q = \frac{H}{\mathcal{D}}, \end{aligned} \tag{7.60}$$

where

$$\mathcal{D}^2 = 3H^2 + \frac{V(\varphi)}{2}. \tag{7.61}$$

This choice sends fixed points for which $\mathcal{D} = 0$ to the asymptotic part of the phase

space. Because of eq. (7.13) this condition reduces to the differential equation

$$\frac{\dot{\varphi}^2}{3\varphi^2} + \frac{V(\varphi)}{2} = 0 \tag{7.62}$$

which, given the form of the potential, represents the solution associated to the asymptotic limit of the phase space. Using variables (7.60), the cosmological equations are equivalent to the dynamical system

$$\Omega_{,\mathcal{N}} = -\frac{3Q\Omega}{2\left(E^2 - 3Q^2\right)}\left[E^2\left(3Q^2-1\right)\mathbb{V} + E^2(w+1) + 3wQ^2\left(\Omega^2-1\right)\right], \tag{7.63}$$

$$E_{,\mathcal{N}} = -\frac{3EQ}{2\left(E^2 - 3Q^2\right)}\left[\left(E^2-1\right)\left(3Q^2-1\right)\mathbb{V} + E^2 + w\Omega^2\left(3Q^2-1\right) - 1\right], \tag{7.64}$$

$$Q_{,\mathcal{N}} = -\frac{3Q^2}{2\left(E^2 - 3Q^2\right)}\left(3Q^2-1\right)\left[\left(E^2-1\right)\mathbb{V} + w\Omega^2 + 1\right], \tag{7.65}$$

together with the decoupled equation

$$\mathcal{D}_{,\mathcal{N}} = \frac{3\mathcal{D}^2 Q}{2\left(E^2 - 3Q^2\right)}\left[E^2\left(3Q^2-1\right)\mathbb{V} + 3Q^2\left(w\Omega^2+1\right)\right], \tag{7.66}$$

and the constraint

$$E^2 + Y^2 + \Omega^2 = 1 \tag{7.67}$$

where we have defined

$$X_{,\mathcal{N}} = \frac{1}{\mathcal{D}}\dot{X} \tag{7.68}$$

and

$$\mathbb{V} = \mathbb{V}\left(\frac{E^2}{6\varepsilon Q^2}\right) = \left.\frac{\varphi V'(\varphi)}{V(\varphi)}\right|_{\varphi = E^2/6\varepsilon Q^2} \tag{7.69}$$

The constraint (7.67) implies that the phase space is compact.

In the following, however, we will consider the case $w = 0$. For this value of the barotropic factor the cosmological equations (7.19) imply that $\rho = \beta\varphi$,

where $\beta = \rho_0/\varphi_0$ is a constant. This means that the phase space will loose one dimensions. Therefore, if $w = 0$, we can choose the variables

$$\bar{Y} = \sqrt{\frac{(m+2\beta)\varphi}{2\mathcal{D}^2}}, \qquad E = \sqrt{\frac{2\epsilon\dot{\varphi}^2}{3\varphi\mathcal{D}^2}}, \qquad Q = \frac{H}{\mathcal{D}}, \tag{7.70}$$

so that the dynamical equations can be written as

$$E_{,\mathcal{N}} = -\frac{3EQ\left(E^2-1\right)\left[\left(3Q^2-1\right)\mathbb{V}+1\right]}{2\left(E^2-3Q^2\right)}, \tag{7.71}$$

$$Q_{,\mathcal{N}} = -\frac{3Q^2\left(3Q^2-1\right)\left[\left(E^2-1\right)\mathbb{V}+1\right]}{2\left(E^2-3Q^2\right)}. \tag{7.72}$$

with the constraint

$$\bar{Y}^2 = 1 - E^2. \tag{7.73}$$

The above system is still not compact in the variable Q. We can obtain a compact two-dimensional system with the transformation

$$E = \cos\theta, \qquad \bar{Y} = \sin\theta, \qquad Q = \frac{\bar{Q}}{1-\bar{Q}}, \tag{7.74}$$

which leads to the system

$$\bar{Q}_{,\mathcal{N}} = \frac{3\bar{Q}^2\left[2\bar{Q}\left(\bar{Q}+1\right)-1\right]\left(\bar{\mathbb{V}}\sin^2\theta-1\right)}{2\left(\bar{Q}-1\right)^2\cos^2\theta-6\bar{Q}^2}, \tag{7.75}$$

$$\theta_{,\mathcal{N}} = \frac{3\bar{Q}\sin\theta\cos\theta\left\{\left[2\bar{Q}\left(\bar{Q}+1\right)-1\right]\bar{\mathbb{V}}+\left(\bar{Q}-1\right)^2\right\}}{2\left(\bar{Q}-1\right)\left[\left(\bar{Q}-1\right)^2\cos^2\theta-3\bar{Q}^2\right]}, \tag{7.76}$$

with the decoupled equation

$$\mathcal{D}_{,\mathcal{N}} = \frac{3Q\mathcal{D}^2\left[E^2\left(3Q^2-1\right)\bar{\mathbb{V}}+3Q^2\right]}{2\left(E^2-3Q^2\right)}, \tag{7.77}$$

where

$$\bar{\mathbb{V}} = \mathbb{V}\left(\frac{\left(\bar{Q}-1\right)^2\cos^2\theta}{\bar{Q}^2}\right). \tag{7.78}$$

We will now use the data analysis above to determine the point of the phase space which corresponds to the current state of the universe. Using this result and the dynamical system above we will deduce, for each type of potential, information on the entire cosmic history that is associated with the observations.

7.7.1 The case $V(\varphi) = V_0\varphi^\alpha$

If one considers the power law potential $V(\varphi) = V_0\varphi^\alpha$, then

$$\begin{aligned}
\bar{Q}_{,\mathcal{N}} &= \frac{3\bar{Q}^2\left[2\bar{Q}\left(\bar{Q}+1\right)-1\right]\left(\alpha\sin^2\theta-1\right)}{2\left(\bar{Q}-1\right)^2\cos^2\theta-6\bar{Q}^2},\\
\theta_{,\mathcal{N}} &= \frac{3\bar{Q}\sin\theta\cos\theta\left\{\left[2\bar{Q}\left(\bar{Q}+1\right)-1\right]\alpha+\left(\bar{Q}-1\right)^2\right\}}{2\left(\bar{Q}-1\right)\left[\left(\bar{Q}-1\right)^2\cos^2\theta-3\bar{Q}^2\right]},
\end{aligned} \tag{7.79}$$

and

$$\mathcal{D}_{,\mathcal{N}} = \frac{3\bar{Q}\mathcal{D}^2\left[E^2\left(3\bar{Q}^2-1\right)\alpha+3\bar{Q}^2\right]}{2\left(E^2-3\bar{Q}^2\right)}, \tag{7.80}$$

The system (7.79) has invariant submanifolds at $\bar{Q}=0$, $\bar{Q}=\frac{1}{2}\left(\sqrt{3}-1\right)$, $\theta=k\pi$, $\theta=\pi/2+k\pi$ with k integer number. It is also singular in

$$\bar{Q} = \frac{\cos(2\theta)\pm 2\sqrt{3}\cos\theta+1}{\cos(2\theta)-5} \qquad \bar{Q}=1 \tag{7.81}$$

However, as we have seen, the divergence in $\bar{Q}=1$ is just an artifact of our variable choice.

Setting $(\bar{Q}_{,\mathcal{N}}=0, \theta_{,\mathcal{N}}=0)$ shows the presence of two physical fixed points in $[0,2\pi]$ and a fixed line. The stability of these points and their associated solutions are given in Table 7.4. The line $\mathcal{L}$ is composed of non hyperbolic fixed points

and one should calculate the Centre manifold for these points. However, since the total dimension of the phase space is two, the stability of these points can be calculated simply taking the second derivative of the equation for $\bar{Q}$ at second order at $\bar{Q} = 0$. It turns out that for

$$\alpha > 1, \quad k\pi < \theta < (2k+1)\frac{\pi}{2} \tag{7.82}$$

$$\alpha < 1, \quad (2k+1)\frac{\pi}{2} < \theta < k\pi \tag{7.83}$$

where $k \in \mathbb{Z}$, these points are unstable. Since on the line $\mathcal{L}$ fixed points can lead to unstable static solutions, we can conclude that these cosmologies admit bounces and turning points only for certain values of α.

Comparing with the work in [76], we see that there are some differences; in particular, some of the fixed points do not appear in the compact version of the phase space. This is due to two different occurrences. The first is that in these points the function $\mathcal{D}$ is either zero or divergent and in this case there is no connection between the different variable systems. In the case of the power law potential we have

$$\mathcal{D} = 0 \Rightarrow \dot{\varphi}^2 + V_0 \frac{3}{2}\varphi^{\alpha+2} = 0 \tag{7.84}$$

which implies via eq. (7.13)

$$a = a_0(t - t_0)^{\frac{2}{3\alpha}}. \tag{7.85}$$

if V_0 is negative. This implies that for $V_0 < 0$ orbits approaching the asymptotic border will represent a Universe whose expansion approaches to the evolution above.

The second occurrence is that some of these points correspond to special cases in which two of the coordinates are one divergent and the other complex

divergent. In this case the constraint (7.67) is still satisfied. However, in the new formulation we have assumed that φ is positive, whereas these points are compatible with a negative φ. We can say therefore that they have no relevance if $\varphi_0 > 0$ and that our compact formulation catches the true degrees of freedom of the cosmological model. Similar reasonings can be made for the other models we will consider here.

The data analysis above indicates the following values of the quantities appearing in the cosmological equations at present[1]:

$$\begin{aligned} &\varepsilon \to 10^{-7}, \quad H_0 \to 69.6, \quad \rho_0 \to 3851.11, \quad \varphi_0 \to 0.006, \\ &V_0 \to -40344.1, \quad \alpha \to 0.12, \quad m \to 1.8 \end{aligned} \tag{7.86}$$

In Fig. 7.11 we have represented the compact phase space and the position representing the state of the Universe related to the data analysis of the previous sections. It is evident that the past attractor of the dynamics is a singular state reached coasting the invariant submanifold $\bar{Q} = \frac{1}{2}\left(\sqrt{3}-1\right)$ and the Universe approaches the $\bar{Q} = 1$ boundary after transiting close the fixed point $\mathcal{A}_1$. This behavior can be observed directly plotting the behavior of the dynamical variables in time (see Fig. 7.12). Indeed, plotting the behavior of the deceleration factor q (see Fig. 7.13) one can conclude that, as expected, the observational data represent a cosmology which present cosmic acceleration and determine the value of q on the boundary. This result is consistent with the interpretation we have given of the $\bar{Q} = 1$ boundary. In fact the solution (7.85) for the value of α given in (7.86) corresponds to an accelerated solution. The solution (7.85) was also an attractor in the phase space analysis of [76], but it was not obvious that the

[1]In order to correctly evaluate the magnitude of the fitted values in the SI units, it is worth noting, here and in the cases of the other potentials, that we are using natural units. Moreover, the Hubble constant is usually estimated as $H_0 = 100h\frac{Km}{Mpc}s^{-1}$, and the conversion factor from Km to Mpc is $\zeta \simeq 3.24\,10^{-20}$. Actually, for $h = 0.696$ the actual dark matter density is $\rho_0 = 2.41\,10^{-27}\,Kg/m^3$, as expected.

Table 7.4: The fixed points and the solutions of the Non Minimal Coupling model with dust matter and $V = V_0\varphi^\alpha$. Here S stays for saddle, A for attractor and R for repeller.

Point	$[\theta, \bar{Q}]$	Scale Factor	Stability
$\mathcal{A}_k$	$\left[\frac{\pi}{2} + k\pi, \frac{1}{2}\left(1 - \frac{1}{\sqrt{3}}\right)\right]$	$a = a_0 (t - t_0)^{2/3}$	S
$\mathcal{L}$	$(\theta_*, 0)$	$a = a_0 t^{\frac{2\cos\theta_*}{3(\alpha-1)}}$	R $\alpha > 1$, $k\pi < \theta < (2k+1)\frac{\pi}{2}$ R $\alpha < 1$, $(2k+1)\frac{\pi}{2} < \theta < k\pi$ A $\alpha > 1$, $(2k+1)\frac{\pi}{2} < \theta < k\pi$ A $\alpha < 1$, $k\pi < \theta < (2k+1)\frac{\pi}{2}$

initial conditions (7.86) would lead to it.

7.7.2 The case $V(\varphi) = V_0 \exp(-\lambda\varphi)$

If one consider the exponential potential $V(\varphi) = V_0 \exp(-\lambda\varphi)$, then

$$\begin{aligned}
\bar{Q}_{,\mathcal{N}} &= \frac{3\left[1 - 2\bar{Q}\left(\bar{Q}+1\right)\right]\left[\lambda(\bar{Q}-1)^2\cos^2(\theta)\sin^2\theta + \bar{Q}^2\right]}{2\left(\bar{Q}-1\right)^2\cos^2\theta - 6\bar{Q}^2}, \\
\theta_{,\mathcal{N}} &= \frac{3\sin\theta\cos\theta\left\{\lambda(\bar{Q}-1)^2\left[1 - 2\bar{Q}\left(\bar{Q}+1\right)\right]\cos^2(\theta) + \bar{Q}^2\left(\bar{Q}-1\right)^2\right\}}{2\bar{Q}\left(\bar{Q}-1\right)\left[\left(\bar{Q}-1\right)^2\cos^2\theta - 3\bar{Q}^2\right]},
\end{aligned} \tag{7.87}$$

and

$$\mathcal{D}_{,\mathcal{N}} = \frac{3\mathcal{D}^2\left[E^2\left(3\bar{Q}^2-1\right)\left(1-\bar{Q}\right)^2\cos^2(\theta) + 3\bar{Q}^4\right]}{2\bar{Q}\left(E^2 - 3\bar{Q}^2\right)}, \tag{7.88}$$

The system (7.87) has invariant submanifolds at $\bar{Q} = \frac{1}{2}\left(\sqrt{3}-1\right)$, $\theta = k\pi$, $\theta = \pi/2 + k\pi$ with k integer number. It is also singular in

$$\bar{Q} = \frac{\cos(2\theta) \pm 2\sqrt{3}\cos\theta + 1}{\cos(2\theta) - 5} \qquad \bar{Q} = 0 \qquad \bar{Q} = 1 \tag{7.89}$$

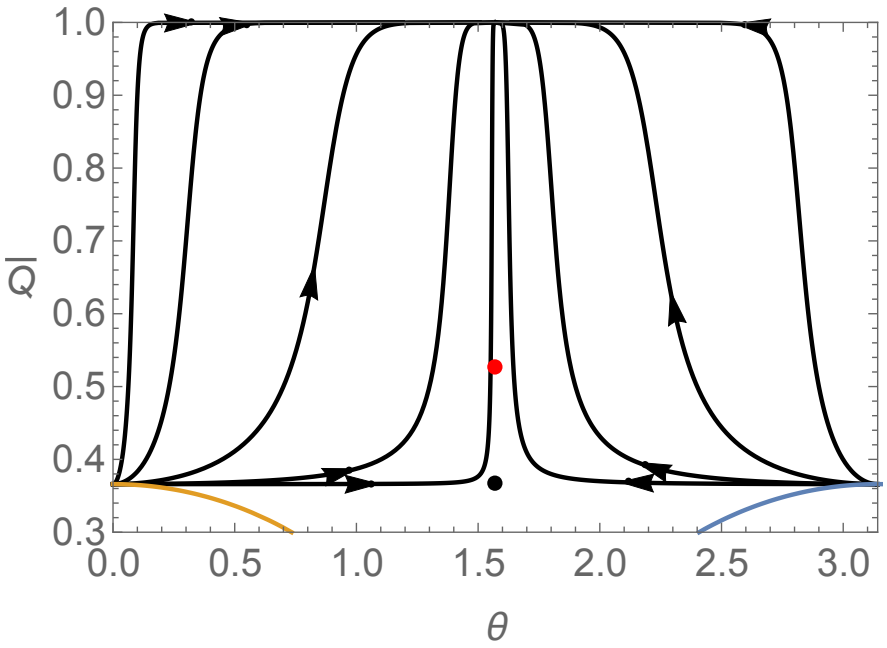

Figure 7.11: Portion of the phase space of equations (7.79). Here the black dot represents the fixed point $\mathcal{A}_1$, the orange and the blue lines the singularity of the dynamical system. The red dot represents the state of the universe as indicated from the observational analysis of Sections 4, 5 and 6.

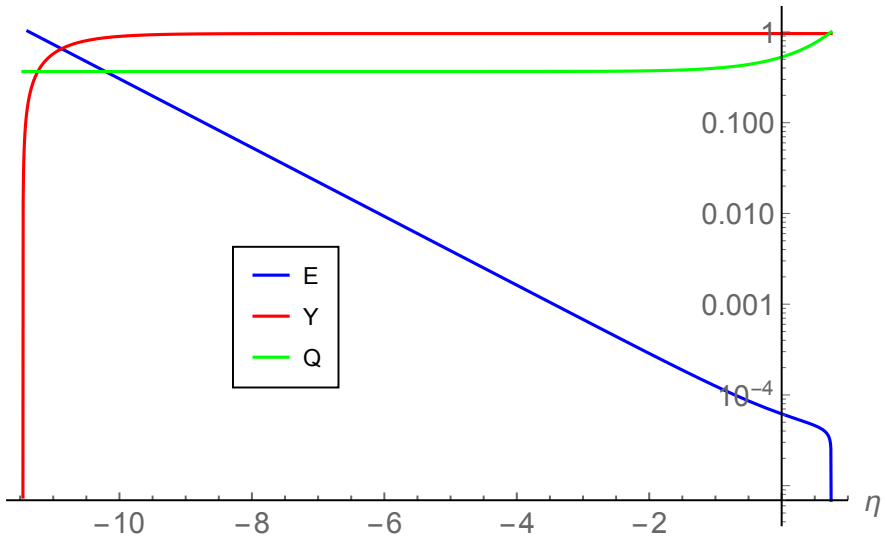

Figure 7.12: Semilogarithmic plot of the evolution of the dynamical system variables along the orbit associated with the conditions (7.86).

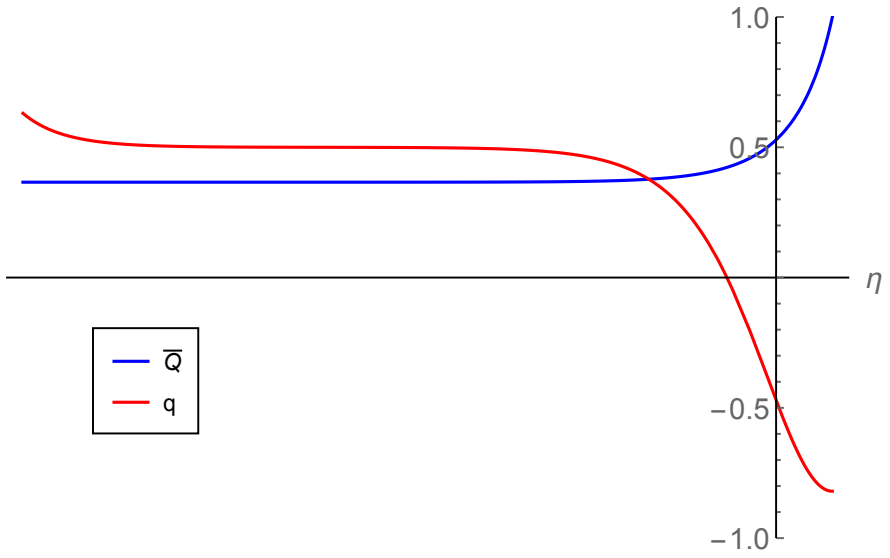

Figure 7.13: Plot of the evolution of the variable $\bar{Q}$ and the deceleration factor q along the orbits of the phase space for the potential $V(\varphi) = V_0\varphi^\alpha$ associated with the conditions (7.86).

The system (7.87) admits fixed points given by

$$\mathcal{A}_k \to \left[\frac{\pi}{2} + k\pi, \frac{1}{2}\left(1 - \frac{1}{\sqrt{3}}\right)\right] \tag{7.90}$$

where $k \in \mathbb{Z}$ which are both saddles and associated with the solution

$$a = a_0\,(t - t_0)^{2/3}\,. \tag{7.91}$$

The above data analysis indicates the following values of the quantities appearing in the cosmological equations at present:

$$\begin{aligned} &\varepsilon \to 10^{-7}, \quad H_0 \to 69.6, \quad \rho_0 \to 4069.09, \quad \varphi_0 \to 0.005, \\ &V_0 \to -21116, \quad \lambda \to 1.5, \quad m \to 0.6 \end{aligned} \tag{7.92}$$

In Fig. 7.14 we have represented the compact phase space and the position representing the state of the Universe related to the data analysis of the previous

sections. As in the case of the power law potential, the past attractor of the dynamics is a singular state on the invariant submanifold and the Universe approaches the $\bar{Q} = 1$ boundary after transiting close the fixed point $\mathcal{A}_1$. This is also confirmed by the time evolution of the variables in Fig. 7.15. The solution associated with the boundary $\bar{Q} = 1$ is given by the equation

$$\dot{\varphi}^2 + V_0 \frac{3}{2}\varphi^2 \exp\left(-\lambda\varphi\right) = 0 \tag{7.93}$$

whose solution can only be given parametrically. However, using the (7.13), we can obtain

$$q = -\frac{\ddot{a}a}{\dot{a}^2} = -1 - \frac{3\lambda\varphi_0}{2a^3} \tag{7.94}$$

which for growing a shows that the solution to this equation corresponds to an accelerating cosmology, and indeed to an asymptotically de Sitter solution. This is also confirmed by Fig. 7.13 which plots the behavior of the deceleration factor on the orbit selected by the parameters (7.92). Note also that different initial conditions in this case lead to a final state with a different value of θ.

7.7.3 The case $V(\varphi) = V_0(V_1 + \varphi)^\alpha$

If one consider the exponential potential $V(\varphi) = V_0(V_1 + \varphi)^\gamma$, then

$$\begin{aligned}
\bar{Q}_{,\mathcal{N}} &= -\frac{3\bar{Q}^2[2\bar{Q}(\bar{Q}+1)-1]\left\{\bar{Q}^4 V_1 + (\bar{Q}-1)^4\cos^4(\theta)[1+\gamma(\cos(2\theta)-1)]\right\}}{2\left[(\bar{Q}-1)^2\cos^2(\theta) - 3\bar{Q}^2\right]\left[\bar{Q}^4 V_1 + (\bar{Q}-1)^4\cos^4(\theta)\right]}, \\
\theta_{,\mathcal{N}} &= \frac{3\bar{Q}(\bar{Q}-1)\sin(\theta)\cos(\theta)\left\{\bar{Q}^4 V_1 + (\bar{Q}-1)^2\cos^4(\theta)\left[\frac{2\gamma(2\bar{Q}^2+2\bar{Q}-1)}{(\bar{Q}-1)^2}+1\right]\right\}}{2\left[(\bar{Q}-1)^2\cos^2(\theta) - 3\bar{Q}^2\right]\left[\bar{Q}^4 V_1 + (\bar{Q}-1)^4\cos^4(\theta)\right]},
\end{aligned} \tag{7.95}$$

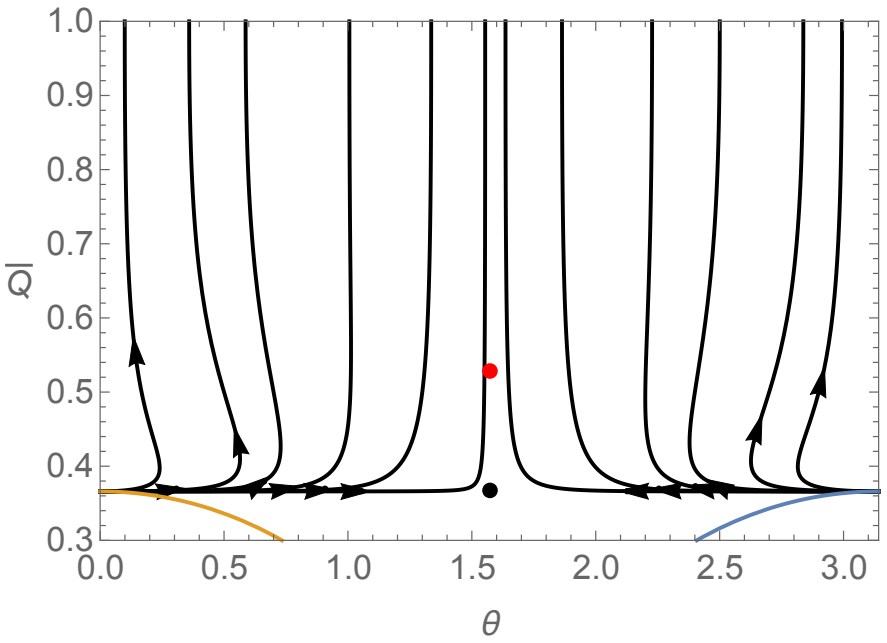

Figure 7.14: Portion of the phase space of equations (7.87). Here the black dot represents the fixed point $\mathcal{A}_1$, the orange and the blue lines the singularity of the dynamical system. The red dot represents the state of the universe as indicated from the observational analysis of Sections 4, 5 and 6.

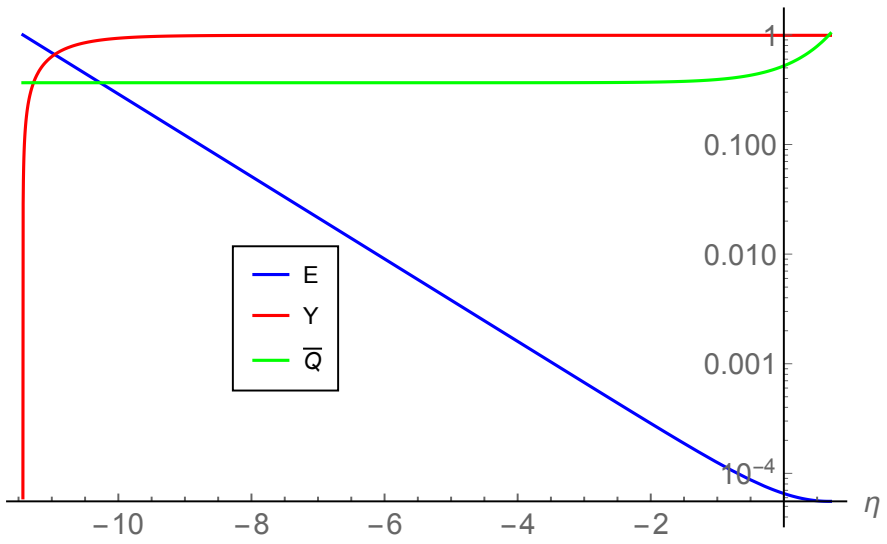

Figure 7.15: Semilogarithmic plot of the evolution of the dynamical system variables along the orbit associated with the conditions (7.92).

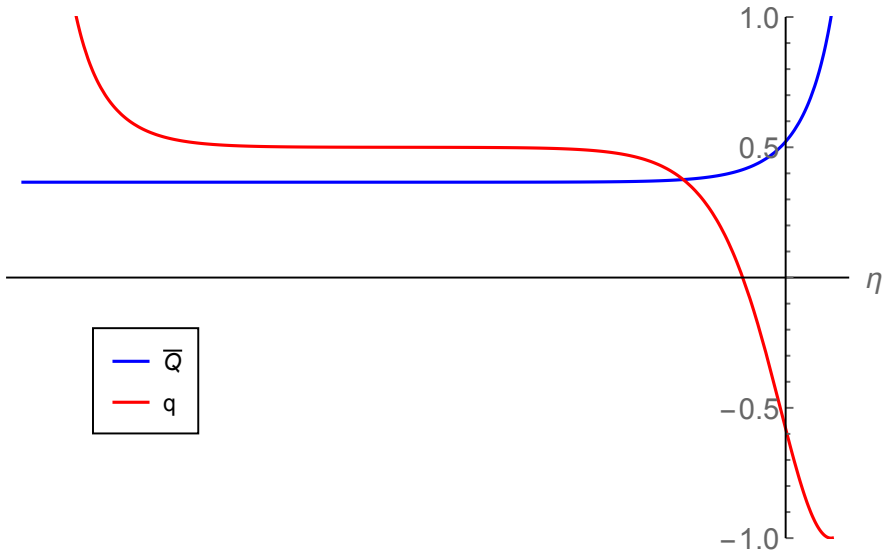

Figure 7.16: Plot of the evolution of the variable $\bar{Q}$ and the deceleration factor q along the orbits of the phase space for the potential $V(\varphi) = V_0 \exp(-\lambda\varphi)$ associated with the conditions (7.92).

and

$$\mathcal{D}_{,\mathcal{N}} = -\frac{3\bar{Q}\mathcal{D}^2\left\{3\bar{Q}^6 V_1 + (\bar{Q}-1)^4\cos^4(\theta)\left[3\bar{Q}^2 + 2\gamma(2\bar{Q}^2+2\bar{Q}-1)\cos^2(\theta)\right]\right\}}{2(\bar{Q}-1)\left\{\left[(\bar{Q}-1)^2\cos^2(\theta) - 3\bar{Q}^2\right]\left[\bar{Q}^4 V_1 + (\bar{Q}-1)^4\cos^4(\theta)\right]\right\}} \tag{7.96}$$

As expected the system above has much in common with the case of Sec. 7.7.1. Therefore we find the same invariant submanifolds, but additional singularities determined by the equation

$$V_1 = -\frac{(\bar{Q}-1)^4\cos^4(\theta)}{\bar{Q}^4} \tag{7.97}$$

The type of fixed points consist of a line and two isolated fixed points and they are the same of the ones in Sec. 7.7.1, in agreement with the analysis of [76] (see Table 7.5). Also the stability of the isolated fixed points is the same. The points

on the line, however, are unstable if

$$\gamma < 1/2 \quad -\frac{1}{\sqrt{2\gamma}} < \sin\theta < \frac{1}{\sqrt{2\gamma}} \tag{7.98}$$

The above data analysis indicates the following values of the quantities appearing in the cosmological equations at present:

$$\begin{aligned} &\varepsilon \to 10^{-7}, \quad H_0 \to 69.7, \quad \rho_0 \to 4080.08, \quad \varphi_0 \to 0.005, \\ &V_0 \to -236, \quad \gamma \to 1.6, \quad m \to 0.55, \quad V_1 \to 16.5 \end{aligned} \tag{7.99}$$

In Fig.7.17 we have represented the compact phase space and the position expressing the state of the Universe related to the data analysis of the previous sections. As in the previous cases, the past attractor of the dynamics is a singular state reached coasting the invariant submanifold $\bar{Q} = \frac{1}{2}\left(\sqrt{3}-1\right)$. The Universe approaches the $\bar{Q} = 1$ boundary after transiting close the fixed point $\mathcal{A}_1$ as indicated by the evolution of the dynamical variables in time (see Fig. 7.18). Indeed, plotting the behavior of the deceleration factor (see Fig. 7.13) one can conclude that the observational data represent a cosmology which present cosmic acceleration. However, differently form the power law case of Sec. 7.7.1, the cosmology in this case approaches a de Sitter evolution ($q = -1$) rather than an accelerated power law. As in Sec. 7.7.2, we cannot give the solution corresponding the time asymptotic state as the key equation

$$\dot{\varphi}^2 + V_0 \frac{3}{2}\varphi^2(V_1 + \varphi)^\gamma = 0 \tag{7.100}$$

does not have a solution that can be put in a useful analytical form, but, using

Table 7.5: The fixed points and the solutions of the Non Minimal Coupling model with matter and $V = V_0(V_1 + \varphi)^\gamma$. Here S stays for saddle, A for attractor and R for repeller.

Point	$[\theta, Q]$	Scale Factor	Stability
$\mathcal{A}_k$	$\left[\frac{\pi}{2} + k\pi, \frac{1}{2}\left(1 - \frac{1}{\sqrt{3}}\right)\right]$	$a = a_0 (t - t_0)^{2/3}$	S
$\mathcal{L}$	$(\theta_*, 0)$	$a = a_0 t^{\frac{2\cos\theta_*}{3(\gamma-1)}}$	R $\gamma < 1/2 \quad -\frac{1}{\sqrt{2\gamma}} < \sin\theta < \frac{1}{\sqrt{2\gamma}}$ A otherwise

eq. (7.13), we can give the form of the decelerating factor

$$q = -\frac{\ddot{a}a}{\dot{a}^2} = -1 + \frac{3\gamma\varphi_0^2}{a^6 V_1 + \varphi_0^2 - 1} \tag{7.101}$$

which approaches -1 for large a. As in the model of Sec. 7.7.2, and in contrast with the model of Sec. 7.7.1, different initial conditions lead to a final state with a different value of θ.

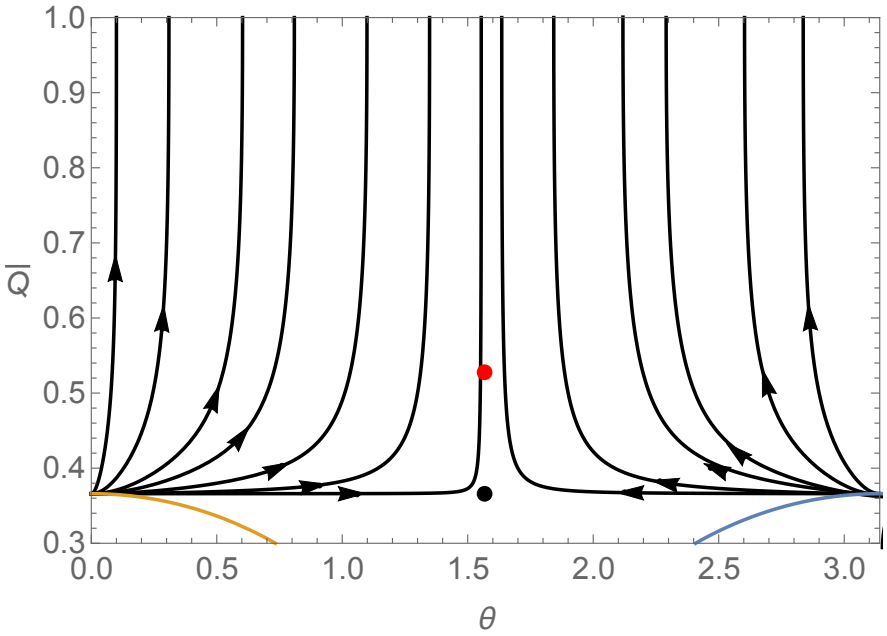

Figure 7.17: Portion of the phase space of equations (7.95). Here the black dot represents the fixed point $\mathcal{A}_1$, the orange and the blue lines the singularity of the dynamical system. The red dot represents the state of the universe as indicated from the observational analysis of Sections 4, 5 and 6.

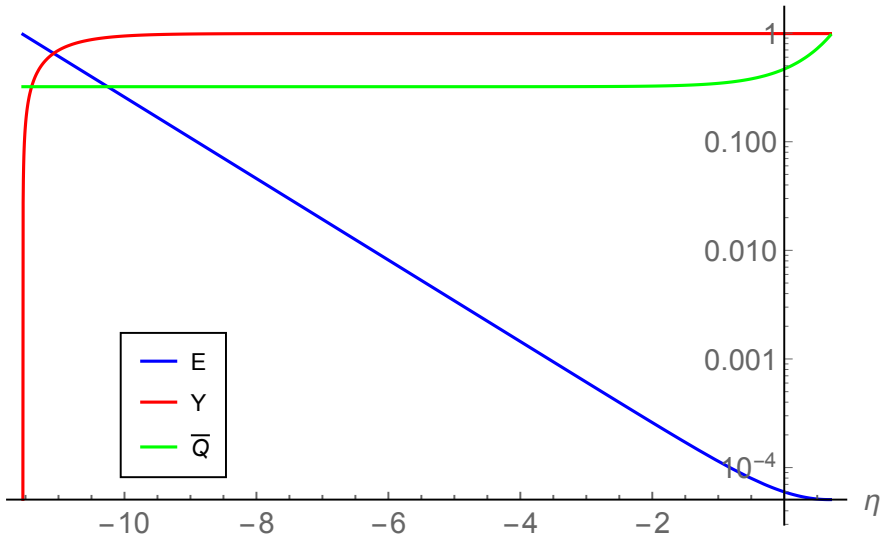

Figure 7.18: Semilogarithmic plot of the evolution of the dynamical system variables along the orbits of the phasespace for the potential $V(\varphi) = V_0(V_1 + \varphi)^\gamma$ associated with the conditions (7.99).

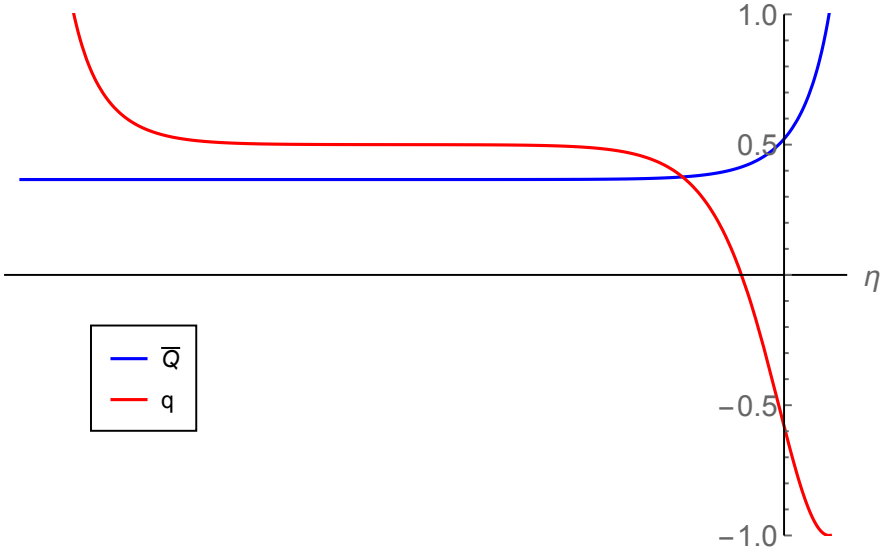

Figure 7.19: Plot of the evolution of the variable $\bar{Q}$ and the deceleration factor q along the orbit associated with the conditions (7.99).

Chapter 8

Discussion and conclusions

In this thesis, we have seen how possible astrophysical and cosmological applications of Extended Theories of Gravity can be obtained. Indeed, on astrophysical scales, we have seen how a higher order theory can describe and predict massive Neutron Stars not justified by General Relativity or, on cosmological scales, thanks to a non-minimally coupled theory, compare theoretical predictions with observations for a class of cosmological models in which the dark energy component is modeled as a Fermionic condensate, non-minimally coupled with the gravitational field and characterized by some specific self-interaction potentials.

The first step that was done, was to derive the stellar structure equations for compact objects using two known formalisms by General Relativity and, in Palatini formalism, introducing the torsion and spin, where the additive terms that emerge could be sources of gravitational field and justify observations of massive Neutron Stars [7; 8; 10; 11; 253] that appear to exceed the Chandrasekhar's limit. In his theory, Chandrasekhar considering degenerate matter, fixed a theoretical upper limit for the stability of a static Neutron Stars at $1.44 M_{\odot}$ [6] but some observations have measured higher mass values [7; 8; 10; 11; 253]. Thus, a good estimate of the Neutron Star mass, would provide further information on the behavior of matter at extreme regimes.

It is well known that the structure of a Neutron Star is strictly correlated with the equation of state, *i.e.* the relation between pressure and density in its interior [2]. Considering instead spin fluids, in addition to the relation between pressure and density, it is necessary to have an additional equation of state that relates the spin to the same density. For any Neutron Stars, in principle, a corresponding maximal mass can be derived, giving an equation of state and plotting the mass-radius ($M - \mathcal{R}$) relation that depends only on the equation of state [254], so describing the evolution of the star's mass according to its radius. Moreover, by finding the ($M - \mathcal{R}$) relation using the Tolman-Oppenheimer-Volkoff equations in both theories, with torsion and/or spin, one could understand what might be, eventually, regions prohibited for the stability of the star.

In fact, in the second step, we have studied the existence of realistic Nuetron Stars in the context of the $f(R) = R + \alpha R^2$ theory both in the purely metric and torsional formulations. The main results concern the computation of the $\mathcal{M} - \mathcal{R}$ diagrams resulting from the two different theoretical frameworks considered. Matter fields have been represented by static and spherically symmetric perfect fluids where the equations of state have been chosen to agree with the recent LIGO-Virgo constraints [50]. The parameter α has been restricted to be smaller than $|\alpha| \leq 0.1$ to avoid unrealistically large oscillations (see e.g. [215]) on our metric potentials and therefore ensuring the(i) fullfillment of junction conditions and (ii) the accurate recovery of the Schwarzschild solution far from the source. These two requirements single out four of the five initial conditions: $p(0)$, $\lambda(0)$,$\psi(0)$ and $R'(0)$, while $R(0)$ remains free. $R(0)$ is ideally defined by choosing this parameter in such a way to match the junction conditions (6.8)(6.9). However, the oscillatory behavior of some solutions for $r \to \infty$ prevents from finding a unique value for $R(0)$. To overcome this issue, we have set $R(0) = R_{GR}$ identical to the General Relativity value. This assumption have been shown to be valid for

small α, being the estimates of the Neutron Star radius only mildly dependent on the $R(0)$ choice, but this is no longer true for $\alpha \gtrsim 1$.

However, a general consideration is in order at this point to justify the assumption $R(0) = R_{GR}$. Let us consider the trace of field equations in metric

$$f'(R)R - 2f(R) + 3\Box f'(R) = 8\pi\Sigma\,, \tag{8.1}$$

and in torsion case

$$f'(R)R - 2f(R) = 8\pi\Sigma\,. \tag{8.2}$$

Substituting $f(R) = R + \alpha R^2$, we have, in the metric case,

$$6\Box R - R = 8\pi\Sigma\,, \tag{8.3}$$

and, in the torsion case,

$$R = -8\pi\Sigma\,. \tag{8.4}$$

For the metric picture, it is reasonable to suppose that, at the center of the star, $\Box R \simeq 0$ because one can assume a constant central density without remarkable variations and gradients [255]. For the torsion picture, we recover exactly the trace of General Relativity. According to these results, the assumption $R(0) = R_{GR}$, besides the above numerical considerations, is fully justified.

In the purely metric theory, the obtained results show a progressive increasing of the total mass as $|\alpha|$ increases, for all the four equations of state considered. This allows for higher masses and more compact Neutron Stars than in General Relativity. This absolute increasing of the mass and compactness could be also reproduced by assuming softer equations of state in full General Relativity, consitent with the recent observations [50]. In the torsion case, the Neutron Star mass tends to decrease for all the equations of state considered. This could be related with the fact that the stable branch of the solutions is flipped with respect

to the purely metric case, in order to ensure the stability of the numerical system. The physical existence of such solutions could help us to describe Neutron Star compact or not, based on astrophysical observations, choosing the appropriate theory by simply constraining whether α is positive or negative. In the torsional framework, the differences about the $\mathcal{M}-\mathcal{R}$ predictions with respect to General Relativity are larger than those obtained in the purely metric case, as a consequence, the allowed intervals on α are poles apart from the two theories. Moreover, the theory with torsion would seem to describe less compact Neutron Star. This would allow to obtain solutions that could be reproduced using equations of state with stiff matter in the limit of General Relativity. Unfortunately, this is in disagreement with the recent LIGO-Virgo discoveries [50]. What comes to the rescue is that given the current accuracy of electromagnetic observations, we can not deny the Neutron Stars observations yet because the differences with the General Relativity are still too small. However, this issues could be addressed by next generation gravitational wave detectors (3G) [256; 257; 258], where the scientific community may have the opportunity to test the results presented in this thesis.

The Mass-Radius diagrams plotted in the two theories, included only perfect fluids because the equations with spin, presenting a further degree of freedom due to the spin, were found to be strongly non-linear and, consequently, the numerical resolutions its turned out to be quite complicated. This is due to the fact that the spin gradients add higher order derivatives that increases the stiffness of our numerical system. We plan to extend these solutions in a future work.

Neutron Stars, furthermore, have a main role in relativistic astrophysics because, since they are the visible objects more denser than the observable universe, their material fields at extreme regimes would allow us to better understand the final phases of stellar evolution. Taking all this into account, a good knowledge of

the equation of state that describes the matter degenerate within it, would allow both to obtain information on the state of degenerate matter and to understand the global behavior of stars in the final stages of their life. Moreover, the Neutron Stars could be an excellent investigation tool, in extreme regimes where General Relativity exhibits some limitations too, both on astrophysical and cosmological scales and could be what is called the *Prova Regina* to test the validity of modified theories of gravity thanks to the huge gravitational field acting on them.

In the third step, on a cosmological scale, we have analyzed some accelerating cosmological models in which dark energy is modeled as a non-minimally coupled selfinteracting fermion condensate. Assuming standard matter to be non relativistic, we have investigated three different forms of potential $V(\varphi)$ that are important in cosmological models with scalar fields.

As a first example, we have considered the power law model $V(\varphi) = V_0\varphi^\alpha$. At early times ($a \approx 0$) the (7.14) implies that the scalar field will have high values and the potential will be negligible ($\alpha < 0$) or dominant ($\alpha > 0$). This situation is reversed at late time ($a \to \infty$). We have obtained a suitable parametrized form of the Hubble function written in terms of redshift, which, with an appropriate choice of parameters, is comparable to the ΛCDM model within a wide range of redshifts and differs at very high redshift.

The second example we have considered has been the exponential potential $V(\varphi) = V_0 \exp(-\lambda\varphi)$ which is commonly used for scalar fields. At late time $\varphi \to 0$ the exponential potential becomes actually a cosmological constant term: indeed, also in this case, the behavior of the function $H(z)$ mimics, for an appropriate choice of the parameters, the standard ΛCDM model.

The third example we have studied has been the potential $V = V_0(\varphi^2 + V_1)^\gamma$ which is a generalization of the power law potential. This potential combines characteristics of both the previous potentials as it behaves as a power law and

generates an effective cosmological constant at late time, related to the value of the constant V_1.

After choosing appropriate parameterizations of these models, we have tested them with some different observational data. To this end, we have used the recently updated Supernovae Cosmology Project union 2.1, a sample of 193 Gamma Ray Bursts Hubble diagram, and a list of 28 $H(z)$ measurements, compiled in [80]. Moreover, we have set Gaussian priors on the distance data from the Baryonic Acoustic Oscillations [243] and the Hubble costant h, in order to help break the degeneracies among the parameters of the different cosmological models. For our statistical analysis, we have used the Markov Chain Monte Carlo Method, running five parallel chains, and using the Gelman-Rubin test to check the convergence. The histograms of the parameters from the merged chains have been then used to infer median values and confidence ranges. In Table 7.2, we have presented the results of our analysis for the main parameters concerning the three different models. The analysis we have performed indicates that a non–minimally coupled self-interacting fermion condensate is compatible with the datasets we have considered.

We have analyzed the three different models using the Akaike Information Criterion AIC [247; 248] and its indicator (7.56). We have found that the model with the lower AIC is the the exponential potential one $V(\varphi) = V_0 \exp(-\lambda\varphi)$. We also used the same method to perform a comparison of the exponential potential model with the Chevallier-Polarski-Linder CPL parametrization for dark energy with an equation of state given by (7.57). Interestingly, it turned out that the exponential model has the lower AIC indicating a weak evidence against the Chevallier-Polarski-Linder model. This result should be confirmed using further data which will be available in the future.

In addition, we have investigated the Euclid experimental possibility to con-

strain our model. We used simulated data assuming an Euclid - like survey of Type Ia Supernovae [251] (plotted in Fig. 7.9) setting the exponential potential model as the fiducial model and considering the simulated Type Ia Supernovae HD as cosmological probes. In Table 7.3 we have summarized the results of the simulation. These results indicate that the mock dataset is able to constraint much better our model.

Finally, using the values of the parameters deduced by the statistical analysis, we have used dynamical system techniques to infer the general behavior of the cosmology and in particular the behavior of the deceleration factor. As expected, it turns out that the three potentials lead to similar behaviors with differences in the final value of q which is -1 for potentials that generate a cosmological constant term and is higher than this value in the other cases. The behavior of the deceleration factor suggests that changes in the expansion rate during the matter dominate era might have repercussions in the large scale structure. Whether these differences are observables, however, cannot be deduced from our calculations and will require further work on the behavior of matter and condensate fluctuations.

We conclude noticing that: the possible astrophysical and cosmological applications of Extended Theories of Gravity presented in this thesis have provided answers fairly consistent with today's astrophysical and cosmological observations. Surely they are not definitive theories to be taken as a reference point, but they could be a good start in order to formulate a more advanced and complete theory. The results present in this thesis will be the subject of future works where, on astrophysical scale, we will try to describe stellar structures with spin plotting the Mass-Radius diagrams and comparing them with the results already obtained in this thesis. We will see how the spin source could behave when the mass of the Neutron Star tends to increase. From the obtained equations we see that the spin could behave as an additional repulsive field, like the torsion, that tends to oppose

the increase of the star mass. This possible information, which could be denied or confirmed, can only be obtained by numerically solving the very complicated Tolman-Oppenheimer-Volkoff equations with the spin fluids that previously we obtained. Instead, on cosmological scale, the results obtained in this thesis take into account the fact that we have considered here standard matter in the form of dust and than the complete description of the cosmic history, in particular at earlier times, requires the inclusion of other forms of matter–energy, like radiation. This analysis is certainly possible with the dynamical system approach we proposed, but it requires a different treatment of the datasets, other than, probably additional sources of data. In addition, as we approach even earlier epochs, the approximation of the semiclassical fermion, which is the cornerstone of the theory we have considered, starts to loose accuracy. This indicates that our approach to the analysis of this type of cosmology is useful but need to be extended with care in order to give meaningful results. Future works will consider this more complicated situation.

Appendix A

Neutron Stars in General Relativity

A.1 Derivation of Tolman-Oppenheimer-Volkoff equations

In General Relativity, a model of an isolated star generally consists of a fluid-filled interior region, i.e. a perfect fluid solution of the Einstein field equation, and an exterior region, which is an asymptotically flat vacuum solution. These two pieces must be carefully matched across the world sheet of a spherical surface, the surface of zero pressure. The exterior region of non-rotating compact objects is given in terms of the Schwarzschild solution. We derive the famous Tolman-Oppenheimer-Volkoff equations which give the hydrostatic equilibrium for relativistic stars. This equations can be derived in a standard way by calculating the Christoffel symbols in Schwarzschild coordinates and from there the Riemann and Ricci tensor. Static and spherically symmetric non rotating stars therefore generate a spacetime of the following form (with $c = 1$)

$$ds^2 = -e^{2\psi(r)}dt^2 + e^{2\lambda(r)}dr^2 + r^2(d\theta^2 + \sin^2\theta d\phi^2). \tag{A.1}$$

The non-null components of the Einstein tensor $G_{ij} = R_{ij} - \frac{1}{2}g_{ij}R$ are:

$$G_{00} = \frac{1}{r^2} - e^{-2\lambda(r)}\left(\frac{1}{r^2} - \frac{2\lambda'}{r}\right) = \frac{1}{r^2}\frac{d}{dr}\left[r\left(1 - e^{(-2\lambda(r))}\right)\right], \tag{A.2}$$

$$G_{11} = -\left[\frac{1}{r^2} - e^{-2\lambda(r)}\left(\frac{1}{r^2} - \frac{2\psi'}{r}\right)\right], \tag{A.3}$$

$$G_{22} = G_{33} = e^{-2\lambda(r)}\left[(\psi')^2 - \psi'\lambda' + \frac{\psi' - \lambda'}{r}\right], \tag{A.4}$$

where $\lambda' = \frac{d\lambda}{dr}$, $\psi' = \frac{d\psi}{dr}$ and $G_{ij} = 0$ for $i \neq j$. The equality of A.4 is a consequence of the isotropy on the sphere. Einstein's equations, provide three equations for the two functions $\lambda(r)$ and $\psi(r)$. In fact, the third equation contains the hydrostatic equilibrium, since the equations of motion are not independent in General Relativity. The matter in the interior of the star is described in terms of the energy-momentum tensor Σ_{ij} that assumes the form of a perfect fluid

$$\Sigma_{ij} = (\rho + p)u_i u_j + p g_{ij}, \tag{A.5}$$

where ρ is the total mass-energy-density, p is the corresponding pressure, u_i is the local fluid 4-velocity and g_{ij} are the covariant components of the metric tensor. For static stars, with the signature used in A.1, the source of the gravitational field has the form

$$\Sigma_{ij} = diag(-\rho, p, p, p). \tag{A.6}$$

Consequently, Einstein's equations (with $G = 1 = c$)

$$G_{ij} = 8\pi\Sigma_{ij}, \tag{A.7}$$

can explicity written as

$$G_{00} = \frac{1}{r^2} - e^{-2\lambda(r)}\left(\frac{1}{r^2} - \frac{2\lambda'}{r}\right) = 8\pi\rho(r), \tag{A.8}$$

$$G_{11} = -\left[\frac{1}{r^2} - e^{-2\lambda(r)}\left(\frac{1}{r^2} - \frac{2\psi'}{r}\right)\right] = 8\pi p(r), \tag{A.9}$$

$$G_{22} = G_{33} = e^{-2\lambda(r)}\left[(\psi')^2 - \psi'\lambda' + \frac{\psi' - \lambda'}{r}\right] = 8\pi p(r). \tag{A.10}$$

The first two equations, provide us two independent equations for the functions $\psi(r)$ and $\lambda(r)$

$$\frac{1}{r^2} - e^{-2\lambda(r)}\left(\frac{1}{r^2} - \frac{2\lambda'}{r}\right) = 8\pi\rho(r), \tag{A.11}$$

$$\left[\frac{1}{r^2} - e^{-2\lambda(r)}\left(\frac{1}{r^2} - \frac{2\psi'}{r}\right)\right] = -8\pi p(r). \tag{A.12}$$

The first equation is equivalent to

$$(re^{-2\lambda(r)})' = 1 - 8\pi\rho(r)r^2, \tag{A.13}$$

which can be integrated with the asymptotic flatness condition to yield the 3-space metric

$$e^{-2\lambda(r)} = 1 - \frac{2M(r)}{r}, \tag{A.14}$$

with the total mass inside radius r given as

$$M(r) = 4\pi\int_0^r \rho(r')r'^2 dr'. \tag{A.15}$$

By subtracting the second equation from the first one, we obtain

$$e^{-2\lambda(r)}(\psi' + \lambda') = 4\pi[\rho(r) + p(r)]r. \tag{A.16}$$

This is equivalent to

$$\frac{d\psi}{dr} = \left(1 - \frac{2M(r)}{r}\right)^{-1}\left(\frac{M(r)}{r^2} + 4\pi r p(r)\right). \tag{A.17}$$

This demonstrates now, how the gravitational force is generalized in General Relativity. In particular, pressure is a source of the gravitational field, and the Schwarzschild metric acts as a modification in the denominator of the force-law. Solving the first and the second equations for λ' and ψ', we obtain

$$-2r\lambda' = (1 - 8\pi r^2\rho)e^{2\lambda(r)} - 1, \tag{A.18}$$

$$2r\psi' = (1 - 8\pi r^2 p)e^{2\lambda(r)} - 1. \tag{A.19}$$

Taking the derivative of (A.19), multiply by r, solving for ψ'', using the (A.18) in the ψ'' equation, using (A.10) in the ψ'' equation which allows us to eliminate all the metric functions and rearranging, we obtain the equation for the relativistic hydrostatic equilibrium

$$\frac{dp}{dr} = -\frac{M(r)\rho(r)}{r^2}\left(1 + \frac{p(r)}{\rho(r)}\right)\left(1 + \frac{4\pi r^3 p(r)}{M(r)}\right)\left(1 - \frac{2M(r)}{r}\right)^{-1}. \tag{A.20}$$

The (A.20) is the Tolman-Oppenheimer-Volkoff equations [52] that, for a given equation of state $p = p(\rho)$, can be easily integrated from the origin with the initial conditions $M(r) = 0$ and an arbitrary value for the central density $\rho_c = \rho(0)$ until the pressure *p(r)* ill vanish at some radius *Rs*. To each possible equation of state, there is a unique family of stars parametrized by central density, i.e. we obtain a sequence of stellar models $M(r) = M(\rho_c)$.

Appendix B

The Friedmann equations and the standard cosmological model

B.1 The Friedmann equations

The Friedmann equations are a set of equations in cosmology that govern the expansion of space in homogeneous and isotropic models of the universe within the context of General Relativity. They were first derived from Einstein's field equations of gravitation starting for the Friedmann–Lemaître–Robertson–Walker metric and a perfect fluid with a given mass density ρ and pressure p [259; 260]. The Friedmann–Lemaître–Robertson–Walker FLRW metric is an exact solution of the Einstein's field equations of General Realtivity; it describes a homogeneous, isotropic, expanding (or otherwise, contracting) universe that is path-connected, i.e. assuming *The Cosmological Principle*. This model is sometimes called the *Standard Model of Modern Cosmology* [261] The metric was derived independently from the authors, arriving at the same result. The final metric has the following form, (with *c=1*), [259; 260]:

$$ds^2 = dt^2 - a^2(t)\left[\frac{dr^2}{1-kr^2} + r^2(d\theta^2 + \sin^2\theta d\phi^2)\right], \tag{B.1}$$

where $a(t)$ is the cosmic scale factor and k is a constant representing the curvature of the space.

The metric (B.1) contains the spatial hypotheses of homogeneity and isotropy and is therefore the most suitable for the study of cosmology. From a general point of view, assigning a given cosmology, in accordance with the *cosmological principle*, means deriving the cosmic scale factor $a(t)$ from the cosmological equations. The cosmic scale factor parameterizes the relative expansion of the universe and this is a key parameter of the Friedmann equations. The parameter k, instead, assigns the curvature of the spatial submanifold. For $k = 1$ we have spatially closed models (3D sphere), for $k = 0$ we have spatially flat models and for $k = -1$ we have spatially open models (hyperbolic models). As a result, this metric assigns all the topologies of the universe.

By inserting the metric (B.1) into Einstein's equations, we obtain all the necessary information on the universe evolutions and the contribution of Einstein's equations, i.e. the matter quantity present in the universe, gives us the nature of k, i.e. the matter present in the universe tells us the space topology. With abundant matter, the universe curves, with little abundant matter the universe expands, instead with matter in equilibrium with energy we have a substantially flat space. Thus, the value of k is assigned by the matter-energy density of a given cosmological model.

Starting from the (B.1), the cosmological equations or Friedmann equations are obtained and written in this form [259; 260]:

$$\left(\frac{\dot{a}}{a}\right)^2 = \frac{8\pi G\rho}{3} - \frac{k}{a^2(t)}, \tag{B.2a}$$

$$\frac{\ddot{a}}{a} = -\frac{4\pi G}{3}(\rho + 3p), \tag{B.2b}$$

and the continuity equations

$$\dot{\rho} + 3\frac{\dot{a}}{a}(\rho + p) = 0. \tag{B.3}$$

The expression of the Ricci scalar in the Friedmann–Lemaître–Robertson–Walker spacetime is

$$R = -6\left[\frac{\ddot{a}}{a} + \left(\frac{\dot{a}}{a}\right)^2 + \frac{k}{a^2}\right]. \tag{B.4}$$

The (B.4) is very important because inside it contains all the cosmological dynamics, i.e. it provides the evolution of the cosmic scale factor, contains the Hubble parameter and the curvature of the universe. The (B.2) are the Friedmann or cosmological equations for a homogeneous, isotropic universe. The (B.2a) is an expansion equation while the (B.2b) is a scale acceleration equation i.e. what type of acceleration the universe undergoes. The (B.2a) and (B.2b) are two equations in three unknowns (ρ, p and $a(t)$). The (B.3), derived from Bianchi's identity considering perfect fluid, establishes a relation between ρ and p. Since the cosmological fluid is not known, in order to complete the cosmological model, a fourth equation is inserted, i.e. the equation of state written in the form

$$p = w\rho, \tag{B.5}$$

where w is the adiabatic index. Having an extra equation, the (B.3) can be used as a constraining equation. The system (B.2), (B.3) and (B.5) represents the standard cosmological model with the three variables ρ, p and $a(t)$ and the two parameters w and k. By assigning the two parameters, we can solve the system and see the type of universe that we are considering.

B.2 The standard cosmological model

The standard cosmological model explains observations consistently in a simple framework. In fact, this model coherently reproduce some of the cosmological observations. For example, allows us to see the recession of galaxies through the Hubble law, thus finding that the universe is expanding. The second observation is compatible with an expanding thermodynamic universe, allowing us to identify an era dominated by radiation and an era dominated by matter. This allows us to calculate, on the one hand, the time that passes from the beginning of the expansion to the time in which matter is decoupled from radiation, and on the other hand, its possible to calculate the time from the present epoch up to when this type of process occurs. We see that, from the beginning of the expansion up to the matter transparency, about 1250 years elapse while, instead, from today's era until the time when this luminous surface was, also called the last scattering surface, about 13.7 billion years elapse. So, we can say that this model provides a series of coherent observations. Furthermore, we can obtain the rate of cosmological fluid variation provided by the Hubble parameter. Consequently, we can get an estimate of the energy density that gives information on how the universe is expanding. This depends on the matter considered in the model.

However, this model presents important inconsistencies. The first problem, and it is also the most obvious one, is the *initial singularity problem*. The standard cosmological model was formulated considering standard matter. The choice of the matter and, consequently, the choice of the adiabatic index w, implies a different temporal evolution of the matter-energy density $\rho(t)$, implies a different temporal evolution of the cosmic scale factor $a(t)$ and, consequently, of the Hubble parameter $H(t) = \frac{\dot{a}(t)}{a(t)}$. For example, for $w = 0$, an universe dominated by dust with zero pressure, i.e. non relativistic matter (baryons), $\rho(t) \sim a^{-3}$, $a(t) \sim t^{\frac{2}{3}}$ and $H(t) = \frac{2}{3t}$ where, in this era, the gravitational interaction is dominant. For

$w = \frac{1}{3}$, an universe dominated by radiation, i.e. dominated by relativistic matter (photons and neutrinos), $\rho(t) \sim a^{-4}$, $a(t) \sim t^{\frac{1}{2}}$ and $H(t) = \frac{1}{2t}$ where, in this era, electromagnetic interaction is dominant or, for $w = 1$, an universe dominated by stiff matter, i.e. compact matter in primordial eras, $\rho(t) \sim a^{-6}$, $a(t) \sim t^{\frac{1}{3}}$ and $H(t) = \frac{1}{3t}$. Thus, whatever the type of matter, the matter-energy density evolves as $\rho(t) \sim \frac{1}{t^2}$.

If we consider the (B.2a), for $k = 0$, we see that $\left(\frac{\dot{a}}{a}\right)^2 \sim \frac{1}{t^2}$. The initial singularity problem emerges when $t \to 0$. In fact, we have the matter-energy density and the Hubble parameter that go to infinite and the cosmic scale factor go to zero, consequently the model is divergent when $t \to 0$. This is due to the fact that, in the standard cosmological model, standard matter was considered. Consequently at infinitely large energies, in a very small volume, a perfect fluid is incompatible in these conditions due to the strong interactions between molecules. Thus, the initial singularity problem implies another problem, namely *the matter problem*, i.e. what kind of matter or source exists in the early universe. In fact, considering the (B.2b), if we use the (B.5) in the (B.2b), for the ordinary matter, we obtain a decelerated expansion of the universe, but the observations show us that the universe expands accelerating. Consequently, for standard fluids, the universe can only expand by decelerating. Experimentally, instead, the universe is expanding accelerated with a cosmic fluid accelerated at negative pressure, $p = -\rho$. Therefore, to justify the observations, the cosmological fluid must have a different nature. This problem, also called *dark energy* concept, represents about 68% of the matter present in the universe. Then, we have the *horizon problem*, i.e. the characteristic length that we observe is not invariant but tends to zero for $t = 0$, whatever the type of matter choose. So, the horizon goes to zero for $t = 0$. To obtain a finite length at the origin, the universe, at some point, must evolve with a cosmic scale factor that includes increasing and decreasing

exponentials that eliminate this singularity. Thus, a temporal evolution of the universe that includes exponentials allows us to eliminate the *horizon problem*.

Another problem of the standard cosmological model is related to the formation of large-scale structures, also called *dark matter* concept. What is observed is that the galaxies and galaxy clusters, in order to assume those structures, need a greater mass than the one observed. When observing autogravitating objects such as galaxies, we note that by studying their rotation curves, considering only the luminous matter, at some point the curves tend to decrease. Instead, what is observed is that the rotation curves, at a certain point, tend to remain stable at a constant velocity. This means that there is another matter that gravitationally interacts but does not interact with light radiation. This quantity of matter represents about 27% of the fluid present in the universe. Therefore, almost 95% of matter/energy is non-baryonic, while only 5% is of baryonic form.

Another problem is the *homogeneity problem*. It is observed that the Cosmic Microwave Background Radiation is isotropic up to an accuracy of the order of $10^{-(4\div5)}$. This implies that the last scattering surface, as mentioned, must be homogeneous within the aforementioned accuracy on a length scale at least as large as the light cone passed, at the recombination time of the primordial elements (last scattering). The problem arises because the light cone passed is larger than the comovent radius of the cone light future at the recombination time. Thus, within the standard cosmology framework, there are no causal processes that can create the observed homogeneity, being causally disconnected volumes of distant universes. So, what happens is that the number of objects observed is more homogeneous than it should be.

Finally, we have the *flatness problem*, where the universe is more homogeneous and isotropic than it should be. Therefore, there must have been a mechanism, before the radiation and the matter epoch, that allowed the universe to expand

in such a way as to have a higher isotropy and homogeneity than what we can observe now. Furthermore, this mechanism must have been able to eliminate the initial singularity because primordial matter cannot be considered as a perfect fluid.

Most of the standard cosmological model inconsistencies are attributable at primordial epochs. The flatness, initial singularity and homogeneity problems, have been studied using inflationary cosmological models where, in the primordial era, inflation hypothesizes that the universe, shortly after the Big Bang, has undergone an extremely rapid expansion phase, due to great negative pressure. In the literature, there are many works that effectively solve these problems of the standard cosmological model. (For more information see [40; 82]). As for the dark matter and dark energy problem, they are current problems that have not yet found a coherent answer with current cosmological models but many theories, including the Extended Theories of Gravity, try to propose models that are consistent with recent observations.

Bibliography

[1] A. W. Steiner, S. Gandolfi, F. J. Fattoyev, and W. G. Newton, *Phys. Rev. C* **91**, 015804 (2015). 1

[2] J. M. Lattimer and M. Prakash, *Phys. Rept.* **621**, 127 (2016). 2, 142

[3] K. Hebeler, J. M. Lattimer, C. J. Pethick, and A. Schwenk, *Astrophys. J.* **773**, 11 (2013). 2

[4] F. Ozel and P. Freire, Ann. Rev. *A&A* **54**, 401 (2016). 2, 90

[5] A. W. Steiner, C. O. Heinke, S. Bogdanov, C. Li, W. C. G. Ho, A. Bahramian, and S. Han, Mon. Not. Roy. *Astron. Soc.* **476**, 421 (2018). 2

[6] S. Chandrasekhar, *Astrophys. J.* **74**, 81 (1931). 2, 141

[7] O. Barziv *et al.*, *A&A* **377**, 925 (2001). 2, 141

[8] M.L. Rawls *et al.*, *Astrophys. J.* **730**, 25 (2011). 2, 141

[9] F. Mullally, C. Badenes, S.E. Thompson and R. Lupton, *Astrophys. J.* **707**, L51 (2009). 2

[10] D. Nice *et al.*, *Astrophys. J.* **634**, 1242 (2005). 2, 141

[11] P.B. Demorest, T. Pennucci, S.M. Ransom, M.S.E. Roberts, J.W.T. Hessels, *Nature* **467**, 1081 (2010). 2, 141

[12] A. V. Astashenok, S. Capozziello, S. D. Odintsov, *Physics Letters B* **742**, 160 (2015). 2

[13] A. V. Astashenok, S. Capozziello and S. D. Odintsov, *JCAP* **1312**, 040 (2013). 2

[14] A. V. Astashenok, S. Capozziello and S. D. Odintsov, *Phys. Rev. D* **89**, 103509 (2014). 2

[15] A. V. Astashenok, S. Capozziello and S. D. Odintsov, *Astrophys. Space Sci.* **355**, 333 (2015). 2

[16] A. V. Astashenok, S. Capozziello and S. D. Odintsov, *JCAP* **1501**, 001 (2015). 2

[17] S. Capozziello, M. De Laurentis, R. Farinelli and S. D. Odintsov, *Phys. Rev. D* **93**, 023501 (2016). 2, 88

[18] S. Perlmutter *et al.* [Supernova Cosmology Project], *Astrophys. J.* **517**, 565 (1999). 2, 5, 14

[19] A. G. Riess *et al.* [Supernova Search Team], *Astron. J.* **116**, 1009 (1998). 2, 5, 14

[20] A. G. Riess *et al.* [Supernova Search Team], *Astrophys. J.* **607**, 665 (2004). 2, 5, 15

[21] D. N. Spergel *et al.* [WMAP Collaboration], *Astrophys. J. Suppl.* **148**, 175 (2003). 2, 5, 15

[22] C. Schimdt *et al.*, *Astron. Astrophys.* **463**, 405 (2007). 2, 5

[23] P. McDonald *et al.*, (SDSS) *Astrophys. J. Suppl.* **163**, 80 (2006). 2, 5

[24] N.A. Bahcall *et al.*, *Science* **284**, 1481 (1999). 2, 5

[25] K. Bamba, S. Capozziello, S. Nojiri, S.D. Odintsov, *Astrophys.Space Sci.* **342**, 155 (2012). 2, 5

[26] A. Joyce, B. Jain, J. Khoury, M. Trodden, *Phys.Rept.* **568**, 98 (2015). 2, 5

[27] S. Capozziello, *Int. J. Mod. Phys. D* **11**, 483 (2002). 2, 6, 16, 18

[28] S. Capozziello, S. Carloni, A. Troisi, Recent Res. Dev. Astron. *Astrophys.* **1**, 625 (2003). 2, 6

[29] S. Nojiri, S.D. Odintsov, *Phys. Rev. D* **68**, 123512 (2003). 2, 3, 6

[30] S. M. Carroll, V. Duvvuri, M. Trodden and M. S. Turner, *Phys. Rev. D* **70**, 043528 (2004). 2, 6

[31] G. J. Olmo, *Int.J.Mod.Phys. D* **20**, 413 (2011). 2, 6, 75

[32] S. Nojiri and S. D. Odintsov, *Phys. Rept.* **505**, 59 (2011). 2, 6

[33] S. Capozziello and V. Faraoni, *Beyond Einstein gravity: A Survey of gravitational theories for cosmology and astrophysics*. Fundamental Theories of Physics. **170**, Springer (2010), ISBN 978-94-007-0164-9. 2, 6, 11

[34] S. Capozziello and M. De Laurentis, *Phys. Rept.* **509**, 167 (2011). 2, 6

[35] A. de la Cruz-Dombriz and D. Saez-Gomez, *Entropy* **14**, 1717 (2012). 2, 6

[36] S. Capozziello and M. De Laurentis, *Annalen Phys.* **524**, 545 (2012). 3, 77

[37] J. A. R. Cembranos, *Phys. Rev. Lett.* **102**, 141301 (2009). 3

[38] A. de la Cruz-Dombriz and A. Dobado, *Phys. Rev. D* **74**, 087501 (2006). 3

[39] P. A. R. Ade *et al.* [Planck Collaboration], *Astron. Astrophys.* **571**, A22 (2014). 3

[40] A. A. Starobinsky, *Phys. Lett. B* **91**, 99 (1980). 3, 14, 159

[41] S. Ferrara, A. Kehagias and A. Riotto, *Fortsch. Phys.* **62**, 573 (2014). 3

[42] L. Sebastiani, G. Cognola, R. Myrzakulov, S. D. Odintsov and S. Zerbini, *Phys. Rev. D* **89**, 023518 (2014). 3

[43] K. Bamba, R. Myrzakulov, S. D. Odintsov and L. Sebastiani, *Phys. Rev. D* **90**, 043505 (2014). 3

[44] K. Bamba, S. Nojiri, S. D. Odintsov and D. Saez-Gomez, *Phys. Rev. D* **90**, 124061 (2014). 3

[45] S. Nojiri, S. D. Odintsov and D. Saez-Gomez, *Phys. Lett. B* **681**, 74 (2009). 3

[46] E. Elizalde and D. Saez-Gomez, *Phys. Rev. D* **80**, 044030 (2009). 3

[47] A. de la Cruz-Dombriz, A. Dobado and A. L. Maroto, *Phys. Rev. D* **77**, 123515 (2008). 3

[48] A. Abebe, A. de la Cruz-Dombriz and P. K. S. Dunsby, *Phys. Rev. D* **88**, 044050 (2013). 3

[49] A. Abebe, M. Abdelwahab, A. de la Cruz-Dombriz and P. K. S. Dunsby, *Class. Quant. Grav.* **29**, 135011 (2012). 3

[50] B. Abbott *et al.* (Virgo, LIGO Scientific), *Phys. Rev. Lett.* **119**, 161101 (2017). 3, 142, 143, 144

[51] F. W. Hehl, P. Von Der Heyde, G. D. Kerlick and J. M. Nester, *Rev. Mod. Phys.* **48**, 393 (1976). 3

[52] J.R. Oppenheimer & G.M. Volkoff *Phys. Rev.* **55**, 374 (1939). 4, 73, 75, 152

[53] S. Capozziello, M. De Laurentis, I. De Martino, M. Formisano and S. D. Odintsov, *Phys. Rev. D* **85**, 044022 (2012). 4

[54] S. Capozziello, M. De Laurentis, S. D. Odintsov and A. Stabile, *Phys. Rev. D* **83**, 064004 (2011). 4

[55] D. Psaltis, *Living Reviews in Relativity*, **11**, 9 (2008). 4

[56] B.A. Bassett, M. Kunz, D. Parkinson, C. Ungarelli, *Phys. Rev. D* **68**, 043504 (2003). 5, 16

[57] S. Weinberg, *Rev. Mod. Phys.* **61**, 1 (1989). 5

[58] Planck Collaboration, *Planck 2013 results. XVI. Cosmological parameters*, arXiv:1303.5076. 6

[59] Planck Collaboration, *Planck 2015 results. XIII. Cosmological parameters*, arXiv:1502.01589. 6, 119

[60] A. G. Riess, L. G. Strolger, S. Casertano, H. C. Ferguson, B. Mobasher et al., ApJ, **659**, 98 (2007). 6

[61] Suzuki et al.. (The Supernova Cosmology Project), ApJ, **746**, 85 (2012). 6, 114

[62] Capozziello et al., *Int. J. Mod. Phys. D* **12**, 1969 (2003). 6

[63] M. Demianski et al., *Astron. Astrophys.* **454**, 55 (2006). 6

[64] V. Perrotta, C. Baccagalupi, S. Matarrese, *Phys. Rev. D* **61**, 023507 (2000). 6

[65] J.C. Hwang, H. Noh, *Phys. Lett. B* **506**, 13 (2001). 6

[66] S. Capozziello, P. Jovanović, V. B. Jovanović and D. Borka, arXiv:1702.03430 [gr-qc] (2017). 6

[67] J. M. Overduin and P. S. Wesson, *Phys. Rept.* **283**, 303 (1997). 7

[68] N. D. Birrell, and P. C. W. Davies, *Cambridge University Press*, **7**, (1984). 7

[69] C. Armendariz-Picon and P. B. Greene, *Gen. Rel. Grav.* **35**, 1637 (2003). 7, 96

[70] B. Saha, *Astrophys. Space Sci.* **357**, 28 (2015). 7

[71] B. Saha, *The European Phys. J Plus* **131**, 242 (2016). 7

[72] M. O. Ribas, F. P. Devecchi and G. M. Kremer, *Mod. Phys. Lett. A* **31**, 1650039 (2016). 7

[73] R. C. Souza and G. M. Kremer, *Class. Quant. Grav.* **25**, 225006 (2008). 7

[74] M. O. Ribas, F. P. Devecchi and G. M. Kremer, *Europhys. Lett.* **81**, 19001 (2008). 7

[75] G. Grams, R. C. de Souza and G. M. Kremer, *Class. Quant. Grav.* **31**, 185008 (2014). 7

[76] S. Carloni, S. Vignolo and R. Cianci, *Class. Quant. Grav.* **31**, 185007 (2014). 7, 8, 95, 97, 112, 129, 130, 136

[77] S. Vignolo, S. Carloni and L. Fabbri, *Phys. Rev. D* **91**, 043528 (2015). 7

[78] J. Wainwright and G. F. R. Ellis, *Cambridge University Press*, 1997 (see also references therein). 7

[79] S. Bahamonde, C. G. Böhmer, S. Carloni, E. J. Copeland, W. Fang and N. Tamanini, arXiv:1712.03107 [gr-qc] and references therein. 7

[80] O. Farroq and B. Ratra, *ApJ*, **766**, L7 (2013). xvi, 7, 113, 116, 117, 118, 146

[81] S. Weinberg, *Gravitation and Cosmology* (Wiley, New York, 1972). 12, 18, 22, 38

[82] A.H. Guth, *Phys. Rev. D* **23**, 347 (1981). 12, 159

[83] I.L. Buchbinder, S.D. Odintsov, I. Shapiro, *Effective Action in Quantum Gravity* (IOP Publishing, Bristol, 1992). 12, 13

[84] H. Bondi, *Cosmology* (Cambridge University Press, Cambridge, 1952). 13, 25

[85] C.H. Brans, R.H. Dicke, *Phys. Rev.* **124**, 925 (1961). 13, 25, 36, 38

[86] S. Capozziello, R. de Ritis, C. Rubano, P. Scudellaro, *Riv. Nuovo Cimento* **4**, 1 (1996). 13

[87] D.W. Sciama, *Mont. Not. R. Astron. Soc.* **113**, 34 (1953). 13, 25

[88] N.D. Birrell, P.C.W. Davies, *Quantum Fields in Curved Space* (Cambridge University Press, Cambridge, 1982). 13, 14, 31

[89] G. Vilkovisky, *Class. Quantum Grav.* **9**, 895 (1992). 13

[90] P. Duruisseau, R. Kerner, *Gen. Relat. Gravit.* **15**, 797 (1983). 14

[91] D. La, P.J. Steinhardt, *Phys. Rev. Lett.* **62**, 376 (1989). 14

[92] S. Capozziello, R. de Ritis, A.A. Marino *Gen. Relat. Gravit.* **30**, 1247 (1998). 14

[93] S. Gott, H.-J. Schmidt, A.A. Starobinsky, *Class. Quantum Grav.* **7**, 893 (1990). 14, 31

[94] K. Maeda, *Phys. Rev. D* **39**, 3159 (1989). 14

[95] P. Teyssandier, P. Tourrenc, *J. Math. Phys.* **24**, 2793 (1983). 14

[96] D. Wands, *Class. Quantum Grav.* **11**, 269 (1994). 14

[97] L. Fatibene, M. Ferraris, M Francaviglia, M. Godina, *Gen. Relat. Gravit.* **9**, 1371 (1998). 14

[98] L. Amendola, A. Battaglia-Mayer, S. Capozziello, S. Gottlober, V. Muller, F. Occhionero, H.-J. Schmidt, *Class. Quantum Grav.* **10**, L43 (1993). 14

[99] R. Arnowitt, S. Deser, C.W. Misner, in *Gravitation: An Introduction to Current Research*, ed. by L. Witten (Wiley, New York, 1962). 14

[100] B.S. DeWitt, in *Battelle Rencontres*, ed. by C. DeWitt, J.A. Wheeler (Benjamin, New York, 1968). 14

[101] C. Itzykson, J.-C. Zuber, *Quantum Field Theory* (McGraw-Hill, New York, 1980). 14

[102] C.W. Misner, in *Magic Without Magic*, ed. by J. Klauder (Freeman, San Francisco, 1972). 14

[103] C.W. Misner, in *Relativity*, ed. by M. Carmeli, L. Fickler, L.Witten (Plenum, San Francisco, 1970). 14

[104] J.A. Wheeler, *Rev. Mod. Phys.* **29**, 463 (1957). 14

[105] R.A. Knop *et al., Astrophys. J.* **598**, 102 (2003). 14

[106] J.L. Tonry *et al., Astrophys. J.* **594**, 1 (2003). 14

[107] P. de Bernardis *et al., Nature* **404**, 955 (2000). 14

[108] R. Stompor *et al., Astrophys. J. Lett.* **561**, L7 (2001). 14

[109] G. Hinshaw *et al., Astrophys. J. Suppl.* **148**, 135 (2003). 15

[110] D.N. Spergel *et al.* [WMAP Collaboration], *Astrophys. J. (Suppl.)* **170**, 377 (2007). 15

[111] V. Sahni, A.A. Starobinsky, *Int. J. Mod. Phys. D* **9**, 373 (2000). 15

[112] E.J. Copeland, M. Sami, S. Tsujikawa, *Int. J. Mod. Phys. D* **15**, 1753 (2006). 15

[113] T. Padmanabhan, *Phys. Rep.* **380**, 235 (2003). 15

[114] S. Capozziello, V.F. Cardone, E. Elizalde, S. Nojiri, S.D. Odintsov, *Phys. Rev. D* **73**, 043512, (2006). 16

[115] V.F. Cardone, A. Troisi, S. Capozziello, *Phys. Rev. D* **69**, 083517 (2004). 16

[116] A. Lue, R. Scoccimarro, G. Starkman, *Phys. Rev. D* **69**, 044005 (2004). 16

[117] K. Freese, M. Lewis, *Phys. Lett. B* **540**, 1 (2002). 16

[118] G.R. Dvali, G. Gabadadze, M. Porrati, *Phys. Lett. B* **485**, 208 (2000). 16

[119] S. Nojiri, S.D. Odintsov, *Int. J. Geom. Meth. Mod. Phys.* **4**, 115 (2007). 16, 18

[120] S. Capozziello, V.F. Cardone, E. Piedipalumbo, M. Sereno, A. Troisi, *Int. J. Mod. Phys. D* **12**, 381 (2003). 16

[121] S. Capozziello, V.F. Cardone, S. Carloni, A. Troisi, *Int. J. Mod. Phys. D* **12**, 1969 (2003). 16

[122] B. Li, J.D. Barrow, *Phys. Rev. D* **75**, 084010 (2007). 16

[123] B. Li, J.D. Barrow, D.F.Mota, *Phys. Rev. D* **76**, 104047 (2007). 16

[124] C.M. Will, *Theory and Experiment in Gravitational Physics*, 2nd edn. (Cambridge University Press, Cambridge, 1993). 17, 19, 28, 29, 30, 31

[125] K.S. Stelle, *Phys. Rev. D* **16**, 953 (1977). 17

[126] R.H. Sanders, *Ann. Rev. Astron. Astrophys.* **2**, 1 (1990). 17

[127] M. Ferraris, M. Francaviglia, G. Magnano, *Class. Quantum Grav.* **5** L95 (1988). 17

[128] G. Magnano, M. Ferraris, M. Francaviglia, *Gen. Relat. Gravit.* **19**, 465 (1987). 17

[129] G. Magnano, L.M. Sokolowski, *Phys. Rev. D* **50**, 5039 (1994). 17, 18, 33

[130] L.M. Sokolowski, *Class. Quantum Grav.* **6**, 2045 (1989). 17

[131] A. Einstein, *Sitzung-ber. Preuss. Akad. Wiss.,* 414 (1925). 17

[132] R.M. Wald, *General Relativity* (Chicago University Press, Chicago, 1984). 18, 20

[133] M. Ferraris, M. Francaviglia, I. Volovich, *Class. Quantum Grav.* **11**, 1505 (1994). 18

[134] B. Li, K.-C. Chan, M.-C. Chu, *Phys. Rev. D* **76**, 024002 (2007). 18

[135] B. Li, M.-C. Chu, *Phys. Rev. D* **74**, 104010 (2006). 18

[136] D.N. Vollick, *Phys. Rev. D* **68**, 063510 (2003). 18

[137] M. Di Mauro, L. Fatibene, M.Ferraris, M.Francaviglia, *Int. J. Geom. Meth. Mod. Phys.* **7**, Issue: 5, 887 (2010). 18, 67

[138] L. Fatibene, M.Ferraris, M.Francaviglia, S.Mercadante, *Int. J. Geom. Meth. Mod. Phys.* **7**, Issue: 5, 899 (2010). 18

[139] I. Quandt, H.-J. Schmidt, *Astron. Nachr.* **312**, 97 (1991). 19

[140] P. Schneider, J. Ehlers, E.E. Falco, *Gravitational Lenses* (Springer, Berlin, 1992). 19

[141] L.M. Krauss, M. White, *Astrophys. J.* **397**, 357 (1992). 19

[142] A. Einstein, *Ann. der Physik* **49**, 769 (1916). 20

[143] L.P. Eisenhart, *Riemannian Geometry* (Princeton University Press, Princeton, 1955). 20

[144] E. Schrodinger, *Space-Time Structure* (Cambridge University Press, Cambridge, 1960). 20

[145] M. Lockwood, *The Labyrinth of Time*, 2nd edn. (Oxford University Press, Oxford, 2007). 20

[146] C. Barcelo, M. Visser, *Class. Quantum Grav.* **17**, 3843 (2000). 20

[147] S.M. Carroll, *Spacetime and Geometry: An Introduction to General Relativity* (Addison-Wesley, San Francisco, 2004). 20

[148] T. Levi-Civita, *The Absolute Differential Calculus* (Blackie and Son, London, 1929). 23

[149] R.H. Dicke, *Phys. Rev.* **125**, 2163 (1962). 26, 27, 32

[150] J.O. Dickey *et al., Science* **265**, July 1994. 28

[151] H. Taylor, J.M. Weinberg,*Astrophys. J.* **235**, 908 (1982). 28

[152] T.P. Sotiriou, S. Liberati, V. Faraoni, *Int. J. Mod. Phys. D* **17**, 393 (2008). 30

[153] T. Damour, G. Esposito-Farese, *Class. Quantum Grav.* **9**, 2093 (1992). 32

[154] V. Faraoni, S. Nadeau, *Phys. Rev. D* **75**, 023501 (2007). 32

[155] S. Capozziello, M. De Laurentis *Phys. Rep.* **509**, 4-5 (2011). 35

[156] M. Fierz, *Helv. Phys. Acta* **29**, 128, (1956). 36

[157] P. Jordan, *Naturwiss.* **26**, 417, (1938). 36

[158] P. Jordan, *Schwerkraft und Weltfall, Grundlagen der Theoretische Kosmologie* Vieweg & Sohns, Braunschweig, (1952). 36

[159] V. Faraoni, *Class. Quantum Grav.* **26**, 145014, (2009). 36

[160] L.D. Landau, E.M. Lifschitz, *The Classical Theory of Fields*, Pergamon Press, Oxford, (1989). 37

[161] T. Matsuda, *Prog. Theor. Phys.* **47**, 738, (1962). 38

[162] C. Romero, A. Barros, *Astr. Sp. Sci.* **192**, 263, (1992). 38

[163] C. Romero, A. Barros, *Phys. Lett. A* **173**, 243, (1993). 38

[164] C. Romero, A. Barros, *Gen. Relat. Gravit.* **25**, 1305, (1993). 38

[165] M.A. Scheel, S.L. Shapiro, S.A. Teukolsky, *Phys. Rev. D* **51**, 4208, (1995). 38

[166] N. Banerjee, S. Sen, *Phys. Rev. D* **56**, 1334, (1997). 38

[167] V. Faraoni, *Phys. Lett. A* **245**, 26, (1998). 38

[168] L.A. Anchordoqui, S.E. Perez-Bergliaffa, M.L. Trobo, G.S. Birman, *Phys. Rev.D* **57**, 829, (1998). 38

[169] V. Faraoni, *Phys. Rev. D* **59**, 084021, (1999). 38

[170] V. Faraoni, *Cosmology in Scalar-Tensor Gravity* ,Kluwer Academic, Dordrecht, (2004). 38

[171] B. Bertotti, L. Iess, P. Tortora, *Nature* **425**, 374, (2003). 38

[172] F. W. Hehl, J. D. McCrea, E. W. Mielke and Y. Ne'eman, *Phys. Rept.* **258**, 1, (1995). 43

[173] Y. Mao, M. Tegmark, A. Guth, S. Cabi, *Phys. Rev. D* **76**, 104029, (2007). 43

[174] S. Capozziello, R. Cianci, C. Stornaiolo and S. Vignolo, *Physica Scripta*, **78**, 065010, (2008). 43, 66, 68

[175] S. Capozziello, R. Cianci, C. Stornaiolo and S. Vignolo, *Class. Quantum. Grav.* **24**, 6417, (2007). 44, 66, 68, 78

[176] S. Capozziello and M. Francaviglia, *Gen. Rel. Grav.*: *Special Issue on Dark Energy* **40**, 357, (2007). 50, 51

[177] G.J. Olmo, *Phys. Rev. Lett.* **95**, 26110, (2005). 51

[178] G. Germán, *Phys. Rev. D.*, **32**, 3307, (1985). 51

[179] N. K. Glendenning, *Compact Stars. Nuclear Physics, Particle Physics and General Relativity*, Springer-Verlag, New York, Berlin, Heidelberg. (2nd edition: 2000). 54

[180] D. D. Osheroff, R. C. Richardson, and D. M. Lee *Phys. Rev. Lett.* **28**, 885 (1972). 61

[181] D. D. Osheroff, W. J. Gully, R. C. Richardson, and D. M. Lee *Phys. Rev. Lett.* **29**, 920 (1972). 61

[182] A.B. Migdal, *Nuclear Physics* **13**, 655 (1959). 61

[183] L. N. Cooper, *Phys. Rev.* **104**, 1189 (1956). 61

[184] P. Haensel, A.Y. Potekhin, D.G. Yakovlev, *Neutron Stars 1* Springer (2007). 61

[185] V. Dwivedi *Phys 569: Emergemt States of Matter* (2012). 61

[186] J.A. Sauls, *NATO ASI Series C* **262**, 457 (2019) arXiv:1906.09641. 61

[187] F. W. Hehl and B. K. Datta, *J. Math. Phys.* **12**, 1334 (1971). 66

[188] S. Capozziello, R. Cianci, C. Stornaiolo and S. Vignolo, *Int. J. Geom. Meth. Mod. Phys.* **5**, 765 (2008). 66, 68, 89

[189] S. Capozziello, R. Cianci, M. De Laurentis and S. Vignolo, *Eur. Phys. J. C* **70**, 341 (2010). 66, 68

[190] S. Capozziello and S. Vignolo, *Ann. Phys. (Berlin)* **19**, 238 (2010). 66, 68, 78

[191] S. Capozziello and S. Vignolo, *Class. Quantum Grav.* 26, 175013 (2009). 67

[192] S. Capozziello and S. Vignolo, *Int. J. Geom. Meth. Mod. Phys.* **9**, 1250006 (2012). 67

[193] A. Mana, L.Fatibene, M.Ferraris *JCAP* **040**, 1510 (2015), DOI: 10.1088/1475-7516/2015/10/040; arXiv:1505.06575. 67, 75

[194] S. Capozziello, M. De Laurentis, L. Fatibene, M. Francaviglia *Int. J. Geom. Meth. Mod. Phys.*, **09**, 12500 (2012). 67

[195] S. Capozziello, M. De Laurentis, L. Fatibene, M. Ferraris, S. Garruto *SIGMA*, **12**, 006 (2016). 67, 101

[196] S. Vignolo and L. Fabbri, Int. J. Geom. Meth. Mod. Phys. **9**, 1250054 (2012) 68

[197] R. Cianci, S. Carloni and S. Vignolo, *Class. Quantum Grav.* **31**, 185007-185030 (2014). 68

[198] R. Cianci, L. Fabbri and S. Vignolo, *European Phys. J. C* **75**, 478 (2015). 68

[199] Y. N. Obukhov and V. A. Korotky, *Class. Quantum Grav.* **4**, 1633 (1987). 68

[200] F. W. Hehl, P. von der Heyde and G. D. Kerlick, *Phys. Rev. D* **10**, 1066 (1974). 68

[201] E.Barausse, T. P. Sotiriou, J. C. Miller, *Class. Quantum Grav.* **25**, (6), 062201, (2008). 75

[202] S. Capozziello, A. Stabile and A. Troisi, *Phys. Rev. D* **76**, 104019 (2007). 77

[203] S. Capozziello, A. Stabile and A. Troisi, *Mod. Phys. Lett. A* **24**, 659 (2009). 77

[204] B. Whitt, *Phys. Lett. B* **145**, 176 (1984). 79

[205] S. Mignemi and D. L. Wiltshire, *Phys. Rev. D* **46**, 1475 (1992). 79

[206] N. Deruelle, M. Sasaki and Y. Sendouda, *Progress of Theoretical Physics* **119**, 237 (2008). 79

[207] S. Vignolo, R. Cianci and S. Carloni, *Class. Quantum Grav.* **35**, 095014 (2018). 79

[208] D. Radice, A. Perego, F. Zappa, and S. Bernuzzi, *Astrophys. J.* **852**, L29 (2018). 80

[209] M. Alford, M. Braby, M. W. Paris, and S. Reddy, *Astrophys. J.* **629**, 969 (2005). 80

[210] H. Mueller and B. D. Serot, *Nucl. Phys.* **A606**, 508 (1996). 80

[211] F. Douchin and P. Haensel, *Astron. Astrophys.* **380**, 151 (2001). 80

[212] R. B. Wiringa, V. Fiks, and A. Fabrocini, *Phys. Rev. C* **38**, 1010 (1988). 80

[213] J. S. Read, C. Markakis, M. Shibata, K. Uryu, J. D. E. Creighton, and J. L. Friedman, *Phys. Rev.D* **79**, 124033 (2009). 80

[214] T.P. Sotiriou, *Class. Quant. Grav* **23**, 5117 (2006). 82

[215] M. Aparicio Resco, A. de la Cruz Dombriz, F. J. Llanes Estrada, and V. Zapatero Castrillo, *Phys. Dark Univ.* **13**, 147 (2016). x, 82, 83, 84, 85, 142

[216] W. R. Inc., *Mathematica, Version 11.3*, champaign, IL, (2018). 83

[217] L. Lombriser, *et al.*, *Phys. Rev. D* **85**, 102001 (2012). 83

[218] C. W. F. Everitt *et al.*, *Phys. Rev. Lett.* **106**, 221101 (2011). 84

[219] R. P. Breton, V. M. Kaspi, M. Kramer, M. A. McLaughlin, M. Lyutikov, S. M. Ransom, I. H. Stairs, R. D. Ferdman, F. Camilo, and A. Possenti, *Science* **321**, 104 (2008). 84

[220] J. Naf and P. Jetzer, *Phys. Rev. D* **81**, 104003 (2010). 84

[221] D.D. Doneva, *et al.*, *Astrophys. J.* **781**, L6 (2013). 86, 88

[222] H. B. Lawson, M. L. Michelsohn, *Spin Geometry*. Princeton Mathematical Series. Princeton Univ Pr (1990), ISBN: 0-6910-8542-0. 95

[223] L. Fatibene, M. Francaviglia, *Natural and gauge natural formalism for classical field theories. A geometric perspective including spinors and gauge theories*. Kluwer Academic Pub, Dordrecht, (2003), ISBN: 1-4020-1703-0. 95

[224] L. Fatibene, M. Francaviglia, *Acta Phys. Polon. B* **29**, (4), 915 (1998). 95

[225] L. Fabbri, S. Vignolo and S. Carloni, *Phys. Rev. D* **90**, 024012 (2014). 96

[226] P. Pinto, L.Del Vecchio, L.Fatibene, M.Ferraris, *JCAP* **11**, (2018), arXiv:1807.00397 [gr-qc]. 101, 105

[227] A. A. Andrianov, F. Cannata, A. Yu. Kamenshchik, *Phys. Rev. D*, **86**, 7303A (2012). 103

[228] L.Del Vecchio, L.Fatibene, S.Capozziello, M.Ferraris, P.Pinto, S.Camera, *Eur. Phys. J. Plus*, **134**, (5), (2019). 105

[229] C. Bambi, M. Giannotti, F. L. Villante,*Phys. Rev. D* **71**, 123524 (2005). 112

[230] E. V. Pitjeva, *Astron. Lett.* **31**, 340 (2005). 112

[231] S. Nesseris, A. Mazumdar, *Physical Review D* **79**, 104006 (2009). 112

[232] E. Piedipalumbo, P. Scudellaro, G. Esposito, C. Rubano *General Relativity and Gravitation* **44**, 2477 (2012). 112

[233] A. G. Riess, A. V. Filippenko, P. Challis, A. Clocchiatti, A. Diercks et al., *ApJ*, 116,1009 (1998). 114

[234] S. Perlmutter, G. Aldering, G. Goldhaber, R. A. Knop, P. Nugent et al., *ApJ*, **517**, 565 (1999). 114

[235] L. Amati, C. Guidorzi, F. Frontera, M. Della Valle, F. Finelli, R. Landi and E. Montanari, *MNRAS*, **391**, 577 (2008). 115

[236] M. Demianski, E. Piedipalumbo, D. Sawant and L. Amati, *A& A*, **598**, (2016). 115

[237] M. Demianski, E. Piedipalumbo, D. Sawant and L. Amati, *A& A*, **598**, (2016). 115

[238] W. J. Percival, B. A. Reid, D. J. Eisenstein, N. A. Bahcall, T. Budavari, et al., *MNRAS*, **598**, 2148 (2010). 115

[239] D. J. Eisenstein and W. Hu, *ApJ*, **496**, 605 (1998). 116

[240] E. Aubourg, S. Bailey, J. E. Bautista et al., *Phys. Rev. D*, **92**, 123516 (2015). 116

[241] O. Farroq, D. Mania, B. Ratra, *ApJ*, **764**, 13 (2013). 116

[242] M. Moresco, A. Cimatti,R. Jimenez, et al., *JCAP*, **08**, 006 (2012). 117

[243] N. G. Busca, T. Delubac, J. Rich, S. Bailey, A. Font-Ribera, et al., *A&A*, **552**, 18 (2013). 117, 146

[244] A. G. Riess et al., *ApJ*, **699**, 539 (2009). 119

[245] J. R. Bond, G. Efstathiou, M. Tegmark, *MNRAS*, **291**, L33 (1997). 119

[246] G. Efstathiou, J. R. Bond, *MNRAS*, **304**, 75 (1999). 119

[247] H. Akaike, *IEEE*, **19**, 716 (1974). 122, 146

[248] A. R. Liddle, *MNRAS*, **377**, L74 (2007). 122, 146

[249] M. Chevallier, D. Polarski, *Int. J. Mod. Phys. D*, **10**, 213 (2001). 122

[250] E. V. Linder, *Phys. Rev. Lett.*, **90**, 091301 (2003). 122

[251] L. Amendola, S. Appleby, A. Avgoustidis, et al, *Living reviews in Relativity*, **21**, 2 (2018). 123, 147

[252] A. G. Kim, E. V. Linder, R. Miquel, N. Mostek, *MNRAS*, **347**, 909 (2004). 124

[253] T. Munoz-Darias, J. Casares, I.G. Martinez-Pais, *ApJ* **635**, 520 (2005). 141

[254] L. Lindblom, *Astrophys. J.* **398** 569 (1992). 142

[255] R. Kippenhahn, A. Weigert, A. Weiss, *Stellar Structure and Evolution*, Springer, Dordrecht (2012). 143

[256] B. Sathyaprakash *et al.*, *Class. Quant. Grav.* **29**, 124013 (2012). 144

[257] R. Essick, S. Vitale, and M. Evans, *Phys. Rev. D* **96**, 084004 (2017). 144

[258] P. Amaro-Seoane, *et al.*, ArXiv e-prints 1702.00786 (2017). 144

[259] A. Friedmann, *Zeitschrift für Physik A* **10**, 377 (1922). 153, 154

[260] A. Friedmann, *Zeitschrift für Physik A* **21**, 326 (1924). 153, 154

[261] L. Bergström, A. Goobar *Cosmology and Particle Astrophysics*, (2nd ed.) Sprint (2006). 153